CAPITAL UNIVERSITY OF SCIENCE AND TECHNOLOGY, ISLAMABAD

Mixture Theory Modeling of Multiphasic Deformation

by

Usman Ali

A thesis submitted in partial fulfillment for the
degree of Doctor of Philosophy

in the
Faculty of Computing
Department of Mathematics

2021

Mixture Theory Modeling of Multiphasic Deformation

By

Usman Ali

(DMT-151010)

Dr. Anuar Ishak, Professor

University of Kebangsaan, Selangor, Malaysia

(Foreign Evaluator 1)

Dr. Mustafa Turkyilmazoglu, Foreign Evaluator 1

University of Hecettepe, Ankara, Turkey

(Foreign Evaluator 2)

Dr. Shafqat Hussain

(Thesis Supervisor)

Dr. Muhammad Sagheer

(Head, Department of Mathematics)

Dr. Muhammad Abdul Qadir

(Dean, Faculty of Computing)

DEPARTMENT OF MATHEMATICS

CAPITAL UNIVERSITY OF SCIENCE AND TECHNOLOGY

ISLAMABAD

2021

Copyright © 2021 by Usman Ali

This dissertation is dedicated to my teachers, parents and family.

CAPITAL UNIVERSITY OF SCIENCE & TECHNOLOGY ISLAMABAD

Expressway, Kahuta Road, Zone-V, Islamabad
Phone:+92-51-111-555-666 Fax: +92-51-4486705
Email: info@cust.edu.pk Website: https://www.cust.edu.pk

CERTIFICATE OF APPROVAL

This is to certify that the research work presented in the thesis, entitled **"Mixture Theory Modeling of Multiphasic Deformation"** was conducted under the supervision of **Dr. Shafqat Hussain**. No part of this thesis has been submitted anywhere else for any other degree. This thesis is submitted to the **Department of Mathematics, Capital University of Science and Technology** in partial fulfillment of the requirements for the degree of Doctor in Philosophy in the field of **Mathematics**. The open defence of the thesis was conducted on **November 19, 2021**.

Student Name :   Usman Ali (DMT-151010)

The Examining Committee unanimously agrees to award PhD degree in the mentioned field.

Examination Committee :

(a)   External Examiner 1:   Dr. Mudassar Nazar
Professor
CASPAM, BZU, Multan

(b)   External Examiner 2:   Dr. Meraj Mustafa Hashmi,
Associate Professor
NUST, Islamabad

(c)   Internal Examiner :   Dr. Rashid Ali
Associate Professor
CUST, Islamabad

Supervisor Name :   Dr. Shafqat Hussain
Professor
CUST, Islamabad

Name of HoD :   Dr. Muhammad Sagheer
Professor
CUST, Islamabad

Name of Dean :   Dr. Muhammad Abdul Qadir
Professor
CUST, Islamabad

AUTHOR'S DECLARATION

I, **Usman Ali (Registration No. DMT-151010)**, hereby state that my PhD thesis entitled, '**Mixture Theory Modeling of Multiphasic Deformation**' is my own work and has not been submitted previously by me for taking any degree from Capital University of Science and Technology, Islamabad or anywhere else in the country/ world.

At any time, if my statement is found to be incorrect even after my graduation, the University has the right to withdraw my PhD Degree.

(Usman Ali)

Dated: November, 2021   Registration No : DMT-151010

PLAGIARISM UNDERTAKING

I solemnly declare that research work presented in the thesis titled **"Mixture Theory Modeling of Multiphasic Deformation"** is solely my research work with no significant contribution from any other person. Small contribution/ help wherever taken has been duly acknowledged and that complete thesis has been written by me.

I understand the zero tolerance policy of the HEC and Capital University of Science and Technology towards plagiarism. Therefore, I as an author of the above titled thesis declare that no portion of my thesis has been plagiarized and any material used as reference is properly referred/ cited.

I undertake that if I am found guilty of any formal plagiarism in the above titled thesis even after award of PhD Degree, the University reserves the right to withdraw/ revoke my PhD degree and that HEC and the University have the right to publish my name on the HEC/ University Website on which names of students are placed who submitted plagiarized thesis.
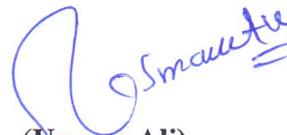
(Usman Ali)

Dated: November, 2021   Registration No : DMT-151010

List of Publications

It is certified that following publication(s) have been made out of the research work that has been carried out for this thesis:-

1. **U. Ali**, J. I. Siddique, "Visco-elastic behavior of articular cartilage under applied magnetic field and strain-dependent permeability" *Computer Methods in Biomechanics and Biomedical Engineering*, vol. 23, pp. 536-547, 2020.

2. J. I. Siddique, **U. Ali**, A. Ahmed, "Effects of magnetic field on porosity and solid deformation for radial fluid flow through deformable porous shells" *Computers and Mathematics with Applications*, vol. 80, pp. 1104-1116, 2020.

Usman Ali
DMT151010

Acknowledgement

I would like to thanks "Allah Almighty", the most Gracious, the most Merciful, Who helps me, give me potential, good health, and ability that I try to contribute in the ocean of endless knowledge. I would not finds the word, how to thanks His blessings upon me? Without His blessing, I would not be able to achieve my goal. The author invoke blessing upon the last Holy Prophet (PBUH), Whose teachings are the way of great knowledge as well as a remarkable source of endless gaudiness for the humanity.

I would like to dedicate this work to my teachers, specially to Prof. Dr. Javeed Iqbal Siddique and Prof. Dr. Shafqat Hussain, who gave me courage and guide me, at every step of this journey. I also acknowledge their positive and constructive criticism throughout the course of my research work. They were always with me, whenever I need. They bear all of my mistakes with great tolerance and give me a great opportunity to learn allot that will be helpful in future. I feel that I am lucky to work under their supervision. No doubt, they are not only good researchers but also good teachers.

I pay great respect as well as sincere gratitude to Prof. Dr. Muhammad Sagheer, head of department of mathematics for all his gaudiness, encouragement, support, and providing an excellent as well as learning environment in the department. He was always be there, when ever I need his assistance both in the course work and research. Moreover, I personally learn allot the subject he taught advance numerical techniques. It is worth mentioning that the subject he teach helps me in my research work, specially when I was solving different problems related to the partial differential equations. I would also likes to thanks Dr. Rashid Ali, Dr. Abdul Rehman Kashif, Dr. Afzal Mehmood and all other staff of the mathematic department for their moral support, giving me courage and valuable discussion during my stay in the department. Their advises help me in handling different projects that I have completed in my research work. I pay great attribute to my parents for their love, care, financial support, and prayers through out the course of my academic career. Their valuable advises are always with me which play

Abstract

In this dissertation, the bio-mechanical response of a fiber reinforced solid matrix (soft tissue) has been formulated. A constant magnetic field effects has been incorporated in the binary mixture of fluid and porous solid. The governing dynamics involved in the multiphasic deformation was based upon the loading imposed at the rigid bony interface. The fluid flow through the cartilage network depends upon the rate of applied compression as well as strain-dependent permeability of the soft tissues. The components of the mixture were assumed intrinsically incompressible; however, in the derivation of governing dynamics, visco-elastic behavior of the solid and an interstitial fluid were developed. The continuum mixture theory approach is employed in modeling solid deformation and local fluid pressure. In deriving the governing dynamics, strain-dependent permeability has been incorporated in the governing equations of binary mixture. The governing nonlinear coupled system of partial differential equations was developed for the solid deformation and fluid pressure, in the presence of Lorentz forces. In the case of permeability dependent flow, a numerical solution is computed, whereas, an exact solution is provided for constant permeability case. Graphical results highlight the influence of various physical parameters both on the solid displacement and fluid pressure.

In the second problem, the mechanical response of a radially constrained elastic porous shell during the passage of charged fluid has been formulated . The motion of fluid as well as solid deformation were based upon the rate of applied compression at the inner radius of the shell. A nonlinear diffusion equation applicable to plana and radial geometries was developed for the porosity along with informal integral boundary conditions on both the extremities. An equation for solid deformation is derived in the form of an integral equation. The governing system of equations is solved numerically for the transient case, whereas, an exact solution is provided for the steady-state problem. In the case of linear permeability, an excellent agreement is noticed between both the solutions. The comparison of the fluid flow through the planar, cylindrical, and spherical shell is used in exploring

the process of fluid flow affected by the geometrical constraint. Graphical results highlight the influence of different physical parameters on the porosity and solid displacement. Moreover, a detailed analysis of the fluid flow through a thick and thin wall elastic porous shell is also presented.

Finally, for the same geometry as was in the second problem, the mathematical model describing visco-elastic behavior of an elastic porous shell during passage of non-Newtonian fluids was developed. In formulating the flow behavior, power-law model was used in the constitutive equations of the mixture theory. The dominant mechanism of the fluid flow was considered outwardly directed when loading imposed at the inner radius of the shell. The outer boundary of the shell is considered as rigid mesh which offers negligible resistance for the passage of fluids. The general system of equations is derived for the porosity and solid deformation both for planar and radial geometries. The governing system of equations is solved analytically for steady-state case, whereas, numerical solution is computed for the transient problem. The significance of power-law index on the porosity and solid displacement is presented graphically.

Contents

List of Figures

Symbols

V_E	Volume of empty space	V_T	Total volumee
ϕ	Porosity	$\mathbf{u}, \mathbf{v}$	Velocity vectors
α	Different phases	ρ	Density
$\mathbf{T}$	Stress tensor	$\boldsymbol{\pi}$	Drag forces
$\mathbf{J}$	Current density	$\mathbf{B}$	Magnetic field
χ	Smooth function	χ^{α}	Inverse function
$\mathbf{V_p}$	Pore volume	$\mathbf{V_b}$	Bulk volume
τ	Shear stress	F	Deformation gradient
f	Function dependent variable	x	Spatial coordinate
$\mathbf{v^s}$	Solid velocity	$\mathbf{v^f}$	Fluid velocity
$\mathbf{D^f}$	Fluid deformation tensor	$\mathbf{b}$	Body forces
$\mathbf{D^s}$	Solid deformation tensor	$H(t)$	Heaviside function
s, f	Solid and fluid phases	σ	Stress
K	Coefficient of diffusive resistance	k	Permeability
$\mathbf{I}$	Identity tensor	$\mathbf{E}$	Electric field
σ_{θ}	Electric conductivity	M	Magnetic parameter
β	Different geometries	λ, μ	**_Lame_** constants
N	Numbers of components	a, b	Radii of shell $(a > b)$
∇P	Applied pressure	D	Diffusion coefficient
n	Power-law index	u	Solid displacement
k_0, m	Material constants	t	Normalized time
μ	Viscosity	$\nabla x, h$	Thickness
Q	Total discharged fluid	L	Length parameter

$p_2 - p_1$	Pressure difference	q	Fluid flux
A	Area of cross-section	H_a	Aggregate modulus
$\mathbf{X}$	Position with respect to some reference	T	Transpose
r	Capillary forces	σ_0	Electric conductivity
$\mathbf{B_0}$	Impose magnetic field	σ_{rr}	Radial direction
$\mathbf{B_1}$	Induced magnetic field	t	Normalized time
μ_c	Primitivity of free space	$\sigma_{\theta\theta}$	Annular direction
Ψ_0, Ψ_1	Functions of time	$\mathbf{E_s}$	Elasticity of solid
ϕ^s	Solid volume fraction	ϕ^f	Fluid volume fraction
$\dot{\lambda}_s, \dot{\mu}_s$	Visco-elastic moduli	λ_s, μ_s	Elastic moduli
λ_f	Bulk viscosity	μ_f	Dynamical viscosity
K_c	Diffusive interaction	Γ	Spin tensor

Chapter 1

Introduction

The basic motivation in this dissertation was in formulating the visco-elastic behavior of a fiber reinforced solid matrix enriched with the fluids in different loading conditions. Present work described the dynamics of fluid flow both for biological and non-biological settings. Particularly, mathematical models describing the fluid-solid interaction during passage of fluids through a soft biological tissue as well as fluid fluxes through a deformable shell are derived in different Chapters. From the modeling point of view, derivation of the governing dynamics reported in different problems are based upon the continuum mixture theory approach. Furthermore, various problems reported in this dissertation have been modeled by considering constant as well as strain-dependent permeability flow dynamics. On the other hand, kinematics involved in the motion of fluids and solid deformation in different problems depend upon the loading imposed either on the soft or rigid interface of the solid matrix. In formulating the multiphasic deformation, numerous theoretical studies have been reported in literature. Few of the well-known are finite elasticity[1–3], visco-elasticity [4, 5], growth and remodeling [6, 7], and continuum mixture theory [8–12] approach, etc. In 2003, a comprehensive review describing these theories has been discussed by Humphrey [13].

When fluids flow through the elastic porous materials, forces associate with the flow result in the solid matrix deformation. This deformation not only changes the shape and porosity of the deformable porous materials but also effects the passage

of fluids. This particular behavior of deformable porous solids is reported due to establishing complex coupling between the fluids motion and solids deformation. More precisely multiphasic deformation takes place simultaneously, when fluid flows through the deformable porous materials. The continuum mixture theory successfully employed [14, 15] in addressing these types of ephemerons, in which more than one phase simultaneously moves. In the following, the problem statement is given that is followed by objective, scope and significance of the present study.

1.1   Problem Statement

In this dissertation, mathematical investigation of the fluid flow through the elastic porous materials is reported. Particularly, motivated from the importance of coupling between the solid matrix and fluid phase in a physiological system while passage of fluid through an elastic tissue and permeation of fluid through a deformable porous shell have been considered in formulating governing models reported in different Chapters.

The main goal in the present study was to gain a better understanding of the dynamical processes as well as mechanical response involved in solid-fluid interaction both in biological and non-biological settings.

A summary of the theory used in formulating the fluid flow through deformable porous medium along with an overview of the applications of such flows to biological tissue deformation have been included in this thesis. Particularly, present work describes the mathematical formulations of the fluid flow through different geometries for industrial applications and mathematical modeling of fluid flow through a soft biological tissue.

Although, accurate and direct biological modeling is avoided, but study provided a reasonable framework for gaining an insight into the deformation phenomena

of elastic porous solid, if not, described the derivation of multiphasic deformation involved in a variety of fluid flow dynamics through deformable porous materials.

1.1.1 Objective and Scope

Mathematical models have been routinely used in describing the physical nature of different materials in engineering and biological sciences that help in understanding complex biological systems as well as optimize industrial processes. As the purpose of modeling is to increase our understanding of the physical world exist around us along with the validity of a model depends upon the empirical observations that provide theoretical background for the available experiments data. Keeping in view such a problem, the influence of magnetohydrodynamics (MHD) during passage of fluids through a soft biological tissue and multiphasic deformation of an elastic porous shell have been formulated in Chapter 3 and 4, respectively. Moreover, non-Newtonian fluid flow behavior is molded using power-law model while passage of fluid through a deformable porous shell in Chapter 5. On the other hand, after developing a theoretical model of any existing physical system, it is natural to develop an algorithm that will allows one to estimate the quantitative behavior of the system. The main focus was in developing the mathematical models reported in different Chapters which are more feasible for the computational point view along with the good approximation of the governing behavior. Quantitative results from mathematical models and their comparison with available data to identify a model's strengths and weaknesses was the main goal in the present research work.

1.1.2 Significance of Study

Various models for the flow induced deformation of the porous materials have been examined using the continuum mixture theory approach leading to a non-linear finite deformation model being proposed. Theory has been generalized and revisited by incorporating nonlinear permeability of the porous solids, in fact, strain-dependent permeability of the solid matrix in the constitutive equations of

the mixture theory modeling. In general, linear mixture theory modeling is combined with strain-dependent permeability in the presences of different physical parameters while deriving the governing models in different Chapters. This particular consideration helps in formulating an accurate physical behavior of a given problem, however, experimental verification still need to improve the findings of present research work. In the following, a historical background of the present work is presented.

1.2   Background

Porous materials are divided into two main classes, i.e., rigid and deformable porous materials. In the case of rigid porous materials, size as well as shape of the solid matrix remain invariant in loading circumstances, unless their threshold elastic limit do not reach. The pioneer work in the area of fluid flow through the rigid porous materials is due to the study of Washburn [16]. He derived the capillary rise phenomenon of fluid through the rigid porous materials. In modeling the governing dynamics of fluid infiltration, he assumed that the porous solid consists of small cylindrical capillaries, whereas, fluid flow through these capillaries was considered as Poiseuille flow. A continuous pressure difference was taken between the interfaces that infiltrated the fluid through these capillaries. In the absence of gravity, he concluded that volume of the liquid penetrated in time t was proportional to $\sqrt{t}$, whereas, in the presence of gravity, initial behavior still follows the same power law approximation for time ($\sqrt{t}$). On the other hand, for the longer time, fluid infiltrated in the porous solid and attained a finite height before achieving equilibrium.

Later on, Zhmud *et al.* [17] have formulated the dynamics of fluid flow through the rigid porous materials. They examined different models including the Washburn model and validated early time Washburn's finding, but for the longer time fluid flows dynamics, theoretical results deviated from the Washburn's equilibrium predictions. Moreover, recent experiment studies [18, 19] have proved that

the capillary rise phenomenon of fluid through the rigid porous materials follow a different power-law approximation for the time ($t^{0.2}$).

Davis and Hocking [20, 21] derived the dynamics of viscous fluid spreading and imbibition through a porous base. In their first study [20], they assumed that the porous solid having anisotropic as well as uniform behavior. However, in the second article [21], an extension in the previous model was made by including spreading of fluid over an initially dry porous solid. From the modeling view point, they assumed no cross-linking of the liquid occurred among the capillaries that was the case in the Washburn's study. They computed the shape of fluid penetration through the rigid porous materials. These studies modified as well as improved the results presented in the Washburn's study.

In the above paragraphs, some work related to the fluid flows through the rigid porous materials is summarized. In contrast to these materials, elastic porous solids reshape themselves in attaining equilibrium under applied shear or normal stress. Therefore, a special kind of visco-elastic behavior depending upon the nature of a porous solid has been reported in modeling the fluid flow through these materials. Our particular interest in this area is due to their close resemblance with many types of processes take place in animal body structure [22–24] as well as their numerous industrial applications [25–27]. Most common examples of the deformable porous materials includes sponge, foam, soil, articular cartilage, arteries, and soft biological tissues, etc.

Parker *et al.* [28] have formulated one-dimensional fluid flow through a deformable porous solid. In this study, dynamics of an incompressible fluid flow through an elastic porous solid were considered while deriving multiphasic deformation. They assumed that the stiffness and permeability of the porous solid both are the functions of local strain gradient. The governing system of equations is solved analytically for several simple constitutive relationships. Moreover, they measured the stiffness and permeability of one particular porous solid (foam) and using these results proved that the fluid flow and solid deformation both depend upon the

applied pressure function. A good qualitative agreement can be found between both the theoretical predictions and experimental findings.

Barry *et al.* [29] have developed the dynamics of fluid flow through a layer of deformable porous material. The main focus in this study was subcutaneous injections and subterranean of fluid through the soil. In formulating governing dynamics, they assumed that the porous solid matrix had an isotropic, homogeneous, and linearly elastic in nature. The governing system of equations is derived for an axis-symmetric geometry using the linear pore-elasticity. Moreover, governing system of equations is solved analytically using Hankel transform technique [30], however, Hankel inversion integrals were approximated numerically. The pressure contours and displacement of the solid matrix have been reported for various values of source heights and elastic parameters. Results of this study indicated the swelling of the porous medium as well as subsequent deformation of the free surface. Furthermore, they find the regions upon which one dimensional models have been applicable.

When loading impose on a deformable porous solid, fluid flows outwardly by squeezing the elastic solid matrix nonlinearly. This multiphasic deformation results a non-linearly link between the constituents of the mixture, i.e., between fluid and porous solid. In this particular physical phenomenon, void ratio (porosity) as well as permeability of the deformable porous materials change dramatically; hence, affects the passage of fluids through these materials. In the derivation of governing dynamics of multiphasic deformation in these types of problems, low speed flows have been formulated using the Darcy's law, whereas, high speed flows behaviors have been molded on the basis of nonlinear Forcheimer's law. The multiphasic nature of these problems limits in the use of single phasic description, even though these approaches have been reported in literature for some special circumstances, i.e., after achieving equilibrium. The pioneer work in the area of fluid flow through the elastic porous materials dates back to the study of Terzaghi [31]. Moreover, these types of multiphasic deformation phenomenons successfully described using the continuum mixture theory approach [32, 33]. This theory successfully employed in driving the multiphasic deformation phenomenons produced

during fluid flows through the deformable porous solids as well as passage of fluids through the soft biological tissues.

The mixture theory is based upon the idea of continuum mechanics which state that "individual components of the mixture are manipulated in such a way that every particle of medium is occupy by each constituent of the mixture". In the mid of nineteenth century, pioneer work in the development of this theory was due to the study of Fick [34], which was followed by Darcy [8]. Later on, necessary and relevant details have been discussed by Truesdell [9], Atkin and Craine [10], and Bowen [11] as well. However, most recent developments in the governing equations of this theory were found in the book written by Rajagopal and Tao [12]. The classical modeling approach described in this theory has provided the foundation to derive the dynamics of fluid lubrication through biological and non-biological settings. The description of governing dynamics of multiphasic deformation in this theory is based upon the conservation laws of mass and momentum balance. Later on, more reliable theoretical results have been achieved by incorporating nonlinear permeability in the governing equations of this theory.

In 1965, Christopher and co-author [35] modified Darcy's law into Blake-Kozeny equation for the power-law fluids along with the laminar flow through a packed tube. Their model was experimentally tested by passing a dilute polymer solution through the packed tube. Theoretical results for this particular study were then compared to the Sadowski study [36], who was working on an identical problem using an Ellis fluid model. Later on, Hayes *et al.* [37] used the volume averaging approach (method) and examined the power-law fluids model. They investigated the velocity and pressure changes in a porous bed packed with the spherical particles. In this study, their focus was in modifying and improving the Darcy's law and intrinsic permeability used in modeling the power-law fluids that has been examined by many authors, i.e., Kemblowski and Michniewicz [38], 1979; Fariss and Pinder [39], 1987; etc.

It is worth mentioning that one-dimensional fluid flow through a deformable porous

slab has been investigated to some extent, but less emphasis was given in accommodating the fluid fluxes through radially constrain geometry. The understanding of radial flow through radial shells has direct relevance with many types of industrial application, particularly, with permeability dependent flow behavior through the arterial wall [40–42], and industrial focused application focusing ultrafiltration of hollow [43]. Moreover, another interesting biological application is flow of proteins through the arterial wall was associated with the type of arteriosclerosis [44, 45]. The deformation in the tissue could be a possible cause for this, particularly, if nonlinearity in the deformation of tissue is enough to impede the flux of proteins for this accumulation as well. The modeling of these filters could be done using cylindrical shells, as was reported in [46], and a comparison could be made between planar and radial filters. Kenyon [47] investigated the fluid flux through an unconfined deformable cylindrical porous medium. He studied the deformation produced in the solid matrix by step changes in the pressure. Later on, Jayaraman [48] extended this work and examined the oscillatory flow in the arterial wall. In this study, the boundary conditions were associated with the initial boundary position instead of the final position. Klanchar and Tarbell [49] prescribed the nonlinear model in which they studied velocity and pressure variation in the cylindrical confined geometry. The flow of organic matter through the cylindrical arteries is an example of fluid-solid interaction for the elastic porous tissues, particularly be an interesting case, when non-Newtonian fluid flows through them. An effort was made in modeling the radial flow through cylindrical and spherical shells along with the comparison for the planar case [50]. A perturbation solution is calculated for small-time and slow deformation with the numerical solution for the time-dependent problems. The useful finding in this study is comparison of fluid flow through planer and radial geometries.

In the above paragraphs, some detail describing the fluid-solid interaction in different physical conditions have been summarized, particularly, when fluid flow through the rigid and deformable porous materials. Now, the main focus is to discuss the fluid flows through the soft tissues along with their effects on the swelling behavior of solid matrix. Our interest in this regard is to elaborate theories and

formulations used in deriving the governing dynamics of fluid flow through the soft biological tissues (articular cartilage), in the presence of Lorentz forces. It is well established fact that the morphology between interconnecting tissues like, skin, cornea, cartilage, and aorta is identically; however, their functioning in the living organisms is totally different.

The organic mixture composition of these tissue consists of glycogenolyses, salt, fluid, glycoprotein, and cellular network. The articular cartilage is a complex biological tissue composed of dense woven type collage fabric matrix covered and filled with proteoglycan aggregate fluid. The organic mixture composition of the solid matrix consists of approximately 65 percent of collagen, 25 percent proteoglycans, and remaining 10 percent other glycoproteins, in the dry weight. This composition depends upon numerous factors, such as depth, topographical positioning, age, degeneration, ultra-structural fixation, and inter-molecular arrangement, etc. On the micro level, this complex organic mixture behaves like a fiber reinforced deformable porous solid. The governing dynamics involve in the solid deformation depend upon the forces associated with the fluid fluxes through the tissues network, either by the inner molecular movement or by external pressure. Until the mid-nineteenth century, this soft tissue was considered to be devoid from all the biological activities. This consideration was due to the fact that the cartilage tissues are virtually isolated from the body structure of living organisms. It is worth mentioning here, cartilage tissues have no blood flow along with complete isolation from the lymphatic and nervous system of the body. Later on, in the advancement of modern technology, a variety of different pictures of this soft biological tissue have been presented using radioactive tracer, electronic microscopy scanning, and bio-mechanical technology, etc. These studies opened a new era for researchers in understanding the dynamics of fluid lubrication as well as solid deformation take place in the cartilage and other such a types of soft biological tissues.

It was challenging for researcher to elaborate the exact nature of many types of elastic tissues theoretically without performing experiments due to their complex mixture compositions. An unsolved problem was the pertaining fluid flow through

the cavities of diarthrodial joints that was the main obstacle which need to be accommodate [51]. The fluid-solid interaction during loading circumstances in these tissues was challenging, because motion of fluid and solid deformation take place all together [52, 53]. Furthermore, a nonlinear link has been reported between the components of the mixture while passing of fluids through the deformable tissues [54, 55]. Later on, more reliable theoretical results of this non-linearity have been achieved using strain-dependent permeability while deriving governing dynamics. After this classical modification more feasible theoretical results of the linear mixture theory have been achieved. This modification helps in understanding the dynamics involve in the fluid flows and solid deformation take place in soft biological tissues.

Mow *et al.* [56] have examined the creep and stress relaxation behavior of articular cartilage. They considered that the mechanical properties of constituents (solid matrix) as well as physical interaction between different phases exhibit rheological behavior. In this study, cartilage solid matrix and fluid phase both were considered intrinsically incompressible, and non-dissipative. They formulated the governing dynamics using constant permeability that was independent of the rate of solid deformation produced in the tissues network. Moreover, volume-metric ratio of solid to fluid was taken in such a way that it changed in accordance with the depth of the specimen taken for the analysis. In this study, a large separation in the permeability coefficient was found due to the fixed rate of the solid deformation. Their theoretical results were inconsistent with experimental findings that justify the theory used in deriving the governing dynamics.

Later on, Myers *et al.* [57] studied an ion induced swelling behavior of cartilage tissues. They placed a thin dimensionally measured specimen in the ionic bath of sodium chloride solution (NaCl solution in water). An ion-induced swelling behavior has been reported in the cartilage tissues that conformed an isotropic inhomogeneous nature of the solid matrix. They found a linear contraction in the tissue network by increasing molar concentration (α_c) of the solution. Their work extended the binary mixture theory model to a triphasic model, in which an ion-induced strain was introduced. Theoretical prediction of this particular

study successfully explained the transient forced history described in an isometric experiment.

Armstrong *et al.* [58] have modeled an unconfined compression of articular cartilage. They examined creep stress-relaxation behavior of a cylindrical specimen. In this study, a saturated tissue was placed between impermeable plates to measure the elasticity of the solid matrix. The tissue equilibrium was maintained with surrounding during radial fluid flow through the tissues. They found an analytical solution of the governing systems of partial differential equations that was used in describing the solid deformation produced in the cartilage network.

Spilker *et al.* [59] have employed finite element method in solving governing system of equations, and used these results in exploring stress relaxation behavior of the cartilage tissues. In this study, a thin layer of hydrated tissue of circular plane was investigated. They divided the tissue domain into both thin and thick wall specimens while exploring the solid deformation affected by the wall thickness of the tissues. This study predicted that rigid bony interface has negligible influence on tissue response far away from the interface.

In recent past, Guo *et al.* [60] have investigated the mechanical behavior of a soft tissue (articular cartilage). They formulated the confined compression of one dimensional deformation of cartilage tissues as well as movement of the interstitial fluid through the tissue surface using a biphasic finite element method. In formulating the governing dynamics, they assumed that tissue having an inhomogeneous, non linear biphasic elastic material with mechanical properties depend upon the depth and strain-dependent material. The loading conditions are divided into two categories. In first case, a superficial zone was considered in loading circumstances with a porous platen, later on, the deep zone was loaded with the porous platen. They find that removing the superficial zone results in the increase of all the mechanical parameters that decrease the fluid support ratio within the tissues network. On the other hand, a linear change in the apparent permeability was noticed when superficial zone is removed in the normal test, whereas, apparent permeability did not alter in the upside down test. These two tests for different

specimen orientations reported a large difference in the apparent permeability. This study described the importance of superficial zones on the properties of the articular cartilage and other types of soft tissues.

In 1998, Cohen *et al.* [61] employed biphasic theory on the hydrated soft tissues and developed a transversely isotropic model. They found an analytical solution for an unconfined compression of radially constrained disk plate tissues that compressed between two rigid platens having frictionless interface. Particularly, they reported the stress relaxation behavior of applied compression and ramp displacements. The solution of the governing system of equations is then used in validating the theoretical results by comparing these results with experimental data obtained in finding the biphasic material parameters. They found an excellent agreement between theoretical predictions and experimental results that are much better than the previously achieved results in an isotropic model.

Later on, Mow *et al.* [62] provided an overview of the different bio-mechanical factors used in analyzing the interpret biological data found in the experiments. They presented a detail describing some mechano-electrochemical events that occurred in the articular cartilage during loading circumstances. Furthermore, a provocative discussion of applied pressure effects on the soft tissues has been presented. They have considered different loading cases, like, hydrostatic pressure, osmotic pressure, pressure loading, confined compression, and unconfined compression. The effects of these loadings on the solid matrix, fluid, solute and ion flows, deformation, and electrical fields have been discussed in detail. Particularly, similarities and differences in these parameters for different types of loading circumstances was the main goal in this study. They found that the understanding of these differences help in describing the insights into the mechano-electrochemical events that take place in tissues during different loading conditions.

In the articular cartilage, proteoglycan aggregate (PGA) are immobilized as well as restrain within the tissues network. These PGAs contain sufficiently large molecules range between 1×10^8 to 2×10^8 [63]. These molecules contain negatively charged ions in large proportion ($S0_3^-$, $C00^-$), with their glycosaminoglycan

(GAG) network. These movable charges have efficiency to generate an induced magnetic field due to the relative motion between different phases. The motivation of present work was to model the governing dynamics involved in the application of external magnetic field on the mobile charge fluid within the tissue network. This particular consideration will helps in understanding the influence of external magnetic fields on the swelling behavior of cartilage as well as other types of elastic porous tissues. We used an identical modeling technique as was in [15, 50, 56, 57], with suitable modification for incorporating the magnetohydrodynamics (MHD) and power-law effects in the governing dynamics of different problems reported in coming Chapters.

Siddique and Kara [64] employed binary mixture theory in formulating the effects of MHD on a capillary rise of liquid through a sponge type elastic porous solid. Later on, Naseem *et al.* [65] derived the MHD dynamics for the fluid flow through a deformable porous material. The main idea used in modeling the MHD process is the forces interaction between the applied and induced magnetic fields. These processes have relevance in various contexts, like, MRI (magnetic resonance imaging), study of plasma, drug targeting, and separation of nuclear isotopes, etc. In the field of computational biomechanics, Ahmed *et al.* [66] have studied the influence of MHD on the tissues deformation using the continuum mixture theory approach.

In the above paragraphs, some work related to the mixture theory modeling have been summarized for the fluid fluxes through the porous materials and soft biological tissues. On the other hand, this theory also employed in modeling the composite manufacturing process [67]. These processes are well known and used in the preparation of different industrial products. The composite manufacturing is usually referred as a resin transfer molding technique (RTM), structural resin molding (SRIM), and squeeze casting (SC). These phenomenons have been schematized based on the fluid infiltration through initially dry porous materials. In recent past, these processes have paid much attention due to their low cast investment, less energy requirement, simple curing cycle, environment friendly, etc. Most often, rigid porous materials have been considered in these processes,

however, there are several papers reported in literature [68–71] that focused on the solid deformation as well as described the importance of stress monitoring in the derivation of governing dynamics. In fact, in many physical situations the applied compression was taken large enough to generate the considerable deformation, particularly to the face of porous solid having direct contact with the fluids.

Preziosi *et al.* [72] have formulated the infiltration of an incompressible fluid through a deformable porous solid. Particularly, they considered the liquid flow through a sponge type porous material that obey the slug flow approximation. The resulting boundary value problem in this study was the Stefan-type with suitable interfaced boundary conditions that described the saturation domain of porous solid. They predicted different models and their dependence upon the inertial and stress factors.

Ambrorosi *et al.* [73] have derived a new model that described an injection molding process under the isothermal conditions. These processes are generally governed by initially dry deformable porous solids. From the modeling point of view, the specimen for analysis was divided into two sub-intervals, i.e., dry and wet porous performed. Their model predicted that the porous solids reshaped themselves under loading circumstances and this deformation altered the properties of the porous material within the prescribed domain without effecting the other (specimen separated by an interface). They concluded that the inertial forces have maximum effects in the early stage of the infiltration and gradually settled by the elasticity of the solid matrix with the passage of time.

Farina *et al.* [74] have formulated the composite manufacturing of the porous materials on the basis of infiltration processes along with the qualitative results. In this study, the resin moulding and structural resin injection moulding have been discussed. In these processes liquid injected into a porous material consist of fiber reinforced elements. They studied the rheological behavior of the fluid along with the mechanical properties of porous solid that deform during the process of infiltration.

Billi *et al.* [75] have developed different models that help in improving certain industrial processes used in the manufacturing of composite materials. In the derivation of governing dynamics, they assumed unidirectional infiltration through a deformable porous material. They used a set of Lagrangian coordinates fixed on the solid matrix while formulating governing dynamics. This particular consideration helps in changing the dynamics of the problem from moving domain problem to a fix domain problem. This assumption used in simplifying the problem from modeling point of view. In fact, in Eulerian coordinates, such a problem is treated as free boundary value problem characterized by two time-dependent interfaces. By using fixed coordinates system, they are able to obtained a nonlinear Stefan type governing equation for a considered geometry.

Later on, Mesin and coworker [76] have formulated the dynamics of fluid flow and solid deformation. This study helps in understanding the industrial production of a composite material that is based upon the injection moulding technique. They have proved that the inertia having typically sufficient effects during early time fluid flow through the elastic porous solid. On the other hand, model predicted that some ideal assumptions used for energy associated with the system help in estimating the time required for the dissipation of vibrational motion. Motivated from these theoretical studies (reported above), the multiphasic deformation during passage of fluid through a soft tissue [77] and a deformable porous shell [78] have been derived and discussed in different Chapters in this thesis.

The continuum mixture theory is used to elaborate the constitutive motion of the components of the mixture, here these components are the deformable porous solids like a tissue or shell and fluid. Furthermore, due to the availability of different grade fluids, it seems quite interesting to formulate the behavior of non-Newtonian fluid flow through the deformable porous materials and explore their consequences on the solid matrix deformation. The main interest behind this particular area is due to the natural occurrence of varsities of non-Newtonian fluids along with their numerous practical applications, like, injection of cement in soil, infiltration of organic matter in tissues, blood flow through confined arteries, and industrial preparation different products, etc. Furthermore, one of the important

applications from an industrial point of view is the oil recovery (EOP) in petroleum engineering in which a large variety of the non-Newtonian fluids exist (jel, foam, polymers, etc). It is important to mention here that the non-Newtonian fluids exhibit nonlinear behavior that was not reported in the case of Newtonian fluids. In fact, it is important to derive the consequences of non-Newtonian fluids on the solid deformation, particularly, when these fluids flows through the elastic porous materials. The Darcy's law has been used in formulating the fluid fluxes through the deformable porous solids [79], however, the complex coupling between the high speed fluid flows and solid materials are not modeled on the basis of this law [80]. Therefore, by considering a moderate speed fluid flow dynamics, we have formulated the passage of non-Newtonian fluid flow through a deformable porous shell in Chapter 5. On the other hand, another interesting fluid-solid interaction has been reported during passage of electrically conducting fluids through the deformable porous materials [81, 82], in the presences of Lorentz forces. In this dissertation, two Chapters have been devoted to this particular area for both biological and non-biological settings.

In the following, a layout is given that summarizes the relevant details of work presented in this thesis. Different problems have been discussed in different Chapters along with the results and discussions.

1.3   Thesis Outline

The continuum mixture theory modeling approach has been used in formulating the governing dynamics of different problems reported in this dissertation. Foundation of this remarkable theoretical framework is based on the study of Atkin and Carine [10] and Bowen [11], however, recent developments have been discussed in [12]. In this thesis, the governing dynamic of fluid flow through a deformable porous shell has been derived and a strain-dependent permeability model for the passage fluid through the cartilage tissues is formulated. The mathematical formulations presented in this thesis are based upon the mixture theory modeling

used in [50] and [83] for a deformable porous shell and cartilage tissues, respectively. From the solution point of view, the governing system of equation derived in different Chapters have been solved using numerical scheme method of lines (MOL), whereas, exact solutions are also computed in some special cases. In the following, a short summary of work presented in different Chapters is given.

In Chapter-2, relevant detail of the mixture theory has been summarized that helps in developing the governing dynamics in different Chapters or Sections. This is followed by basic definitions and terminologies about the fluids, porous solids, soft biological tissues, partial differential equations, and numerical scheme method of line. These preliminaries help while developing the mathematical models as well as their numerical simulation.

In Chapter-3, the dynamics of electrically conducting fluid flow through the articular cartilage using mixture theory has been formulated. In order to derive nonlinear interaction between the fluid and solid, strain-dependent permeability is incorporated in the basic constitutive equations of the binary mixture theory approach. The governing system of time dependent diffusion equations is developed for the solid deformation and fluid pressure. An exact solution of the governing system of equations is calculated for the constant permeability along with a numerical solution of permeability dependent flow. Graphical results have been used in describing the effects of exposed magnetic field on the tissue deformation and local fluid pressure. This work is published in "Computer Methods in Biomechanics and Biomedical Engineering" [77], vol (23), pp. 524-535, 2020.

Chapter-4 contains the necessary and relevant detail of mathematical model derived for the exposed magnetic field effects on the mixture of charged fluid and deformable porous shell. The governing nonlinear system of equations is developed for the solid displacement and porosity of the shell. The integral boundary conditions are outlined on both the extremities in the form of unknown function. The numerical solution of the governing system of equations is computed for two different inner radii of the shell for a time dependent problem along with an exact solution for steady state case. A comparison of fluid flow through the radial and

planar geometries is also presented in the form of graphical outcomes. This work is published in "Computer and Mathematics with Application" [78], vol (80), pp. 1104-1116, 2020.

In Chapter-5, the derivation of radial flow of non-Newtonian fluids through a deformable porous shell has been given. The governing system of equations is derived for the porosity along with an integral equation containing solid deformation using power-law. In case of time dependent problem, numerical solution is computed using the method of lines, whereas, an exact solution is provided for the steady state problem. Revision of this work has been submitted in "International journal of engineering sciences" in December 2019.

In Chapter-6, concluding remarks have been given that is followed by Appendices that contain necessary details of an exact solution of the governing equation for constant permeability reported in Chapter three and numerical algorithms used in solving governing equations reported in Chapters 3, 4 and 5. At the end, the bibliography is furnished that help during the research work presented in this dissertation.

Chapter 2

Preliminaries

In this Chapter, the main focus was on the basic definitions and terminology that will help in the coming Chapters or sections for both modeling and solution point of view.. This includes definition of the fluid, porous materials, mixture theory modeling, magnetohydrodynamics (MHD) formulation, power-law formulation, and numerical scheme "method of lines" (MOL).

2.1 Introduction

It is well established engineering as well as biological practice that elastic porous solids under loading circumstances cannot attain instantaneous deflection but gradually settled to manage the applied stress. The balancing of applied compression results in the solid matrix deformation. These types of deformation processes are important, particularly, in the sand and clay saturation phenomenons, while draining of fluids. The dynamics involve in the settlement is the continuous adaption of the loading effects that causes solid deformation in these materials. This basic phenomenon of deformation is known as soil consolidation.

Early studies of fluid flow through the porous materials were based on the phenomenon of soil consolidation. These types of processes are closely link with the squeezing of fluid, particularly, flow of water through the deformable porous solids.

The pioneer work in this area is due to the study of Biot [84–86]. In 1941, he developed a general theory of three-dimensional consolidation. This study opened a new era for researcher to model and understand the lubrication processes occurs in the porous materials, both in the biological and non-biological settings. Before advance to the modeling of these types of phenomenons, it is important to go through the basic terminology related to the fluids.

2.2 Fluids Flow

Fluid is a state of matter that reshape itself to adopt the shape of confined geometry. On the other hand, description of the fluid flow or more precisely liquid flow required to specify the velocity vector. The average kinetic energy associates with any fluid, in fact, is due to the velocity with which fluid flow through any medium. So, this is the basic requirement to specify the velocity of the fluid at each and every instant within the given domain of fluid flow. The velocity vectors generally denoted by $\boldsymbol{u}$ or $\boldsymbol{v}$ and quantitatively define as "the rate of change of displacement or space with respect to the time". A fluid flow is said to be study, if and only if, the velocity $\boldsymbol{u}$ is independent of the time, i.e., $\partial u/\partial t = 0$, at any time t, otherwise, the flow is said to be unsteady. The flow behavior dependents upon different factors, like, applied pressure, dimension of the plane through which fluid flow occurs, and the nature of the fluid as well. In general fluids are divided into two main categories, Newtonian, and non-Newtonian.

The class of fluids which obey the Newton's law are known as Newtonian and that do not obey the law are known as non-Newtonian fluids. This law plays a very important role in modeling the behavior of fluids when they flow in contact with different types of solids. According to this law, the applied shear stress is directly proportional to the rate of deformation, mathematically it can be written as

$$\tau = \mu \left(\frac{du}{dy} \right), \tag{2.1}$$

where τ corresponds to shear stress, μ is viscosity, and du/dy is the rate of deformation. For the case of non-Newtonian fluids

$$\tau = \mu \left(\frac{du}{dy} \right)^n .$$ (2.2)

The exponent n in the equation (2.2) is generally used to differentiate between Newtonian and non-Newtonian fluids. In case of Newtonian fluids $n = 1$, otherwise a fluid is considered as non-Newtonian. The main interest in this thesis was in modeling the fluid flow through the porous materials, when fluid is of non-Newtonian in nature, i.e., $n < 1$ or $n > 1$. When a fluid passes through elastic porous solids, forces associated with the flow result in solid matrix deformation. During this process, both the porosity and permeability of the material change, hence, effects the passage of fluid. Moreover, a nonlinear coupling has been established between the fluid and solid deformation that depends upon the nature of porous solid as well as fluid. In the following, a detail describing the porous materials is given.

2.3   Porous Materials

A porous material is a type of solid that has empty spaces (pores) within the solid matrix. These pores often filled with liquids, if not, gases phase. The skeletal portion of the solid is called the "matrix" or "frame". There are numerous engineering applications of these materials, e.g., ground water hydrology, reservoir engineering, filtration process in industries, and fluid flow through the soft biological tissues, etc. These materials based upon their structure and inner molecular fixation (arrangement) are divided into rigid and deformable porous materials.

2.3.1   Rigid Porous Materials

Rigid porous solid remain in contact under loading circumstances unless their threshold elastic limit do not reach. These materials bear a specific limit value

of the applied normal or shear stress that vary from one type of material to the other. This specific behavior of the rigid porous solids depends upon their inter-molecular fixation. Fluid infiltration through these materials depend upon the capillaries action along with energy associated with the flows and kind of loading act on them. These materials have numerous application in engineering, like, absorption of mineral and food transports in plants, fluid flows occur through rocks, and bone-interface interaction with soft tissues in animals body structure, etc.

2.3.2   Deformable Porous Materials

Deformable porous solids is the class of porous materials that reshape themselves in balancing the applied stress. When fluid fluxes through these materials, kinematics associated with the flow produces solid deformation that effects the infiltration as well as discharging of fluid through these materials. This phenomenon produces a complex interconnection between the fluid and porous solid. The main responsible components of the multiphasic deformation are the porosity and permeability of the materials.

2.3.3   Porosity

Porosity corresponds to the void or empty spaces present in a porous solid. On the other hand, word porosity particularly used for the rocks, in the engineering terminology, and it can be defined as "ratio of the pore volume of bulk to the pore volume of rock simple". Mathematically, it can be written as

$$\phi = \frac{V_p}{V_b},\tag{2.3}$$

where ϕ is porosity, V_p and V_b are the pore and bulk volume, respectively.

Figure 2.1 shows microscopic view of different types of deformable porous solids. Particularly, empty spaces represented by tiny black holes correspond to the porosity of the porous solids. These pores allow the fluid to pass through the porous materials, however, porosity of the materials depends upon the inner fixation between the molecules of the porous solids as well.
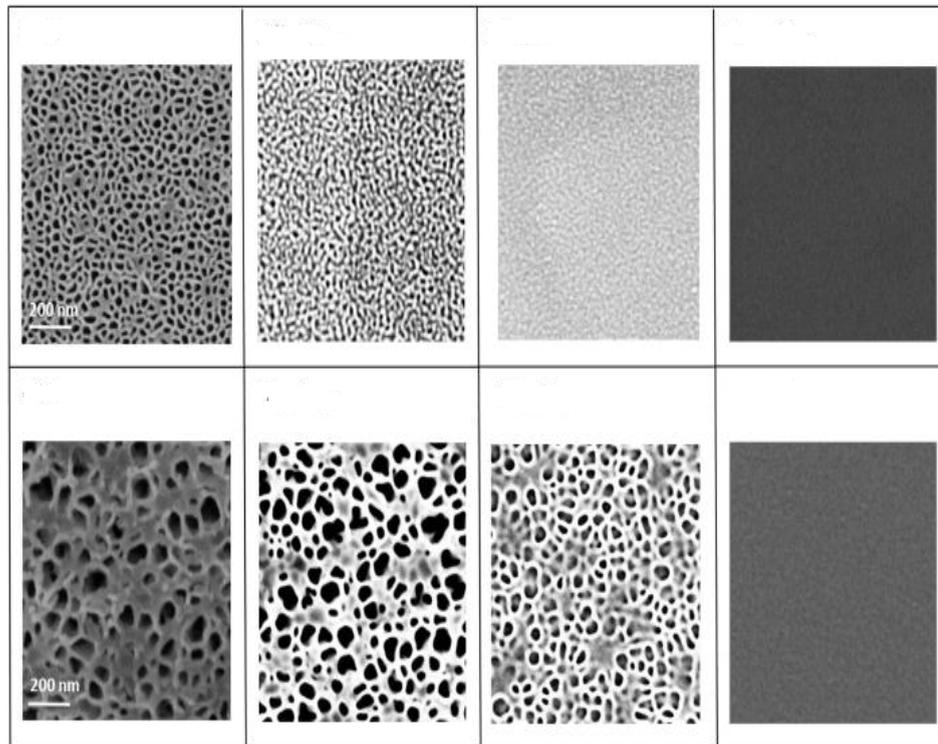
FIGURE 2.1: Microscopic view of different types of the porous materials, for detail see [87].

The porosity is a dimensionless quantity, and it is generally expressed in decimals or percentage. In general, porosity of the material changes when fluid flows occurs through a porous solid due to the repulsion of gas or air phases present in the pores.

In case of dry substrate, these empty spaces are filled with a gas or more precisely air, in equilibrium situation. During the process of infiltration, these gaseous media resist for the passage of fluid which in turn changes the capability of fluid to pass through the porous material, in fact, changing in the permeability of the porous material take place in this process.

2.3.4 Permeability

It is well established fact that properties of an elastic porous medium change in accordance with the deformation of the solid matrix. Particularly, porosity of the deformable porous solid decreases in compression. The mathematical relationship between the permeability and strain is then required for deriving the governing equations for an accurate governing model [88]. This was the first study that described relationship between the porosity and strain. The permeability of a porous material plays an important role while passing of fluids through rigid as well as deformable porous materials. This can be define as "the ability of a porous solid to allow the fluid to pass". On the other hand, permeability of the porous solids is link directly with the porosity, however, permeability also depends upon the shapes of pores present in the solid matrix. In system international of units, permeability is measured in m^2, most appropriate measuring scale used in measuring permeability is Darcy (d) or milli-Darcy (md). Mathematically, permeability can be expressed as follows

$$k = v\frac{\mu\Delta x}{\Delta P},\tag{2.4}$$

where v is the velocity, k is the permeability, Δx is thickness of the porous solid, μ viscosity, and ΔP is the applied compression (applied pressure). A quantitative relation between the driving pressure, permeability of the porous solid, and fluid flow is given by Darcy.

2.4 Darcy Law

In 1856, Henry Darcy was the first scientist to explore the flow of fluid through the porous solids. Particulary, Darcy formulated the amount of sand required for filtration of given flow, specially, water flow. On the basis of experiments, he derived a relationship between the fluid flow and applied pressure.

The Darcy's law states that "fluid flux through the porous solids is directly proportional to the pressure gradient imposed on initially saturated porous solid".

It is worth mentioning; this proportionality relation between the fluid flow and pressure is only valid for the low-speed flow dynamics for both liquids and gases phases. This law can be used in describing the fluid flow behavior through the elastic porous materials in the form of a single parametric equation. Foundation of this mathematical description is based upon the experimental finding of water flow through the bed of sand. This law plays an important role in understanding ground water hydrology that opens new ways of understanding the different governing dynamics in Earth sciences (geophysics). In the absence of gravity, Darcy's law is redefined by Morris which state that there exists a proportional relationship between the fluid flow, pressure difference, and viscosity of the fluid. Mathematically it can be written as

$$Q = -\frac{Ak(p_2 - p_1)}{\mu L},\tag{2.5}$$

where Q is total discharge of fluid, A is the cross-sectional area, k corresponds to the permeability, $p_2 - p_1$ pressure difference or pressure drop, μ dynamical viscosity of the fluid, and L is the length of porous solid. Negative sign in equation (2.5) indicates that the fluid flow directed from high to low pressure, i.e., in direction of decreasing potential. After some mathematical manipulation and using general notation, equation (2.5) can be written as

$$q = -\frac{k}{\mu}\nabla P,\tag{2.6}$$

where q is the fluid flux, and ∇P correspond to the pressure gradient. Darcy's law provided the basis for modeling different kinds of flow through porous materials. Furthermore, lots of modifications have been made to this law to include high speed flow behavior through the deformable materials. For the validation of this law, slow rate of deformation of mixture constituents has been considered in deriving the governing dynamics of different problems reported in this thesis. In this dissertation, this law has been used for incorporating different factors, like magnetohydrodynamics (MHD) and power-law, in the governing dynamics of different problems reported in coming Chapters.

2.5 Magnetohydrodynamics

Magneto-hydrodynamics deals with the forces interaction between the applied and induced magnetic fields. It is well established fact that an electric field setup around a stationary charge, whereas, a moving charge is surrounded with both electric and magnetic fields. Matter under high temperature and pressure consist in ionic form, generally known as plasma. When these charges moves, they have ability to generate an induced magnetic field those magnitude depends upon the strength of the charges as well as velocities with which they move. It is worth mentioning; most part of the universe exist in plasma state, however, inner core of our Earth also exhibit plasmic nature. The mobile charges in the inner core of the Earth establish a strong magnetic field around the Earth that control the atmospheric conditions around the globe. On the other hand, one of the important biological application of these MHD processes is to study the effects of exposed magnetic field on the moving charges in animals body structure. In fact, this particular physical phenomenon have great importance and need to pay attention. The mathematical formulations used in deriving the consequences of magnetic fields on moving charges were first discussed by Swedish mathematician and physicist H. Alfvsen, in 1942. Furthermore, in the derivation MHD process that involve in the fluid flow dynamics, the Maxwell equations are manipulated with the Navier-Stokes equation. These types of studies having grate importance both in engineering and biological sciences.

2.6 Tissue Engineering

In biological science, living organisms are mainly divided into two main categories, i.e., animals and plants. In both these classes, the building block of the body is cell that combine together in forming the body structure. Based upon the organic mixture composition and functioning of the different parts of the body, these cells are divided into soft and rigid bony interface.

It is well established fact that every cell of the living organism enrich with the fluids and it has been estimated that almost 70 percent of cell weight consist in the fluid form, particularly, in water form. This composition of the cell or more precisely tissues convince us to derived the dynamics of fluid-solid interaction, specially, for soft tissues where kinematics associated with the fluid flows having sufficient effects on the tissues deformation. This particular area belong to the tissue engineering in which a combination of cells, engineering, materials methods, and suitable biochemical factors have been discussed.

Figure 4.1 shows a verity of different types of soft biological tissues under the microscope. These tissues are responsible of performing different kinds of activities in the animals body structure. In the case of soft tissues, visco-elastic behavior has been reported in loading circumstances, however, this deformation phenomenon is also observed in some kinds of rigid tissues as well. This characteristic of the elastic as well as stiff tissues legitimate the importance of mathematical and physical description of these tissues for the better understanding of their functioning and composition. On the other hand, the rate of deformation and inertial fluid flow through different tissues having numerous applications both in the medical and clinical point of views.
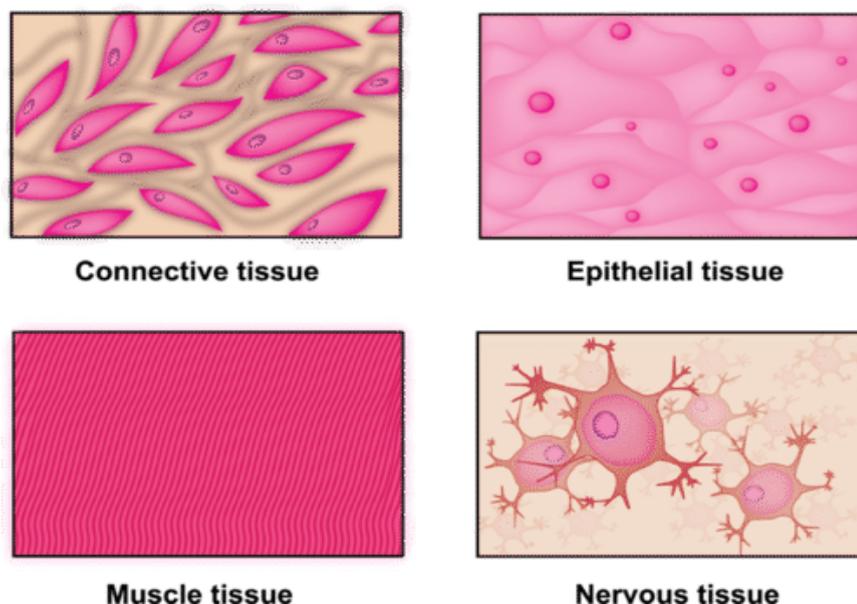
FIGURE 2.2: Microscopic view of different types of soft biological tissues [89]

In elastic tissues, a multiphasic deformation phenomenon has been reported while passing of fluids. There are different theoretical studies that have been used in modeling these types of multiphasic deformation phenomenons. In the beginning of introductory, a proactive discussion of different theory [13] is given that are successfully employed in deriving these types of problems. Particularly, the continuum mixture theory has been used in modeling the visco-elastic behavior of articular cartilage, in the presence of Lorentz forces, in Chapter 3. In following two sections, some basic terminology related to the tissues is given.

2.6.1 Stress Relation Behavior of Tissues

In soft tissues, stress relation is considered as a function of the local strain. In most of the cases, stress is assumed linearly related to the strain while driving the fluid flows through the soft biological tissues. This is known as infinitesimal deformation theory more precisely linear deformation theory. Particularly, the stress tensor for the solid matrix can be written as follows

$$\sigma^s = \lambda e \boldsymbol{I} + 2\mu \boldsymbol{e}, \tag{2.7}$$

where λ, μ are Lame constant, and $e = trace(\boldsymbol{e})$ that can be found as follows

$$\boldsymbol{e} = \frac{1}{2}(\nabla u + (\nabla u)^T). \tag{2.8}$$

2.6.2 Visco-elastic Behavior of Soft Tissues

Visco-elasticity is a property that is associated with many types of biological tissues, particularly, for soft tissues. In this thesis, viscoelastic behavior has been considered in modeling the governing dynamics of fluid flow through a soft biological tissue. Moreover, stress relaxation in tissue is a process where a constant displacement is imposed on the solid matrix that requires a force to hold this displacement. In the case of constant force acting on the medium, tissue creeps

towards the equilibrium displacement by balancing the loading effects. A classical methods used in describing these types of phenomena can be written in the form of following integral

$$T(t) = \int_{-\infty}^{t} G(t - \tau)T(\tau)d\tau, \tag{2.9}$$

where $G(t)$ corresponds to the normalized reduced relaxation function, $T(t)$ is the elastic response, and $T(\tau)$ is continuous stretch. The poro-elastic theory has proved the viscoelastic behavior of the tissues is due to the interaction of the fluid and the solid matrix. In the mixture theory, these types of phenomenons are well explained using the finite time for the passage of fluid within the tissue. On the other hand, when displacement is imposed on the boundary, it causes fluid squeezed out from the tissues by compressing elastic porous media of the tissues. This results in a large stress and reduces the passage of fluid through the tissue while balancing the applied stress.

2.6.3 Creep

Creep is a process in which a coupled stress relaxation behavior of the soft tissues is observed. When a constant stress is imposed to a system (solid matrix), then the surface displacement gradually creeps towards the equilibrium. This particular behavior is due to the fluid motion that drainage through the porous boundary.

2.7 Continuum Mixture Theory

The continuum mixture theory states that "individual components of the mixture are manipulated in such a way that every component of the mixture occupies each and every point within the mixture". This theory has been used in formulating the governing dynamics, when there exists relative motion between different phases of mixture and resistive forces having sufficient effects during deformation. These resistive forces play an important role both on the motion of the fluid and solid deformation. In the literature, mixture theory successfully employed in addressing

the problems of fluid fluxes through biological [13–15] and non-biological [47, 50, 64, 65, 72] settings.

In this thesis, the binary mixture theory has been used in modeling the squeezing phenomenon produced in an elastic porous shell as well as visco-elastic behavior of cartilage tissues during the passage of fluid in the presence of different physical parameters. In general, the power-law model has been developed for the elastic porous shell, whereas, MHD effects have been derived for both an elastic porous shell and a soft biological tissue. In fact, the constitutive theory for the mixture has been presented for the fluid and porous solid. In literature, continuum mixture theory model has been developed for fluids, suspensions, porous solids enriched with fluids, and composite solids as well. In this thesis, the main focused was on the mixture theory formulation related to the porous solid and viscous fluids only.

In deriving basic mixture theory model, assumed a continuum mixture having N different components that are individually incompressible and each component of the mixture having its on identity within the mixture.

The relative motion of constituents is specify by a following smooth function

$$\chi = \chi^\alpha(\boldsymbol{X}^\alpha, t), \tag{2.10}$$

where $\alpha = 1, 2, 3, \cdots, N$, and $\boldsymbol{X}^\alpha$ denote position with respect to some reference configuration.

In the following, we defined an inverse function for χ^α

$$\boldsymbol{\chi}^\alpha = \xi^\alpha(x, t). \tag{2.11}$$

Now, the mass density ρ, for the mixture as whole can be written as

$$\rho = \sum \rho^\alpha, \tag{2.12}$$

where ρ^α corresponds to the density of αth component of the mixture.

The volume fraction ϕ^α, for the αth can be expressed as

$$\phi^\alpha = \frac{\rho^\alpha}{\rho_R^\alpha}, \tag{2.13}$$

where ρ_R^α is used for the density of αth constituent in a homogeneous state.

In the case of saturated configuration, volume fraction can be written as

$$\sum \phi^\alpha = 1. \tag{2.14}$$

The velocity profile $\boldsymbol{v}^\alpha$ and deformation gradient $\boldsymbol{F}^\alpha$ are related to each other by a following relation

$$\boldsymbol{v}^\alpha = \frac{\partial}{\partial t}\boldsymbol{\chi}(\boldsymbol{X}, t), \quad \boldsymbol{F}^\alpha = \nabla\chi^\alpha(\boldsymbol{X}^\alpha, t). \tag{2.15}$$

In equation(2.15), operator ∇ corresponds to gradient with respect to the spatial position. For a homogeneous mixture, we have

$$\boldsymbol{v} = \frac{1}{\rho}\sum \rho^\alpha \boldsymbol{v}^\alpha, \quad \boldsymbol{u}^\alpha = \boldsymbol{v}^\alpha - \boldsymbol{v}, \tag{2.16}$$

where $\boldsymbol{v}$ and $\boldsymbol{u}^\alpha$ represent mean and diffusion velocities, respectively. The total derivative with respect to time can be written as

$$\frac{D^\alpha(\cdot)}{Dt} = \frac{\partial(\cdot)}{\partial t} + ((\boldsymbol{v}^\alpha \cdot \nabla)(\cdot)). \tag{2.17}$$

In the following, we gave the basic law of mass conservation for the mixture

$$\frac{\partial \rho^\alpha}{\partial t} + \nabla \cdot (\rho^\alpha \boldsymbol{v}^\alpha) = \rho^\alpha \phi^\alpha. \tag{2.18}$$

The conservation of linear momentum for the mixture can be written as

$$\frac{\partial}{\partial t}(\rho^\alpha \boldsymbol{v}^\alpha) + \nabla \cdot (\rho^\alpha \boldsymbol{v}^\alpha \otimes \boldsymbol{v}^\alpha) = \nabla \cdot \boldsymbol{T}^\alpha + \rho^\alpha \boldsymbol{b}^\alpha + \boldsymbol{\pi}^\alpha + \rho^\alpha \phi^\alpha \boldsymbol{v}^\alpha \tag{2.19}$$

where $\rho^\alpha \phi^\alpha$ corresponds to the mass flow rate, $\boldsymbol{T}$ the stress tensor, $\boldsymbol{\pi}^\alpha$ interaction

forces, and $\rho^\alpha \boldsymbol{b}^\alpha$ body forces for the αth components of a continuum mixture. Particularly, for the case of binary mixture, $\alpha = 1, 2$ that represent two phases, i.e., liquid and solid. It is worth mentioning; mixture theory is employed with following general assumptions in developing different models in coming Chapters

1. The mixture constituents are considered immiscible, however, they formed homogeneous mixture when mixed together.

2. For a closed system conservation of mass always hold, i.e., neither mass growth nor resorption exist.

3. The mixture constituents considered non reacting, i.e, constituents are chemically stable.

4. The solid matrix was assumed in fully saturated conditions, i.e. whole available space is occupied by every constituents of the mixture.

5. Governing dynamics are depend loading conditions, inertial terms are ignored due to their small contributions.

6. Mixture constituents were considered intrinsically incompressible, and isothermal.

7. There exist no external body forces, i.e., gravity.

In following two section, details of the mixture theory formulation for the derivation of power-law and MHD are given.

2.7.1   Power-law Formulations

The continuum mixture theory has been used in formulating the power-law model. Most of the equations were originated directly from the basic constitutive equations of mixture theory with suitable modification for the problem of our interest.

The conservation of mass for α phase can be written as

$$\frac{\partial \phi^\alpha}{\partial t} + \nabla \cdot (\phi^\alpha \mathbf{v}^\alpha) = \mathbf{0}, \tag{2.20}$$

where $\alpha = s, f$ correspond to solid and fluid phases respectively, v^α is the velocity, and ϕ^α is volume fraction.

A general form of the momentum balance for the mixture can be written as

$$\rho^\alpha \left(\frac{\partial \boldsymbol{v}^\alpha}{\partial t} + (\boldsymbol{v}^\alpha \cdot \nabla) \boldsymbol{v}^\alpha) \right) = \nabla \cdot \boldsymbol{T}^\alpha + \rho^\alpha \mathbf{b}^\alpha + \boldsymbol{\pi}^\alpha, \tag{2.21}$$

where $\mathbf{T}$ is the stress tensor, $\boldsymbol{\pi}$ corresponds to the drag forces, and $\boldsymbol{b}^\alpha$ represent body forces. Following forms of the stress tensor were considered

$$\mathbf{T}^\alpha = -\phi^\alpha pI + \boldsymbol{\sigma}^\alpha, \tag{2.22}$$

and

$$\boldsymbol{\pi}^s = -\boldsymbol{\pi}^f = K(\mathbf{v}^s - \mathbf{v}^f)^n - p\nabla\phi^s, \tag{2.23}$$

where n corresponds to the power law index, $\boldsymbol{\sigma}^\alpha$ represents the stress of mixture, K is the drag coefficient, and p is the fluid pressure. The components of stress tensor for the radial and angular direction can be written as

$$\sigma_{rr} = (\lambda + 2\mu)\frac{\partial u}{\partial r} + \beta\lambda\frac{u}{r}, \tag{2.24}$$

and

$$\sigma_{\theta\theta} = (\lambda + 2\mu)\frac{u}{r} + \lambda\frac{\partial u}{\partial r} + (\beta - 1)\frac{u\lambda}{r}, \tag{2.25}$$

where λ and μ are Lame constants, and β correspond to the geometry.

2.7.2 MHD Formulations

In the derivation of MHD dynamics, we considered the binary mixture of an electrically conducting fluid and deformable porous solid. A continuous magnetic field

effects have been considered on the binary mixture of fluid and porous solid. The components of mixture are considered individually incompressible, homogeneous, non-dissipated, and an-isotropic.

Form modeling point of view, the conservation of mass for MHD having an identical equation as was (2.20), whereas, the momentum balance, in the presence of Lorentz forces can be written as

$$\rho^\alpha(\frac{\partial \boldsymbol{v}^\alpha}{\partial t} + (\boldsymbol{v}^\alpha \cdot \nabla)) = \nabla \cdot \boldsymbol{T}^\alpha + \rho^\alpha \boldsymbol{b}^\alpha + \boldsymbol{\pi}^\alpha + \boldsymbol{J} \times \boldsymbol{B}, \qquad (2.26)$$

where $\boldsymbol{J}$ and $\boldsymbol{B}$ are the current and magnetic flux density, respectively. In the following, we gave the mathematical forms of Maxwell's and Ohms laws. These equation have been used in simplifying the expression $\boldsymbol{J} \times \boldsymbol{B}$, later on

$$\nabla \times \boldsymbol{B} = \mu_c \boldsymbol{J}, \quad \nabla \cdot \boldsymbol{B} = \boldsymbol{0}, \quad \nabla \times \boldsymbol{E} = -\frac{\partial \boldsymbol{B}}{\partial t}, \quad \boldsymbol{J} = \sigma_0(\boldsymbol{E} + \boldsymbol{v}^\alpha \times \boldsymbol{B}), \quad (2.27)$$

where μ_c is the primitivity of free space, σ_0 corresponds to electric conductivity, and $\boldsymbol{E}$ is the electric field strength. The expression $\boldsymbol{J} \times \boldsymbol{B}$ corresponds to the contribution of Lorentz forces effects that can be simplify using relations defined in (2.27) as

$$\boldsymbol{J} \times \boldsymbol{B} = \sigma_0(\boldsymbol{E} + \boldsymbol{v}^\alpha \times \boldsymbol{B}) \times \boldsymbol{B}. \qquad (2.28)$$

It is wort mentioning that $\boldsymbol{B}$ corresponds to the total magnetic filed [90, 91] which is the actually sum of applied and induced magnetic fields ($\boldsymbol{B} = \boldsymbol{B}_0 + \boldsymbol{B}_1$). Furthermore, induced magnetic filed ($\boldsymbol{B}_1$) having negligible influence due to the low magnetic field Reynolds number approximation. In this setting, equation (2.28) can be written as

$$\boldsymbol{J} \times \boldsymbol{B} = \sigma_0(\boldsymbol{E} + \boldsymbol{v}^\alpha \times \boldsymbol{B}_0) \times \boldsymbol{B}_0. \qquad (2.29)$$

Using the rule of vector triple product, equation (2.29) can be written as

$$\boldsymbol{J} \times \boldsymbol{B} = \sigma_0(\boldsymbol{B}_0(\boldsymbol{v}^\alpha \cdot \boldsymbol{B}_0) - \boldsymbol{v}^\alpha(\boldsymbol{B}_0 \cdot \boldsymbol{B}_0)). \qquad (2.30)$$

As, magnetic field having maximum effects for perpendicular direction and zero for the parallel orientation. This fact leads to ignore the term $\boldsymbol{v}^\alpha \cdot \boldsymbol{B}_0$. This leaves the following form of the equation (2.30)

$$\boldsymbol{J} \times \boldsymbol{B} = -\sigma_0 B_0^2 \boldsymbol{v}^\alpha. \tag{2.31}$$

From equations (2.26) and (2.31), we get

$$\rho^\alpha \left(\frac{\partial \boldsymbol{v}^\alpha}{\partial t} + (\boldsymbol{v}^\alpha \cdot \nabla)\right) = \nabla \cdot \boldsymbol{T}^\alpha + \rho^\alpha \boldsymbol{b}^\alpha + \boldsymbol{\pi}^\alpha - \sigma_0 B_0^2 \boldsymbol{v}^\alpha. \tag{2.32}$$

Expression $-\sigma_0 B_0^2 \boldsymbol{v}^\alpha$ gives the magnetic fields (Lorentz) contribution in the governing dynamics.

It is wort mentioning here, equations for the stress tensor are identical to the equations (2.22) to (2.25) given for the power-law formulation. The only difference occurs in the constitutive equation (2.23) either the Newtonian or non-Newtonian fluid flow behavior has been used in the MHD dynamics.

2.8 Solution Technique and ODEs Solver

In general, any physical system is well described by three dimensional space and time that is known as space-time. These space and time coordinates are used in developing any mathematical model in the form of partial differential equations (PDEs). In computing the solution of resulting PDEs, different analytical as well as numerical methods have been reported in literature. In this thesis, we have used numerical scheme "method of lines (MOL)" and successfully solved the resulting partial differential equations (PDEs) reported in different Chapters. MOL required to convert the partial derivatives of spatial variables involved in the governing system of partial differential equations into system of ordinary differential equations using the finite difference. The resulting system of ODEs is than solved

using a well established MATLAB's ODE solver, like odes15, odes23, etc. In order to elaborate the implementation of MOL, we first introduce the some basic terminology about the partial differential equations for the convenience.

2.8.1 General Form of PDE System

The general form of a partial differential equation in the first order is of the following type

$$u_t = f(x, t, u, u_x, u_{xx}, ...),\tag{2.33}$$

where x is vector of spatial coordinates, i.e., planar or radial, u denotes the vectors for n-dependent variables (x), and f is a function. In general, u and f can be written as

$$u = (u_1, u_2, u_3, ...u_n)^T, \qquad f = (f_1, f_2, f_3, ...f_n)^T,\tag{2.34}$$

where T denotes the transpose. As, equation (2.33) is first order in variable t, so, it required just one initial condition of following type

$$u(x, t = 0) = u_0(x, u, u_x, u_{xx}, ...).\tag{2.35}$$

For the case of u, it required n-vectors as follows

$$u_0 = (u_{10}, u_{20}, ...u_{n0})^T.\tag{2.36}$$

In case of derivative function f, we defined boundary conditions (BCs) prior because BCs purely depend upon the highest derivatives involve in the governing PDE. Particularly, we considered that highest derivatives in variable x is of second order, then there are two BCs in solving the given PDE. In general, the BCs for equation (2.33) can be written as

$$f_b(x_b, u, u_x, u_{xx}, ...t) = 0.\tag{2.37}$$

Now, we have a complete system, i.e, a PDE along with associated initial and boundary conditions.

2.8.2 Implementation MOL

It is well established fact that PDEs problem come in infinity variety of modern science, engineering, biomedical applications, and industries manufacturing of different materials. On the other hand, geometric classification (parabolic, elliptic, hyperbolic), class of dependent and independent variables, and types of BCs (boundary conditions), it seen quite difficult to formulate a numerical scheme with any generality which address board spectrum of all PDEs problems. However, the numerical scheme MOL provides a surprising degree of generality, although the output depends upon the experience and inventiveness of analyst to new PDE problem. Now, the focused is toward formulation and implementation of MOL to a PDE problem. The main theme of MOL is to change spatial derivatives (partial derivatives) involve in PDE with algebraic approximation (forward difference, reverse difference, central difference etc). In order to understand the process of implementation of MOL, we consider following simple first order PDE

$$u_t + vu_x = 0. \tag{2.38}$$

Using forward difference, we get

$$u_x \approx \frac{u_i - u_{i-1}}{\Delta x}, \tag{2.39}$$

where i corresponds to an index ($i = 1$ for left end and $i = M$ for right end) along x, and Δx is the spacing between two consecutive mesh points. Now, equation (2.38) can be written as

$$\frac{du_i}{dt} = -v \frac{u_i - u_{i-1}}{\Delta x}, \qquad M \geq i \geq 1. \tag{2.40}$$

Equation (2.40) has only one independent variable that is t also it represents system of M ODEs. This system of ODEs is approximated form the given PDE. In order to solve this system, we need to complete the PDE problem by imposing one initial and one boundary condition of the following types

$$u(x, t = 0) = f(x), \qquad u(x = 0, t) = g(t). \tag{2.41}$$

As, equation (2.40) has M initial value ODEs, so, it required M initial conditions as

$$u(x_i, t = 0) = f(x_i), \qquad 1 \leq i \leq M. \tag{2.42}$$

The boundary condition at $i = 1$ can be written as

$$u(x_1, t) = g(t). \tag{2.43}$$

Now, equations (2.40), (2.42) and (2.43) are complete MOL approximation of equation given PDE, whereas, solution of ODE system is given as

$$u_1(t), u_2(t), u_3(t), ... u_{M-1}(t), u_M(t), \quad at \quad i = 1, 2, 3, ... M. \tag{2.44}$$

The error associated with such a solution depends upon the order of approximation generally known as truncation error. We used first order forward difference to approximate the spatial derivatives, however, for the case of $\Delta x \to 0$ leads to the exact derivatives of original partial differential equation. In practical application, Δx remain finite, so, given PDE remain approximated.

2.9   Example

In this section, we can solved the heat equation using the method of lines and compared this solution with an available exact solution. Heat equation is most widely studied in mathematics, and its analysis is considered as fundamental in the field of partial differential equations.

Numerous nonlinear variants of the heat equation were introduced in differential geometry by James Eells and Joseph Sampson in 1964, inspiring the introduction of the Ricci flow by Richard Hamilton in 1982. On the other hand, heat equation also paly an important role in many fields of science and applied mathematics. Particularly, researches interested in formulating the distribution of heat within the slab. This process is usually derived in the form of time varying ultimately reaches to a steady state. This phenomenon is represented by the parabolic partial differential equations along with appropriate boundary conditions on the extremities. Furthermore, linear and nonlinear parabolic partial differential equations have been discussed in literature.

In the present section, a comparison of analytical and numerical solutions for a parabolic partial differential equations is given. In the following, a general form of the parabolic type PDE is given

$$\frac{\partial u}{\partial t} = \hbar^2 \frac{\partial^2 u}{\partial x^2}, \quad t > 0, \quad 0 < x < 1. \tag{2.45}$$

Let $\hbar = 1$, for the case of simplicity, and equation (2.45) subjected to the following initial and boundaries conditions

$$u(x, 0) = 1, \quad u(0, t) = 0, \quad u(1, t) = 0. \tag{2.46}$$

In solving equation (2.45), consider the domain of spatial variable from 0 to 1.

An exact solution of the partial differential equation (2.45) using the boundary condition (2.46) can be written as follows

$$u(x, t) = \frac{4}{\pi} \sum_{n=0}^{\infty} \frac{1}{2n + 1} \sin[(2n + 1)\pi x] e^{-(2n+1)\pi^2 t}. \tag{2.47}$$

Now, discretizing equation (2.45) using the finite difference, we get

$$\frac{du_j}{dt} = \frac{u_{j+1} - 2u_j + u_{j-1}}{(\Delta x)^2}, \quad j = 1, 2, 3 \cdots, n, \tag{2.48}$$

where $\Delta x = \frac{1-0}{n}$, and $u_0 = 0 = u_n$ (contribution of left and right boundaries). An input of the initial condition can be written as

$$u(x_i, 0) = 1, \quad x_i = i\Delta x. \tag{2.49}$$

Now, we have a system of n ODEs given in equation (2.48) along with the initial condition expressed in equation (2.49). These equation can be solve using Matlab's ODE solver, like ode15, ode23s, etc. In the following, the graphical outcome gives the comparison between the exact and numerical solutions for $t = 0.1$

In Figure 2.3, an excellent agrement has been found between both the solutions, i.e., exact and numerical solutions. Moreover, this graphical result shows that method of lines (MOL) give good accuracy, particularly, in case of parabolic type partial differential equations. In this thesis, most of the governing equations derived in different Chapters are of parabolic types partial differential equations and solved numerically using method of lines.
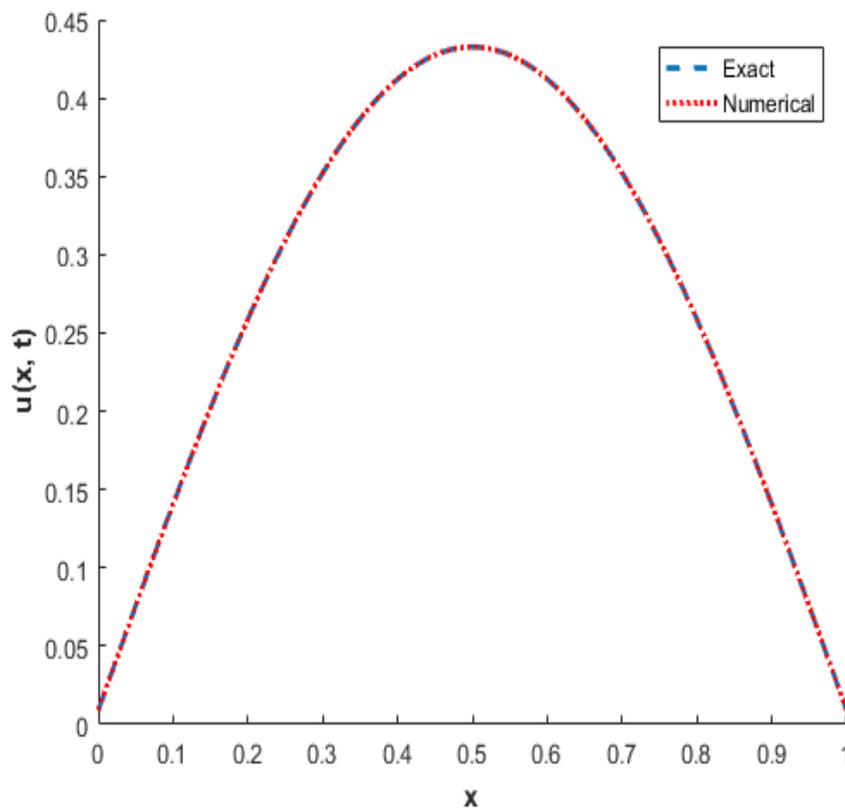
FIGURE 2.3: Comparison between the exact and numerical solutions.

It is worth mentioning that the convergence and stability of MOL also depends upon the order of approximation of partial derivatives involve in the governing equation. This approximation change from one type of PDE to the other as well as nature of governing equation, i.e., equation is linear or nonlinear.

Chapter 3

Visco-Elastic Behavior of Articular Cartilage Under Applied Magnetic Field and Strain-Dependent Permeability

3.1   Introduction

In this Chapter, the problem of fluid flow through an elastic tissue is derived using binary mixture theory approach. The governing dynamics involved in the motion of fluid and solid deformation are formulated for both constant as well as strain-dependent permeability of the solid matrix. A constant magnetic field effects have been incorporated in the governing equations while deriving influence of Lorentz forces on the tissues deformation. The fluid flow and solid deformation were assumed to be depend upon the loading imposed at the rigid bony interface of the cartilage tissues. We employed the continuum mixture theory approach and developed a mathematical model that described the contribution of MHD effects on a soft biological tissue.

The continuum mixture theory successfully used in deriving the problems of fluid-solid interaction during the passage of fluids through the deformable porous materials [19–21, 50, 64, 72, 73, 92]. Present Chapter based upon the research work published in [66] that was the only available model in literature developed for the investigation of MHD effects on a soft tissue using mixture theory approach. However, there are several paper reported in literature that described the derivation of MHD effects based upon the mixture theory during passage of electrically conducting fluids through the deformable porous solids [64, 65, 78].

In formulating the kinematics of the problem, components of the mixture were assumed individually incompressible, homogeneous within the solid matrix, and isotropic. We have derived the governing system of partial differential equations for the solid deformation and local fluid pressure, in the presence of Lorentz forces. The numerical solution is computed using the method of lines for the permeability dependent flow, whereas, an exact solution is provided by the eigenfunction expansion method for the case of constant permeability. The graphical results highlights the influence of magnetic parameter, normalized time, strain-dependent permeability, and dimensionless constant (R) on the fluid pressure and solid deformation. In the following, a summary of the present Chapter is given.

Section 3.2 contains the mathematical formulation, Section 3.3 described the solution methodology, Section 3.4 devoted for the result and discussion. At the end, Section 3.5 contains the concluding remarks.

3.2 Theory and Model

The intrinsic permeability was introduced in modeling multiphasic deformation of soft biological tissues while passage of fluids, in different loading conditions. The elasticity of soft tissues links the consequences of drag forces on the solid deformation hence change the permeability of the solid matrix [93]. Experimental studies have proved that the mechanical response of the cartilage tissues is extremely sensitive, even for a slow rate of compression. The dependence rate of sensation

related to the drag forces is very high; also, this factor plays an important role in modeling the mechanical behavior of cartilage and other types of soft biological tissues. This particular behavior of many types of deformable tissues makes it important to consider the effects of strain-dependent permeability while deriving the governing dynamics.

In the present study, the fluid flow through the tissues network was considered as permeability dependent, and following form of strain-dependent permeability relation has been assumed

$$k = k_0 e^{m\frac{\partial u}{\partial x}}, \tag{3.1}$$

where k_0 and m are the material constants, $\frac{\partial u}{\partial x}$ is the dilatation, and $u(x,t)$ corresponds to the solid displacement. It was assumed that cartilage tissues fixed to the interval $0 \leq x \leq h$, where $x = 0$ and $x = h$ correspond to the soft and rigid bony interfaces, respectively. Due to the symmetry, only non-zero components of the velocities are $\boldsymbol{v}^s = \boldsymbol{v}^s(x,t)$, $\boldsymbol{v}^f = \boldsymbol{v}^f(x,t)$, s and f represent solid and fluid phases, respectively.

Lai *et al.* [83] have found the permeability parameter of the elastic tissues experimentally. They passed Ringer solution through a soft tissue having thickness h. In this study, area A of the specimen was subjected to the pressure P_A imposed at the rigid bony interface of the soft tissues. They have found an apparent value of the permeability as $\frac{Q/A}{P_A/h}$, where, Q corresponds to the volume of fluid flux through the cartilage network. When fluid flow through the cartilage tissues, drag forces associated with the flow result in the solid matrix deformation. This phenomenon plays an important role both in the compactness of the porous solid as well as passage of the fluid. This multiphasic deformation limits the value of strain-dependent permeability to an average value, if not, an apparent value k_{app}. It is worth mentioning here; this apparent value of the permeability parameter links to the driving pressure ∇P [94] that is the main factor change the passage of fluid through the tissues. On the other hand, when k_{app} measured with various values of the clamping strains, it depends upon both applied pressure as well as clamping strain. These experimental justifications given in [95] convinces us to

use the equation (3.1) in the present study. The multiphasic nature of biological tissues limits in the use of single-phasic modeling approaches, even though these approaches have been reported (employed) in some special circumstances, i.e., after attaining equilibrium.
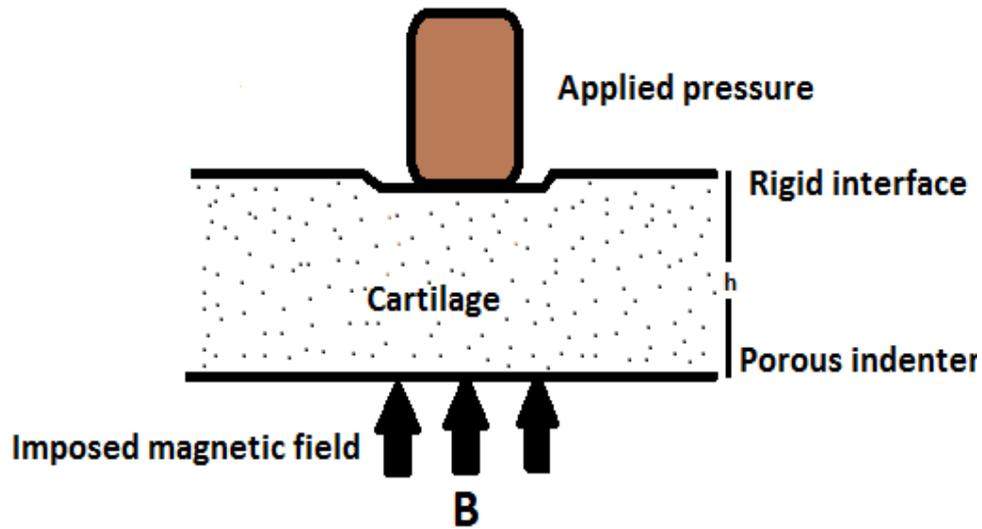
FIGURE 3.1: Geometry of the problem 1 has been given in Figure (3.1). A soft tissue (articular cartilage) in loading circumstances under applied magnetic field of strength B was considered for the analysis.

In the present study, we assumed the bio-rheological behavior of the soft and hydrated tissues that consist of deformable porous solid filled with fluids. The governing dynamics of such a problem deals with the idea of continuum mixture theory. The modeling technique we used in the present article has a relatively brief; however, details can be found in [11], and a compressive review also given in [96–99] as well. In these types of modeling, each constituent of the mixture manipulating in such a way that it occupies at every material positioning within the mixture . The kinematics involved in the derivation of governing dynamics depends upon the components of a mixture, here these components are solid matrix (cartilage body) and fluid phase. Moreover, we fallow a similar modeling approach reported in [83], with suitable modification for the problem of our interest.

We considered that the solid matrix (cartilage tissues) could only be squeezed into a special control volume, when an equal amount of the fluid fluxes in the opposite

direction. The motion of the constituents described using classical conservation laws of the mass and momentum balance. The volume fraction ϕ^α of each phase is defined by $\phi = \frac{V^\alpha}{V}$, other useful relations are $\phi^s + \phi^f = 1$, and $\rho^\alpha = \rho_T^\alpha \phi^\alpha$, where ρ_T^α is true density, ρ^α is density of mixture, and $\alpha = s, f$ used to represents different phases. Using the model of an incompressible binary mixture, conservation of mass can be written as

$$\nabla \cdot \boldsymbol{v}^f = -\xi \nabla \cdot \boldsymbol{v}^s, \tag{3.2}$$

where ξ is the ratio of volume fraction, i.e., $\xi = \frac{V^s}{V^f}$, for articular cartilage tissues $\xi \approx 0.2$ (for an adult joint). In modeling the governing dynamics, the quantitative relation between fluid and solid velocities that is given in equation (3.2) has been reported in numerous studies [58, 83], identical to the present study. The momentum balance for the mixture can be written as

$$\rho^\alpha \left(\frac{\partial \boldsymbol{v}^\alpha}{\partial t} + (\boldsymbol{v}^\alpha \cdot \nabla)\boldsymbol{v}^\alpha \right) = \nabla \cdot \boldsymbol{T}^\alpha + \rho^\alpha \boldsymbol{b}^\alpha + \boldsymbol{\pi}^\alpha + \boldsymbol{J} \times \boldsymbol{B}, \tag{3.3}$$

where $\boldsymbol{T}^\alpha$ is the stress tensor for α phase, $\boldsymbol{b}^\alpha$ represent body forces, $\boldsymbol{\pi}^\alpha$ is drag force between the mixture constituents ($\boldsymbol{\pi}^s + \boldsymbol{\pi}^f \approx 0$), $\boldsymbol{J}$ and $\boldsymbol{B}$ are the current density and applied magnetic field, respectively.

In the case of infinitesimal deformation along with small velocities, the effects of inertial forces become negligible [50]. Barry and coworker [100] considered the contributions of inertial forces, in the derivation of governing dynamics, and proved that these forces had been ignored, when $t_0 > k\rho_T$, where t_0 is the typical time, and k is the permeability. Using these assumptions help us to rewrite the equation (3.3), in the absence of body forces, for both the phases as follows

$$\nabla \cdot \boldsymbol{T}^s + \boldsymbol{\pi}^s + \boldsymbol{J} \times \boldsymbol{B} = \boldsymbol{0}, \tag{3.4}$$

and

$$\nabla \cdot \boldsymbol{T}^f + \boldsymbol{\pi}^f + \boldsymbol{J} \times \boldsymbol{B} = 0. \tag{3.5}$$

It is important to mention here, magnetic field $\boldsymbol{B}$ has maximum effects, when apply perpendicular to the moving charged fluid, and minimum for parallel orientation.

The diffusive resistant forces for the solid and fluid can be written as [66, 83]

$$-\boldsymbol{\pi}^s = \boldsymbol{\pi}^f = K(\boldsymbol{v}^s - \boldsymbol{v}^f), \tag{3.6}$$

where K corresponds to the drag coefficient of the resistance, which is related to the permeability by a relation $K = \frac{1}{(1+\alpha)^2 k}$ [50]. The linear momentum has been affected by the relative velocities of the mixture components, i.e., $\boldsymbol{v}^s - \boldsymbol{v}^f$. Lai and coauthors [101] have studied compressive stress relaxation behavior of soft tissues for transversely isotropic permeability. For the special case, all load carried by the elastic tissues, and binary problem changes to an elasticity problem. Furthermore, for a confined compression, equilibrium strain, as well as lateral expansion, all are controlled by the E_s and v_s [51, 56], where E_s and v_s are the elasticity and velocity of the solid matrix, respectively. In literature, different studies have been reported that used elasticity theory in modeling the behavior of soft tissues [102–104]. In 1678, Robert Hook formulated a quantitative relationship between the stress and strain [105]. In many physical situation, it has been assumed that an accurate governing model for solids, deformations and forces are small. Moreover, in the development of theory of elasticity proved that Hook's law say that strain directly related to the applied stress, whereas, the proportionality factor is not a single real number, but a tensor corresponds to the matrix consist of real numbers. This configuration of the matrix depends upon the solid material taken from seven classes of the crystals [106–108]. On the other hand, elastic solids divided into two classes, i.e., isotropic and anisotropic, in the present study, we considered that solid matrix of the tissues having isotropic nature. These types of solid having properties independent of the direction, whereas, an anisotropic material has property that depends upon direction due to their structure. In literature, many studies have used the isotropic materials [109, 110], for more detail [111–114]. It is well-established fact that visco-elastic behavior of soft tissues purely depends upon the fluid fluxes through the permeable porous solid matrix as well as type of loading condition imposed on it [60]. In the derivation governing dynamics of the present problem, we considered the biological tissues consisting of a porous material that is intrinsically elastic, isotropic, and filled with fluid. We considered

the following forms of stress relations for the solid and fluid phases

$$\boldsymbol{T}^s = -\xi p\boldsymbol{I} + \lambda_s e^s \boldsymbol{I} + 2\mu_s e^s + 2\mu_s \boldsymbol{e} + \dot{\lambda}_s div(\boldsymbol{v}^s)\boldsymbol{I} + 2\dot{\mu}_s \boldsymbol{D^s} - 2K_c\boldsymbol{\Gamma}, \qquad (3.7)$$

and

$$\boldsymbol{T}^f = -p\boldsymbol{I} + \lambda_f div(\boldsymbol{v}^f)\boldsymbol{I} + 2\mu_f \boldsymbol{D}^f + 2K_c\boldsymbol{\Gamma}, \qquad (3.8)$$

where $\boldsymbol{e}$ is the infinitesimal strain tensor, $e^s = trace(\boldsymbol{e})$, $\boldsymbol{D}^s$ is the deformation tensor, Γ is the spin tensor, p local pressure of the fluid, $\boldsymbol{I}$ is identity tensor, $\boldsymbol{D}^f$ is the rate of fluid deformation tensor, λ_s, μ_s are isotropic elastic moduli, $\dot{\lambda}_s$, $\dot{\mu}_s$ are visco-elastic moduli, λ_f, μ_f are bulk and dynamical viscosities of the fluid, and K_c is the diffusive interaction between mixture constituents.

The infinitesimal binary mixture theory described fluid-solid interaction using ten material constants, i.e., ξ, λ_s, μ_s, $\dot{\lambda}_s$, $\dot{\mu}_s$, λ_f, μ_f, K_c, r, K, where r is the contribution of capillary forces. It is difficult, either impossible, to access all these parameters at once both for modeling and solution point of views. Moreover, Mow *et al.* [14] developed a model using following assumptions

1. Solid and fluid phases are linearly elastic,

2. The permeability of the solid matrix is constant,

3. $K_c = 0$, $r = 0$,

4. ξ is constant.

They used the resulting linear equations successfully in addressing the problems of one-dimensional confined compression stress relaxation behavior of cartilage tissues, meniscus, and nasal septum, although these restrictions were quite severe. Using these assumptions, they find the permeability constant $10^{-15}\frac{m^4}{Ns}$ that made an excellent agreement with the available experimental data [94, 115]. On the other hand, Lia and coauthor [83] gave a detailed comparison between stress relaxation experiments with biphasic linear mixture theory findings. They had proved that

certain inconsistencies occurs when theory was generalized by including the non-linear strain-dependent permeability relationship given in equation (3.1). Thus in the present study, we have extended linear mixture theory by including non-linear permeability relation in the presence of magnetic fields, in the constitute equations of binary mixture. In the following, the Maxwell, and Ohm's law are given, which were used in simplifying the expression $\boldsymbol{J} \times \boldsymbol{B}$, later on

$$\nabla \times \mathbf{B} = \mu_c \mathbf{J}, \qquad \nabla \cdot \mathbf{B} = 0, \qquad \nabla \times \mathbf{E} = -\frac{\partial \mathbf{B}}{\partial t} \quad \boldsymbol{J} = \sigma_0(\boldsymbol{E} + \boldsymbol{v}^\alpha \times \boldsymbol{B}), \quad (3.9)$$

where μ_c correspond to the permittivity of the medium, $\mathbf{E}$ is the electric field intensity, and σ_0 is the electric conductivity of the charged fluid. The expression $\boldsymbol{J} \times \boldsymbol{B}$ can be written as

$$\mathbf{J} \times \mathbf{B} = \sigma_0(\mathbf{E} + \mathbf{v}^\alpha \times \mathbf{B}) \times \mathbf{B}, \qquad (3.10)$$

where $\mathbf{B} = \boldsymbol{B_0} + \boldsymbol{B_1}$, i.e., $\boldsymbol{B}$ is sum of the applied and induced magnetic fields. The contribution of induced magnetic field ($\boldsymbol{B_1}$) may be ignored due to the low magnetic field Reynold number approximation [66]. Thus, equation (3.10) for negligible induced magnetic and electric fields can be written as

$$\mathbf{J} \times \mathbf{B} = \sigma_0(\mathbf{v}^\alpha \times \mathbf{B}_0) \times \mathbf{B}_0. \qquad (3.11)$$

After some mathematical manipulation, we get

$$\mathbf{J} \times \mathbf{B} = \sigma_0 \left(\mathbf{B}_0(\mathbf{v}^\alpha \cdot \mathbf{B}_0) - \mathbf{v}^\alpha(\mathbf{B}_0 \cdot \mathbf{B}_0) \right). \qquad (3.12)$$

The term $\mathbf{v}^\alpha \cdot \mathbf{B}_0 \approx 0$ (magnetic field has negligible effects in parallel orientation to the fluid flux). This leaves the following form of the equation (3.12)

$$\mathbf{J} \times \mathbf{B} = -\sigma_0 B_0^2 \mathbf{v}^\alpha. \qquad (3.13)$$

We assumed that the solid and fluid deformations are along the x-direction. Now

what follows, the vector form of equations change into one-dimension form. Using the assumptions of linear binary mixture theory, and employing divergence operator to the equations (3.7) and (3.8), we get

$$\frac{\partial T^s}{\partial x} = -\xi p + H_a\left(\frac{\partial u}{\partial x}\right), \tag{3.14}$$

and

$$\frac{\partial T^f}{\partial x} = -p, \tag{3.15}$$

where $H_a = \lambda_s + 2\mu_s$. Inserting equations (3.6), (3.13), (3.14)-(3.15) into equations (3.4)-(3.5), we obtain

$$-\xi\frac{\partial p}{\partial x} + H_a\frac{\partial^2 u}{\partial x^2} - K(v^s - v^f) - \sigma_0 B_0^2 v^s = 0, \tag{3.16}$$

$$-\frac{\partial p}{\partial x} + K(v^s - v^f) - \sigma_0 B_0^2 v^f = 0. \tag{3.17}$$

From equation (3.2), we get
$$\frac{\partial v^f}{\partial x} = -\xi\frac{\partial v^s}{\partial x}. \tag{3.18}$$

The cartilage was divided into elastic as well as rigid, which correspond to the soft and bony interface, respectively. Integrating equation (3.18), and using condition $v^s = v^f = 0$ for cartilage rigid boundary interface (for adult joint) [83] , we get

$$v^f = -\xi v^s. \tag{3.19}$$

Equation (3.18), yields
$$v^f - v^s = -(1+\xi)\frac{\partial u}{\partial t}, \tag{3.20}$$

where $v^s = \frac{\partial u}{\partial t}$. From equations (3.20) and (3.16)-(3.17), we get

$$\frac{\partial u}{\partial t} = \left(\frac{H_a k_0 e^{m\frac{\partial u}{\partial x}}}{1 + M e^{m\frac{\partial u}{\partial x}}}\right)\frac{\partial^2 u}{\partial x^2}, \tag{3.21}$$

where $K = k^{-1}(1+\alpha)^{-2}$, and $M = k_0(1+\alpha^2)\sigma_0 B_0^2$ is the dimensionless magnetic parameter. Equation (3.21) is the governing nonlinear partial differential equation

for the solid deformation. The nonlinearity is due to the strain-dependent permeability. In the case of $m = 0$, equation (3.21) reduces to the linear form, the resulting linear equation used successfully in describing one-dimensional stress-relaxation behavior of soft tissue, even though this restriction is quite hard. For the case of constant permeability, it is not possible to elaborate on the exact nature of the problem. Therefor, it is important to consider the consequences of strain-dependent permeability that was changed in accordance with tissue deformation, in the presences of the magnetic parameter M. These two factors are the main features, which were considered in the foregoing section, and we reported their effects on both solid deformation and fluid pressure in the section results and discussion.

Now, we turn attention toward the fluid pressure p. For this, adding equations (3.16) and (3.17), we get

$$\frac{\partial p}{\partial x} = \left[\frac{H_a}{1 + \xi} - \frac{H_a M (1 - \xi) e^{m \frac{\partial u}{\partial x}}}{(1 + \xi)(1 + \xi^2)(1 + M e^{m \frac{\partial u}{\partial x}})} \right] \frac{\partial^2 u}{\partial x^2}. \tag{3.22}$$

Equation (3.22) is used in finding the fluid pressure only when solution of the solid deformation u is available. The nonlinear permeability k appeared both in the equations (3.21) and (3.22). However, it seems quite physical without altering the nature of the problem to handle the equation (3.22) for constant permeability, because strain-dependent permeability contribution comes through the calculated solution of u from equation (3.21) into (3.22). In this setting, equation (3.22) can be written as

$$\frac{\partial p}{\partial x} = \frac{H_a}{1 + \xi} \left[1 - \frac{(1 - \xi)M}{(1 + \xi^2)(1 + M)} \right] \frac{\partial^2 u}{\partial x^2}. \tag{3.23}$$

Integrating

$$p(x, t) = \frac{H_a}{1 + \xi} \left[1 - \frac{(1 - \xi)M}{(1 + \xi^2)(1 + M)} \right] \frac{\partial u}{\partial x} + g(t), \tag{3.24}$$

where $g(t)$ is the constant of integration, which can be found using the conditions $p(h, t) = 0$, at the rigid edge. This leaves the following form of equation (3.24)

$$p(x, t) = \frac{H_a}{1 + \xi} \left[1 - \frac{(1 - \xi)M}{(1 + \xi^2)(1 + M)} \right] \left[\frac{\partial u}{\partial x} - \frac{\partial u(h, t)}{\partial x} \right]. \tag{3.25}$$

Equations (3.25) is partial differential equation for the fluid pressure. In order to close the system, we associated following initial and boundary conditions

$$u(0, t) = \dot{P}t(H(t) - H(t - t_0)) + \dot{P}t_0 H(t - t_0), \tag{3.26}$$

$$u(x, t) = 0, \quad u(x, 0) = 0, \quad p(x, t) = 0, \quad at, \quad x = 0, h, \tag{3.27}$$

where $H(t)$ represents Heaviside function. It is important to mention here, our choice of left boundary condition potentially significant. For $0 \leq t \leq t_0$ corresponds to a stage of compression, whereas, $t > t_0$ represents the relaxation. The governing system of equations is converted into the dimensionless form using the following choices

$$\bar{u} = \frac{u}{h}, \quad \bar{h} = \frac{h}{h_0}, \quad \bar{x} = \frac{x}{h}, \quad \bar{t} = \frac{\dot{P}t}{h}, \quad \bar{p} = \frac{p}{H_a}. \tag{3.28}$$

These variables allow us to rewrite the governing system of equations as follows

$$\frac{\partial \bar{u}}{\partial \bar{t}} = R \left[\frac{e^{m\frac{\partial \bar{u}}{\partial \bar{x}}}}{1 + Me^{m\frac{\partial \bar{u}}{\partial \bar{x}}}} \right] \frac{\partial^2 \bar{u}}{\partial \bar{x}^2}, \tag{3.29}$$

$$\bar{p}(\bar{x}, \bar{t}) = \frac{1}{1 + \xi} \left[1 - \frac{(1 - \xi)M}{(1 + \xi^2)(1 + M)} \right] \left[\frac{\partial \bar{u}}{\partial \bar{x}} - \frac{\partial \bar{u}(\bar{h}, \bar{t})}{\partial \bar{x}} \right], \tag{3.30}$$

$$\bar{u}(0, \bar{t}) = \bar{t}(H(\bar{t}) - H(\bar{t} - \bar{t}_0)) + \bar{t}_0 H(\bar{t} - \bar{t}_0), \tag{3.31}$$

$$\bar{u}(1, \bar{t}) = 0, \quad \bar{u}(\bar{x}, 0) = 0, \quad \bar{p}(\bar{x}, \bar{t}) = 0, \quad at \quad x = 0, 1, \tag{3.32}$$

where $\bar{t}_0 = \frac{\dot{P}t_0}{h}$, and $R = \frac{H_a k_0}{\dot{P}h}$. In next section, we present solution methodology employed in solving governing system of equations. Now, we remove over bar from the variables in upcoming sections, because the governing system of equations are obviously in dimensionless form.

3.3   Solution Methodology

The solution of the governing system of the equations is divided into two groups, i.e., constant and strain-dependent permeability solutions. Particularly, an exact solution for constant permeability is calculated using the eigenfunction expansion that is followed by a numerical solution, in case of strain-dependent permeability flow. It is worth mentioning that while considering nonlinear strain-dependent permeability behavior in the governing partial differential changes the dynamics of the problem from linear to highly nonlinear. This particular situation restrict the governing equations to be solved analytically.

3.3.1   Exact Solution

We considered tissue contraction (when applied compression have maximum effects) as well as expansion. The eigenfunction expansion method using Green's formula was employed to solve the governing equation for solid deformation and fluid pressure. The main difficulty in solving the equation for solid deformation was the in-homogeneous left boundary condition. A detail describing the solution methodology is given in Appendix A. The closed form solution for solid displacement and pressure can be written as

$$u(x,t) = t(1-x) + \frac{2}{\varrho^2 \pi^3} \sum_{n=1}^{\infty} \left(\frac{e^{-\varrho^2 (n\pi)^2 t} - 1}{n^3} \right) \sin(n\pi x), \qquad (3.33)$$

and

$$p(x,t) = \frac{2}{\varrho^2 \pi^2 (1+\xi)} \left[1 - \frac{(1-\xi)M}{(1+\xi^2)(1+M)} \right] \ddot{b}, \qquad (3.34)$$

where

$$\ddot{b} = \sum_{n=1}^{\infty} \left[\frac{e^{-\varrho^2 (n\pi)^2 t} - 1}{n^2} \right] (\cos(n\pi x) - \cos(n\pi)).$$

In case of compression, equations (3.33) and (3.34) are the required solutions for the solid displacement and fluid pressure, respectively. On similar dynamics, one can find the exact solution for tissue expansion $(t > t_0)$, which we left as a

trivial case. It is important to note that we obtain a trivial steady-state solution for solid displacement and fluid pressure as suggested by equations (3.33) and (3.34) ($t = 0$), and these solutions are independent of permeability and magnetic parameter effects. In the section below, we discuss some detail related to the numerical algorithm used in solving governing equations numerically for a strain-dependent permeability flow.

3.3.2 Numerical Solution

The method of lines (MOL) is used in solving the governing system of equations for solid deformation and fluid pressure. MOL required to approximate spatial derivatives using the finite difference. This transformation changes the system of partial differential equations (PDEs) into the system of ordinary differential equations (ODEs). The resulting system of ODEs is solved using a well established MATLAB ODE solver like ode15s, ode23 [116, 117], etc. The partial derivatives in equation (3.29) are approximated as follows

$$\frac{\partial u}{\partial x} \approx \frac{u_{j+1} - u_{j-1}}{2 \cdot \Delta x}, \quad \frac{\partial^2 u}{\partial x^2} \approx \frac{u_{j+1} - 2 \cdot u_j + u_{j-1}}{\Delta x^2}. \tag{3.35}$$

Relations (3.35) allows us to rewrite equations (3.29) and (3.30) as follows

$$\frac{\partial u}{\partial t} = R \left[\frac{e^{m\left(\frac{u_{j+1} - u_{j-1}}{2 \cdot \Delta x}\right)}}{1 + M \cdot e^{m\left(\frac{u_{j+1} - u_{j-1}}{2 \cdot \Delta x}\right)}} \right] \left[\frac{u_{j+1} - 2 \cdot u_j + u_{j-1}}{\Delta x^2} \right], \tag{3.36}$$

and

$$p(x,t) = \frac{1}{1+\xi} \left[1 - \frac{(1-\xi)M}{(1+\xi^2)(1+M)} \right] \left[\frac{u_{j+1} - u_{j-1}}{2 \cdot \Delta x} \right], \tag{3.37}$$

where $\Delta x = \frac{b-a}{n}$ ($a = 0$ and $b = 1$) also $j = 1, 2, 3, \cdots n$. Below are the boundary conditions

$$u(0,t) = t(H(t) - H(t - t_0)) + t_0 H(t - t_0), \tag{3.38}$$

$$u(1,t) = 0, \quad u(x,0) = 0, \quad p(x,t) = 0 \quad at \quad x = 0, 1, \tag{3.39}$$

In the section below, the graphical results for the solid deformation and pressure variation for various cases have been presented.

3.4   Result and Discussion

The main objective of the present section is to highlight the influence of different physical parameters on fluid flow through the soft tissues during compression.In Figure-(3.2), a comparison between the exact and numerical solutions is given. In plotting these curves, four different values of the normalized time are considered (0.015-0.1).

Particularly, dotted curves correspond to an exact solution given in equation (3.33); however, dashed curves show numerical solutions of the equation (3.36). An excellent agreement can be noticed between both the solutions, which verify the convergence of the numerical scheme (MOL) used in solving the governing system of equations. In both of these solutions, constant permeability of the solid matrix was considered, however, strain-dependent permeability solutions are also obtained and discussed in coming graphs.

In Figure 3.3, we plotted solid deformation for various values of the magnetic parameter $(M = 0, 1, 2, 3)$. This solution is plotted for constant permeability $(m = 0)$ using both exact and numerical solutions of solid deformation u.

It is clear that the solid volume fraction gradually decreases when the value of magnetic parameter increases. This particular behavior is due to the Lorentz forces associated with the flow of charged fluid, in the presence of magnetic field. This particular behavior become more profound in the middle part of every curve for each value of M, which gradually decreases and become linear at the end. The plots 3.2 and 3.3 are devoted for the justification of numerical scheme, particularly, method of lines that was used in solving governing system of equations in more complex scenarios.
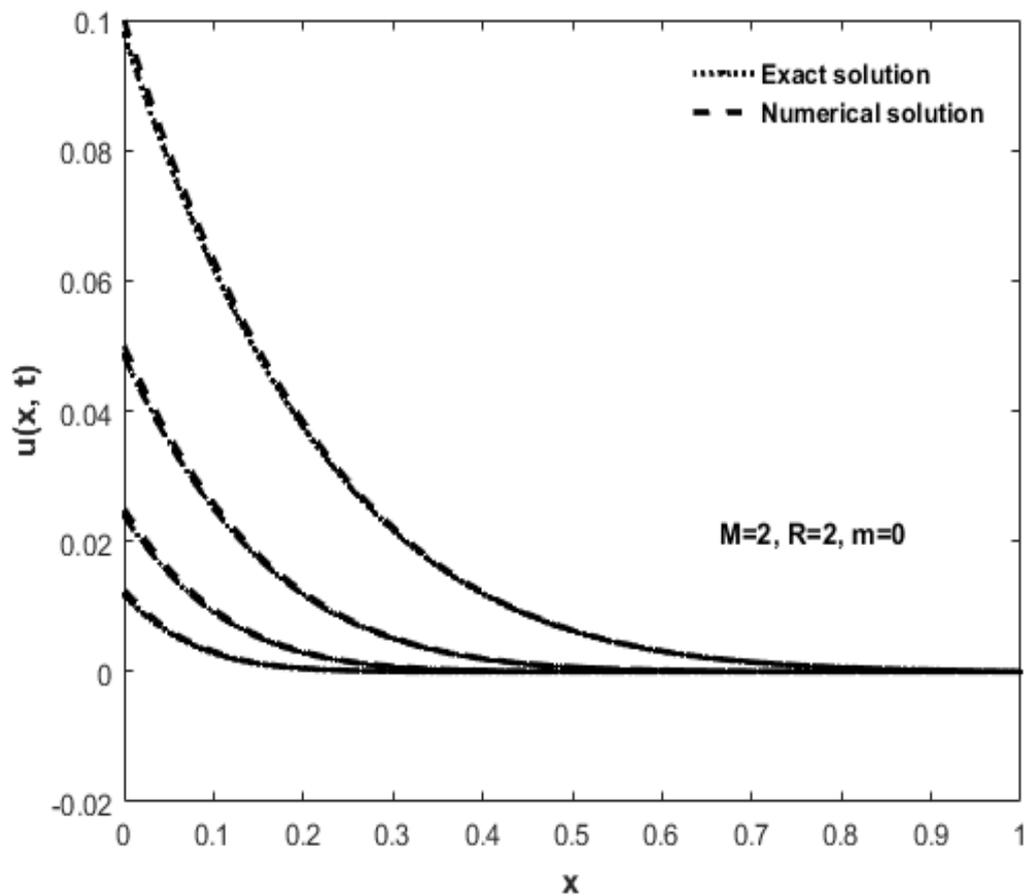
FIGURE 3.2: Comparison between the exact and numerical solutions for various values of the normalized time t, at $k = 1$.

In Figures 3.4, we plotted the solid deformation against the coordinate direction for fixed values of dimensionless constant R and normalized time t. In this plot, we explore the influence of magnetic parameter M on the swelling behavior of the cartilage tissues during compression.

This figure illustrated that the elastic porous medium of the tissues remain in loading circumstance throughout the course of compression; however, every curve undergoes an expansion in the middle part for every value of the magnetic parameter. This fact is due to the annular stretching of the tissues medium, because fluid flows outwardly produced inner region expansion in the solid matrix. On the other hand, swelling behavior of the soft tissues conformed that the macromolecules associated with the fluid flow captured within the tissues medium.
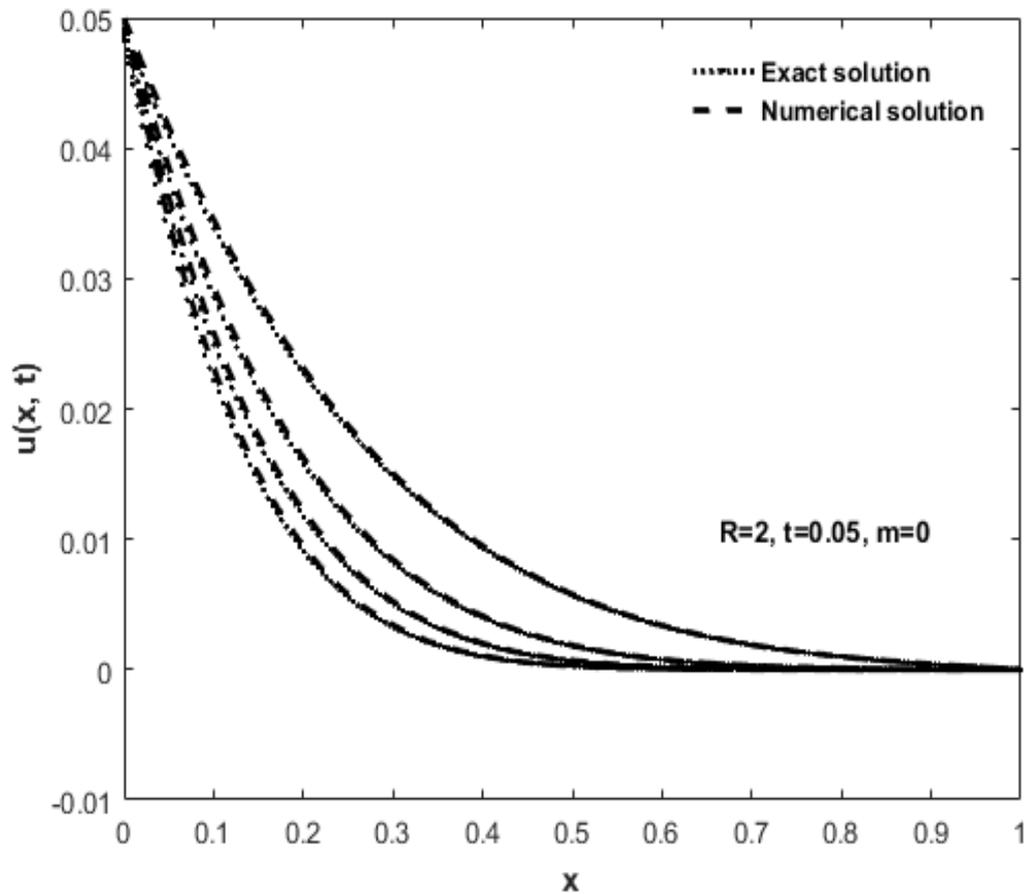
FIGURE 3.3: Comparison between the exact and numerical solutions for various values of the magnetic parameter M, at constant permeability.

Although, average sized particles travel in the tissues network due to which initial behavior of the solid matrix curves fluctuated downward direction. In plotting these curves, four different values of the magnetic parameter are used. As time goes on, solid deformation of the tissue become maximize. The largest value reported at $x = 1$, for every curve, which was the limit of consolidation in the present study. Furthermore, solid volume fraction inversely related with the magnitude of the magnetic parameter. In fact, this particular behavior of the solid matrix was due to the increased of resistance during passage of fluid that changed in accordance with magnitude of Lorentz forces. On the other hand, the predominant effects of applied compression can be seen in the middle part of every curve for every value of the magnetic parameter. This fact is due to the expansion of the elastic porous medium of the tissue during loading circumstances.
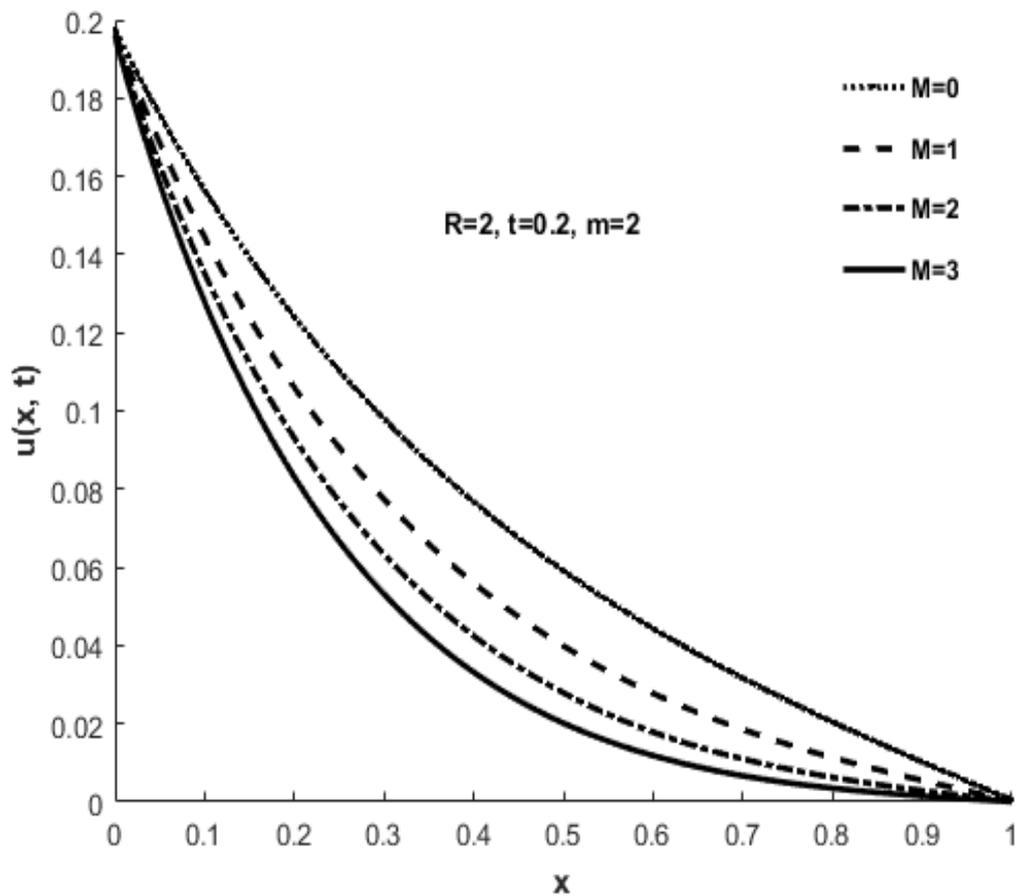
FIGURE 3.4: Solid deformation Vs various values of magnetic parameter M, at $t_0 = 0.2$.

After a while, stress effects were balanced by the elasticity of soft tissues and each curve moves linearly. It is worth mentioning, for $M = 3$, equilibrium reached much faster; the solid curve corresponds to this particular behaviors. Moreover, dotted curve shows change in the solid displacement in the absence of magnetic fields, which clearly indicates maximum deflection.

In Figure 3.5, changes in the solid displacement have been plotted for various value of the normalized time (t). These curves show that the existence of consolidation region grows in accordance with the value of time taken in plotting different curves. During compression, four different curves correspond to four different values of the normalized time t, and maximum deformation occurred when the value of the normalized time reached to 0.2.
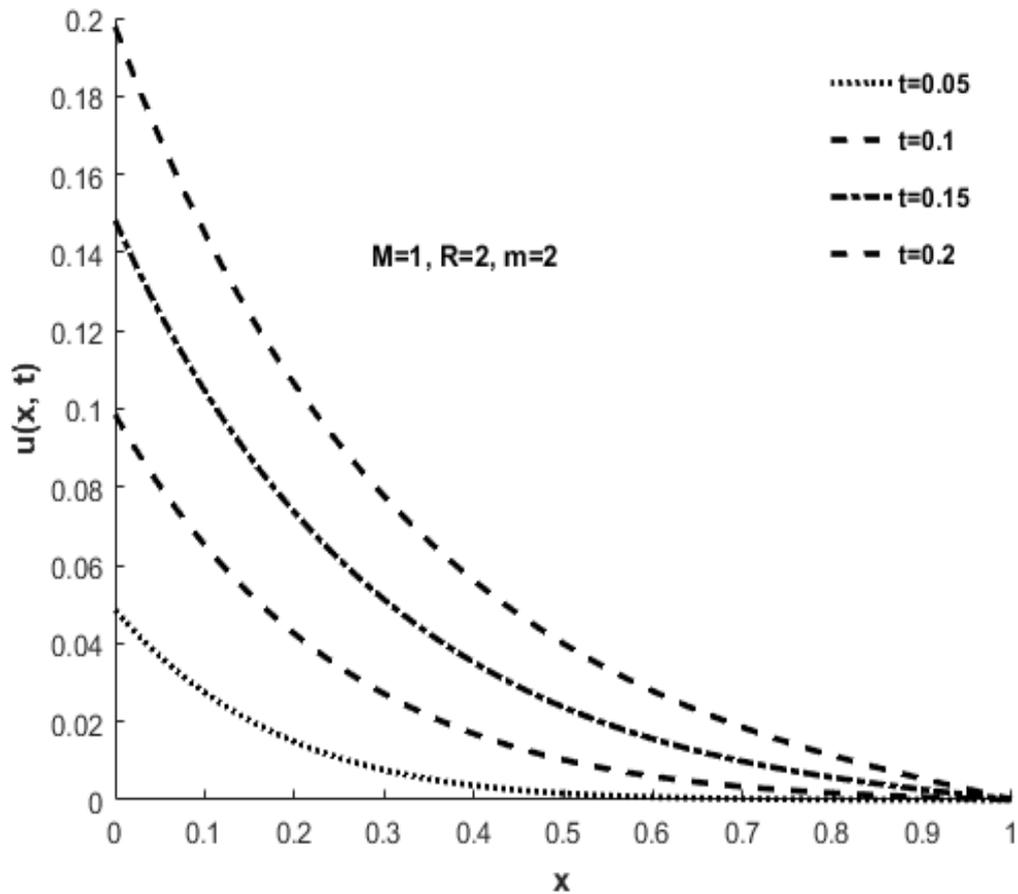
FIGURE 3.5: Solid deformation Vs various values of normalized time t (0.05-0.2.)

These dynamics show that time directly proportional to the deformation produced in the tissue network. It is worth mentioning here that these dynamics are opposite to the fact noted in Figures 3.4. Moreover, maximum deformation is reported at $t = 0.2$ (solid curve), and least for $t = 0.05$ (dotted curve).

In Figure 3.6, we explored the effects of strain-dependent permeability on the tissue deformation. In plotting these curves, we have used fixed values of the magnetic parameter M, dimensionless constant R, and normalized time t. These curves used to study the effects of strain-dependent permeability flow on the soft tissues, particulary, swelling behavior of the tissues was the main focused. The dash-dotted curve shows solid deformation for $m = 4$ that was the limiting value

of nonlinear permeability used in plotting solid deformation, because beyond this value result a sudden change in the solid deformation.
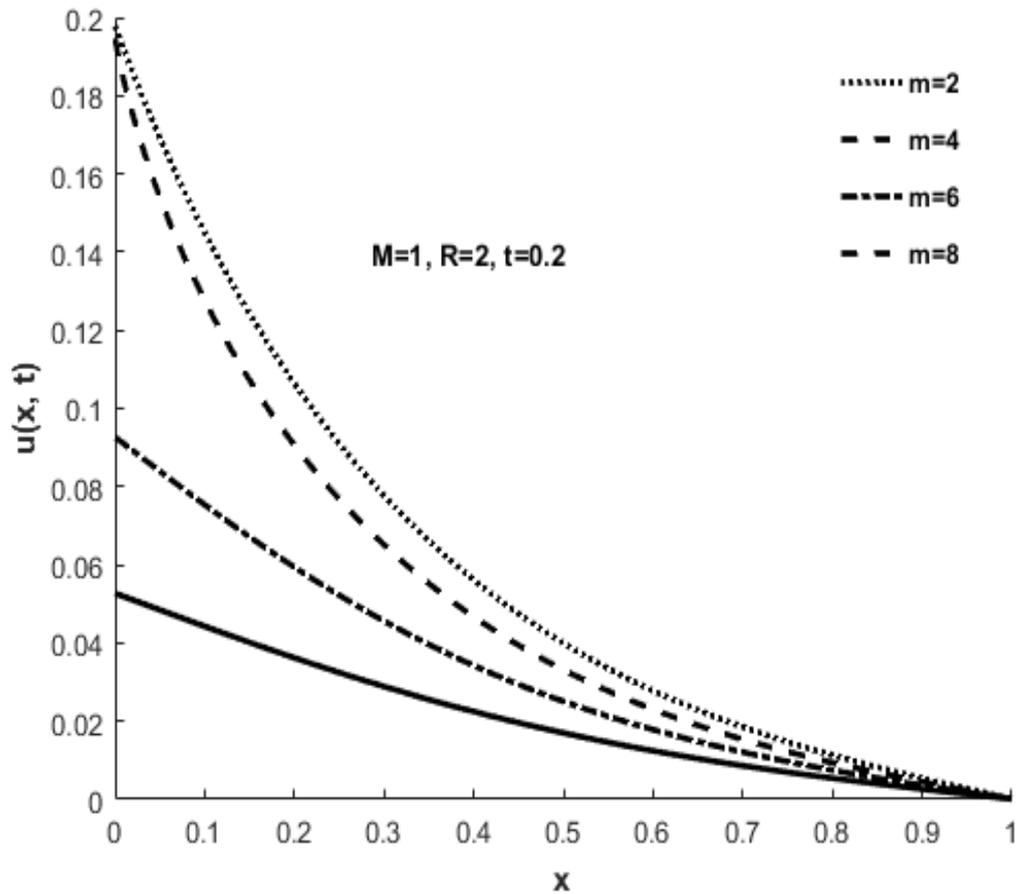
FIGURE 3.6: Solid displacement Vs various values of the strain-dependent permeability k.

This particular situation clearly shows equilibrium stage or more precisely steady state problem in which dominating effects of permeability alter soft tissues into a rigid medium. Large gap between dash-dotted and dashed curves provide a justification for this particular behavior. This effect is observed due to an increase of huge resistance for the passage of fluid through the cartilage tissues. In conclusion, our present study clarifies that in understanding the material nature of soft biological tissues, especially articular cartilage, it is important to consider the fluid flow through the interstitial spaces of the solid matrix. If not, them exact permeability of the solid matrix is required for an accurate governing model for saturated specimen.
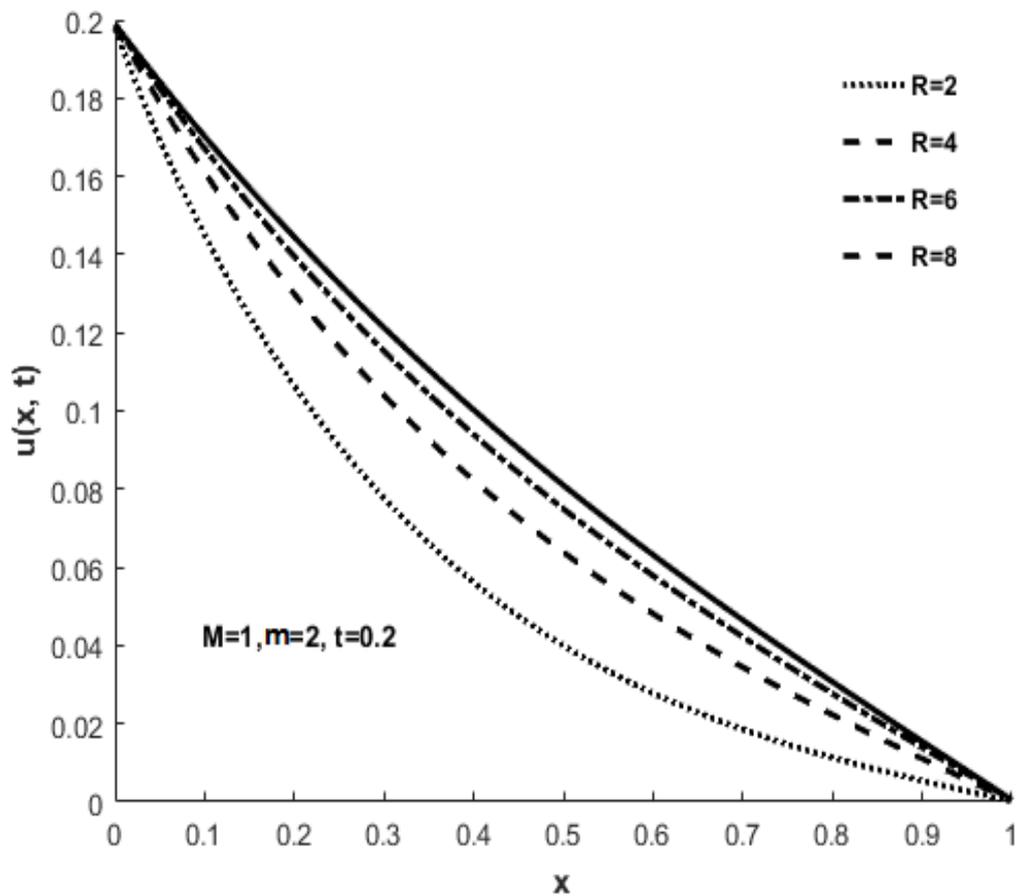
FIGURE 3.7: Solid deformation Vs various values of dimensionless constant R.

So, it is clear that elastic porous tissues were reasonably soft as well as large consolidation occurred; whereas, non-linear effects during fluid flow through cartilage network must be considered. These effects were particularly encounter by considering the non-linear strain-dependent permeability while driving the governing dynamics of these types of problems. This modification in the derivation of governing dynamics by incorporating strain-dependent permeability closely resemble to the exact nature of the cartilage and other types of soft biological tissues. In Figure 3.7, we plotted change in the solid displacement for different values of the constant R. This plot is devoted to study the effects of R on the tissue deformation. It is important to mention here that R is the function of applied compression imposed at the rigid interface of the tissues. Theoretical prediction of applied compression on the binary mixture of fluid and solid shows that stress at the surface

of cartilage tissues is required to overcome on the relative motion of interstitial fluid and solid matrix. Particularly, $R = 2$ correspond to the limiting case for applied compression, after that $(R = 0)$, a linear behavior is observed in the tissues expansion.
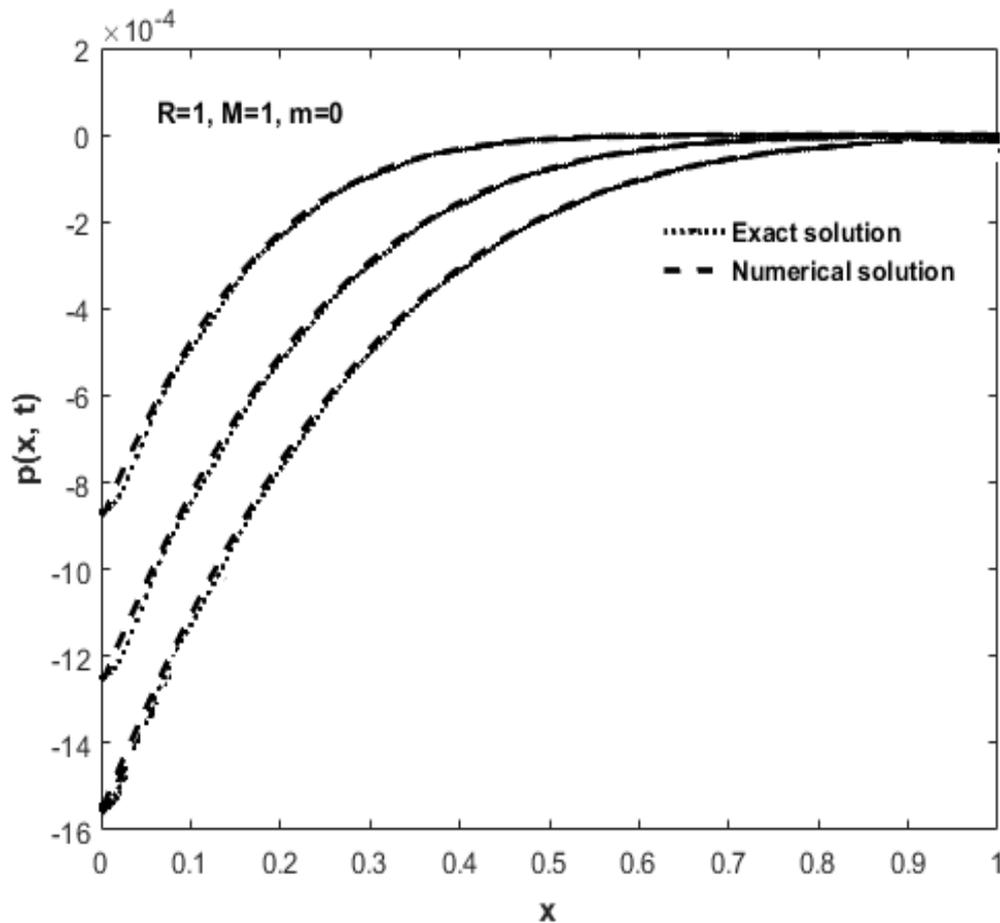
FIGURE 3.8: Compression between the exact and numerical solutions of the fluid pressure, at $k = 1$ (constant permeability).

In Figure 3.8, a compression between an exact and numerical solutions of fluid pressure is presented. Particularly, the dotted curves correspond to the numerical, whereas, dashed curves correspond to the exact solution. In plotting this graph, linear permeability of the solid matrix was considered $(k = 1)$. The pressure gradually increases, and become linear after attaining a specific hight due to the achieving equilibrium with the elastic porous medium of the tissues. In Figure 3.9, changes in the fluid pressure are plotted for various values of the magnetic parameter M. It is interesting to highlight that fluid pressure gradually decreases

after a certain value of space variable, i.e., $x \approx 0.3$. It is due to enhancement of the resistive forces for the passage of fluid.In the beginning, pressure gradually increases for every value of M, and become linear when moves toward the right boundary.
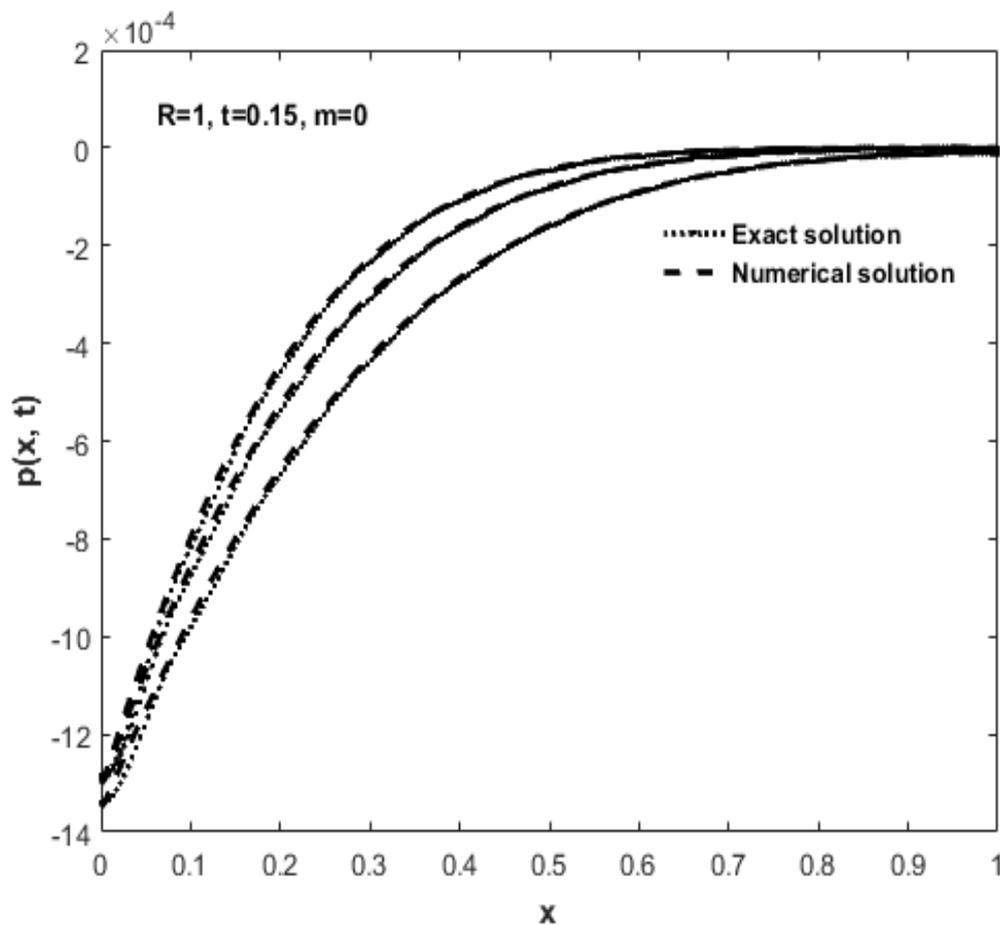
FIGURE 3.9: Compression between the exact and numerical solutions of the fluid pressure for various values of magnetic parameter M.

In plotting Figure 3.10, we have used different values of the material constant m. This variation in the permeability of solid matrix effects the fluid fluxes ability of the soft tissues. Particularly, a dramatic change occurred in the pressure is noticed beyond $m = 2$, i.e., at $m = 4$ and $m = 6$. Moreover, for $m = 0$ to 2, a regular increase in the fluid pressure is seen that suddenly decreased for $m = 4$ and $m = 6$. This peculiar behavior of the fluid pressure is observed by enhancement of non-linear affects in the permeability of the tissues that offer more resistance for the passage of fluid in accordance with nonlinearity of the solid matrix. This

phenomenon confirmed the dependance of pressure changes upon the permeability of solid matrix, which play an important role in understanding of interstitial fluid fluxes through the cartilage and other types of soft biological tissues.
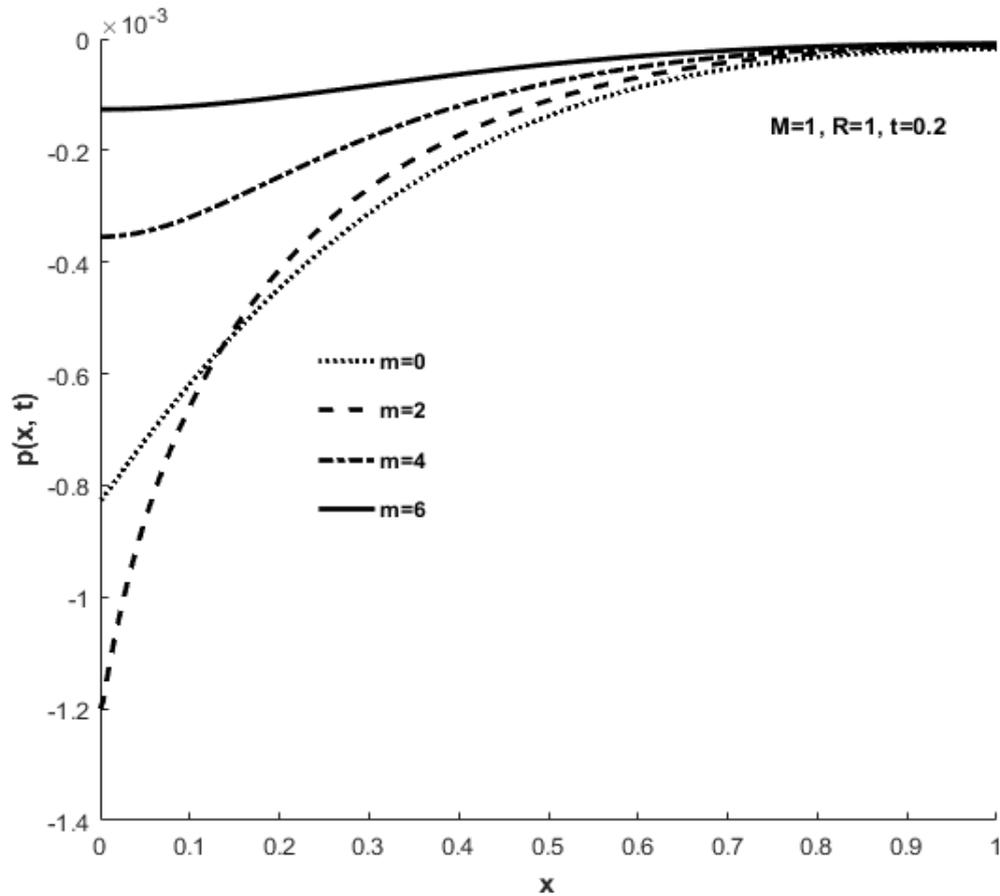
FIGURE 3.10: Fluid pressure Vs various values of strain-dependent permeability k.

These types of studies are very important that established a direct link between the fluid flow and pressure changes as well as their dependance upon the material nature of the solid matrix. In Figure 3.11, changes in the local fluid pressure are plotted for various values of normalized time (0.05 to 0.2) while keeping other parameters fixed. A unique behavior is noticed for every value of the time t. These curves show that the changes occurred in fluid pressure is directly proportional to the magnitude of time taken in each case. At the early stage, pressure gradually increases because the permeability of the tissues is much smaller, in the beginning.

After that, a linear behavior is noted for every value of the time to reach maximum deflection at $x = 1$.
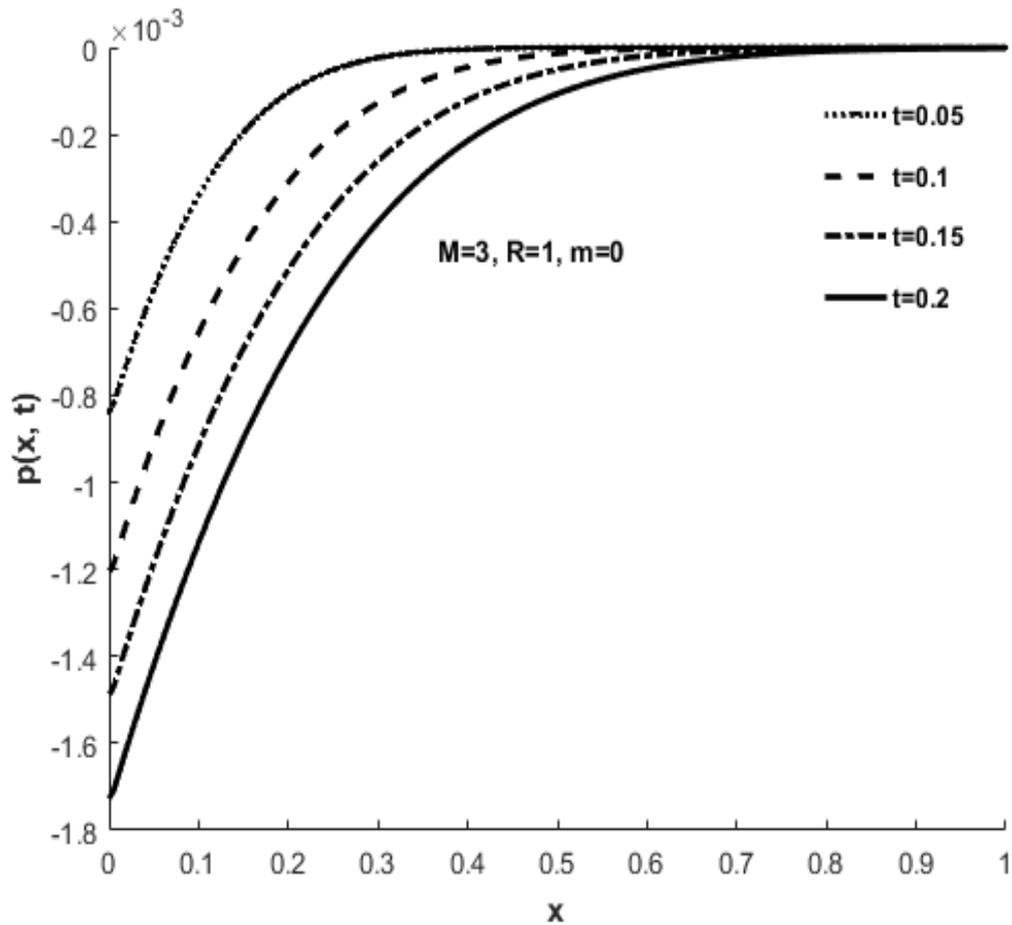
FIGURE 3.11: Fluid pressure Vs various values of normalized time t.

In the section below, a summery of the present Chapter is given.

3.5   Conclusion

In this Chapter, the stress-relaxation behavior of soft tissue during loading circumstances in the presence of applied magnetic field is derived. The problem is divided into two categories, i.e., for compression (when applied pressure have maximum effects), and relaxation (when the applied pressure is balanced by the elasticity of the tissue). We present the summary as follows

1. The magnetic parameter act as a resistive force during fluid flux through the soft tissues.

2. By increasing the time range we observe more deformation for the same applied pressure.

3. The strain-dependent permeability have enough effects during compression.

4. Increasing the value of dimensionless parameter R represents the same effects that were observed for the case of varying the time on the consolidation.

5. The pressure suddenly changed by increasing the non-linear effects in the permeability.

From the modeling point of view, continuum mixture theory is a well-established theoretical framework employed by many researchers in modeling the squeezing phenomenon for both linear and non-linear permeability in biological setting. However, the results of the present study can be further enhanced using more sophisticated forms of the permeability and revisiting the experiments which we are unable to perform due to lack of resources. In conclusion, our present study suggest that governing dynamics is affected predominantly due to permeability and the fluid flow through tissue boundaries. The magnetic parameter behaves like an opposing force on the fluid flow through cartilage tissues.

Chapter 4

The Effects of Magnetic Field on Porosity and Solid Deformation for the Radial Flow through Deformable Porous Shells

4.1   Introduction

In this Chapter, the dynamics of electrically conducting fluid flow through radially directed an elastic porous shell have been formulated. A constant magnetic filed effects have been incorporated in the binary mixture theory formulations while deriving nonlinear interaction between the mixture constituents. The fluid flow as well as solid deformation were assumed to depend upon the rate of applied compression at the inner radii of the shell. The outer edge (boundary) of the shell was considered as rigid mesh that offer negligible resistance during passage of fluid. The permeability dependent flow effects have been formulated by incorporating strain-dependent permeability dynamics while deriving governing behavior of multiphasic deformation. A system of coupled partial differential equation was

developed for the porosity and solid deformation along with the informal integral boundary conditions on both the extremities. The numerical scheme method of lines was used in finding the porosity of the shell, whereas, solid deformation was found by solving the integral equation containing the solid displacement. An analytical solution of the governing equations is provided for study state problem. Graphical results have been used in exploring the effects of different physical parameters on the growth rate of porosity and solid displacement of the elastic porous shell. A detail comparison of fluid flow through different geometries and a comparison of numerical and exact solutions for constant permeability case are also presented.

Barry and Aldis [50] have formulated the radial fluid flow through a deformable porous shell. This particular study gave a comparison between fluid flow through radial and planar geometries, still no comparison has been made between the fluid flow through different geometries, in the presence of Lorentz forces. In this Chapter, we incorporated the applied magnetic field effects in the constitutive equations of mixture theory and made an attempt to study the influence of magnetic parameter on the swelling behavior of an elastic porous shell.

The main idea used in formulating the governing dynamics of MHD using continuum mixture theory having direct relevance with the research work published in [66], for more detail see [64, 118, 119]. The governing system of partial differential equations is derived for the porosity and solid deformation, and fluid pressure while passage of electrically conducting fluid through an elastic porous shell. The governing system of equations is solved numerically for permeability dependent flow along with an exact solution for constant permeability case. A detail comparison between the fluid flow through the radial and planar geometries is presented graphically and using this particular result, we explored the fluid flow affected in different geometries keeping in view the industrial applications of different filters. In the following, a layout of the present Chapter is given.

Section 4.2 contains the mathematical formulation based upon the latest version of mixture theory, Section 4.3.1 contains the relevant details of the steady state

solution of the governing system of equations that is followed by a numerical solution in Section 4.3.2. Finally, Section 4.4 contains a detail summery of the present work (Chapter).

4.2   Theory and Model

It is well established fact that the deformable porous materials response to the loading imposed on them. Moreover, solid deformation produced in these materials not only change the shape of the solid matrix, but also effects the permeability parameter of the materials. In fact, a special kind of multiphasic deformation has been reported during fluid flows through the elastic porous materials. This variation in the physical property of an elastic porous solid control the passage of fluid, however, different loading conditions also play important role in these processes. Therefore, it is important to consider the consequences of strain-dependent permeability while deriving the governing dynamics of fluid flows through these materials.

In the present study, we assumed that the fluid flow depends upon both, i.e., applied pressure as well as permeability of the elastic porous medium of the shell. The permeability of the solid matrix is taken of the following type [50]

$$k(\phi) = k_0 \cdot e^{m\phi} \tag{4.1}$$

where k_0 and m are the material constants. It is worth mentioning; present study is identical in modeling point of view of soft biological tissues such as articular cartilage. These types of problems having more then one constituents, hence limit in the use of single phasic description. We considered that the applied pressure imposed at the inner boundary of the shell which in turn flux the fluid outwardly from the central part of cylindrical or spherical geometry.

The continuum mixture theory, in fact, binary mixture theory was taken into account while deriving complex coupling between the constituents of the mixture.

According to this theory "individual components of the mixture are manipulated in such a way that each point within the mixture is occupied by each constituent of the mixture" [120]. The mathematical formulations used in deriving the governing dynamics in the present Chapter are based on the work of Barry and Aldis [50], however, some modifications have been made for incorporating MHD effects in the governing dynamics of multiphasic deformation. The kinematics of the problem have been modeled using the conservation laws of mass and momentum balance.

Due to the assumption of intrinsic in-impressibility of the components, the solid matrix can only be squeezed into a spacial controlled volume, when an equal amount of the fluid flow from the opposite direction. This assumption leads us to the following equation

$$\frac{\partial \phi^\alpha}{\partial t} + \nabla \cdot (\phi^\alpha \mathbf{v}^\alpha) = 0, \tag{4.2}$$

where α used to specify different phases i.e., $\alpha = f, s$, f and s represent solid and fluid phases, respectively, $\mathbf{v}^s$ and $\mathbf{v}^f$ are the velocities ρ^s and ρ^f are apparent densities along with true densities ρ_T^s and ρ_T^f. Equation (4.2) is the continuity equation (mass conservation) for the α phase reported in numerous studies [20, 50, 64, 66], identical to the present study. Adding equation (4.2) for both phases, we get

$$\nabla \cdot \mathbf{v} = 0, \tag{4.3}$$

where $\mathbf{v} = \phi^\mathbf{s} \mathbf{v}^\mathbf{s} + \phi^\mathbf{f} \mathbf{v}^\mathbf{f}$ represents the microscopic or composite velocity. In the absence of body forces, momentum balance for a homogenous mixture can be written as [100]

$$\rho^\alpha \left(\frac{\partial \mathbf{v}^\alpha}{\partial t} + (\mathbf{v}^\alpha \cdot \nabla) \right) \mathbf{v}^\alpha = \nabla \cdot \mathbf{T}^\alpha + \boldsymbol{\pi}^\alpha + \mathbf{J} \times \mathbf{B}, \tag{4.4}$$

where $\mathbf{T}^\alpha$ represents stress tensor, $\mathbf{J}$ is the current density, $\mathbf{B}$ is contribution of Lorentz force effects, and $\boldsymbol{\pi}^\alpha$ corresponds to the drag forces. For small frequencies and assumption of infinitesimal deformation, effects of inertial forces become negligible [68, 72]. This assumption allow us to rewrite equation (4.4) as follows

$$\nabla \cdot \mathbf{T}^\alpha = -\boldsymbol{\pi}^\alpha - \mathbf{J} \times \mathbf{B}, \tag{4.5}$$

and

$$\mathbf{T}^\alpha = -\phi^\alpha pI + \boldsymbol{\sigma}^\alpha, \tag{4.6}$$

where $\boldsymbol{\sigma}^\alpha$ and K represent stress and coefficient of diffusive resistance, respectively. It is worth mentioning; in the rest of derivation, we considered $\boldsymbol{\sigma}^s = \boldsymbol{\sigma}$, and $\boldsymbol{\sigma}^f = 0$, for detail see [68]. The diffusive resistance between the mixture components can be written as

$$-\boldsymbol{\pi}^s = \boldsymbol{\pi}^f = K(\mathbf{v}^s - \mathbf{v}^f) - p\nabla\phi^s. \tag{4.7}$$

From equations (4.5)-(4.7), we get

$$-\nabla(\phi^s p\mathbf{I}) + \nabla \cdot \boldsymbol{\sigma} = K(\mathbf{v}^s - \mathbf{v}^f) - p\nabla\phi^s - \mathbf{J} \times \mathbf{B}, \tag{4.8}$$

and

$$-\nabla(\phi^f p\mathbf{I}) = -K(\mathbf{v}^s - \mathbf{v}^f) + p\nabla\phi^s - \mathbf{J} \times \mathbf{B}, \tag{4.9}$$

where $\mathbf{I}$ corresponds to the identity tensor. After some mathematical manipulation, equations (4.8)-(4.9), yield

$$\nabla \cdot \boldsymbol{\sigma} = K(\mathbf{v}^s - \mathbf{v}^f) + \phi^s\nabla p - \mathbf{J} \times \mathbf{B}, \tag{4.10}$$

and

$$\mathbf{0} = -K(\mathbf{v}^s - \mathbf{v}^f) + \phi^f\nabla p - \mathbf{J} \times \mathbf{B}. \tag{4.11}$$

In the following, we gave the Maxwell's and Ohm's laws equations which help in simplifying the expression $\mathbf{J} \times \mathbf{B}$, later on

$$\nabla \times \mathbf{B} = \mu_c\mathbf{J}, \quad \nabla \cdot \mathbf{B} = 0, \quad \nabla \times \mathbf{E} = -\frac{\partial\mathbf{B}}{\partial t}, \qquad \boldsymbol{J} = \sigma_0(\boldsymbol{E} + \boldsymbol{v}^\eta \times \boldsymbol{B}), \tag{4.12}$$

where μ_c is the permittivity of free space, and $\mathbf{E}$ represents the electric field intensity. Now, expression $\boldsymbol{J} \times \boldsymbol{B}$ can be simplify using the relations define in (4.12) as follows

$$\mathbf{J} \times \mathbf{B} = \sigma_0(\mathbf{E} + \mathbf{v}^\alpha \times \mathbf{B}) \times \mathbf{B}, \tag{4.13}$$

where σ_0 is the electric conductivity. The strength of magnetic field $\mathbf{B}$ is algebraic

sum of the applied ($\boldsymbol{B_0}$) and induced magnetic ($\boldsymbol{B_1}$) fields. Using the vector triple product, equation (4.13) can be written as

$$\mathbf{J} \times \mathbf{B} = \sigma_0 \left(\mathbf{B}_0(\mathbf{v}^\alpha \cdot \mathbf{B}_0) - \mathbf{v}^\alpha(\mathbf{B}_0 \cdot \mathbf{B}_0) \right). \tag{4.14}$$

It is worth mentioning; contribution of magnetic force parallel to the fluid motion is negligible, because it is vector product of fluid speed with magnetic field influence. This allows us to ignore the term $\mathbf{v}^\alpha \cdot \mathbf{B}$. In this setting, equation (4.14) can be written as

$$\mathbf{J} \times \mathbf{B} = -\sigma_0 B_0^2 \mathbf{v}^\alpha. \tag{4.15}$$

From equations (4.15), (4.10)-(4.11), we get

$$\nabla \cdot \boldsymbol{\sigma} = K(\mathbf{v}^s - \mathbf{v}^f) + \phi^s \nabla p + \sigma_0 B_0^2 \mathbf{v}^s, \tag{4.16}$$

and

$$\mathbf{0} = -K(\mathbf{v}^s - \mathbf{v}^f) + \phi^f \nabla p + \sigma_0 B_0^2 \mathbf{v}^f. \tag{4.17}$$

Eliminating the fluid pressure p from equations (4.16) and (4.17) and using relation $\phi^s + \phi^f = 1$, we get

$$\nabla \cdot \boldsymbol{\sigma} = \frac{K}{\phi^f}(\boldsymbol{v}^s - \boldsymbol{v}^f) + \frac{\sigma_0 B_0^2}{\phi^f}(\boldsymbol{v}^s - \phi^s(\boldsymbol{v}^s + \boldsymbol{v}^f)). \tag{4.18}$$

The relative velocity in the opposite direction to the applied pressure is negligible, because applied compression large enough to flux the fluid as well as produced solid deformation in the direction of applied pressure only. In this setting, factor $\boldsymbol{v}^s + \boldsymbol{v}^f = 0$ in equation (4.18) vanished and it leaves the following form of equation (4.18)

$$\nabla \cdot \boldsymbol{\sigma} = \frac{K}{\phi^f}(\boldsymbol{v}^s - \boldsymbol{v}^f) + \frac{\sigma_0 B_0^2 \boldsymbol{v}^s}{\phi^f}. \tag{4.19}$$

From relation $\boldsymbol{v} = \phi^s \boldsymbol{v}^s + \phi^f \boldsymbol{v}^f$, we have

$$\boldsymbol{v}^f = \frac{\boldsymbol{v} - \phi^s \boldsymbol{v}^s}{\phi^f}. \tag{4.20}$$

Using the value of v^f in equation (4.19), we get

$$\nabla \cdot \sigma = \frac{K}{(\phi^f)^2}\left(\boldsymbol{v}^s - \boldsymbol{v}\right) + \frac{\sigma^2 B_0^2 \boldsymbol{v}^s}{\phi^f}. \tag{4.21}$$

After some mathematical manipulation, equation (4.21) can be written as

$$\nabla \cdot \sigma = \frac{1}{k}\left(1 + M\right)\frac{\partial \boldsymbol{u}}{\partial t} - \frac{\boldsymbol{v}}{k}, \tag{4.22}$$

where $k = \frac{K}{(\phi^f)^2}$ [50, 100], $M = \frac{\sigma^2 B_0^2 \boldsymbol{v}^s}{\phi^f}k$ corresponds to the magnetic parameter [65, 66], and **u** is the solid displacement. The quantitative relation between the pressure and stress can be found using equations (4.16) and (4.17) as follows

$$\nabla \cdot \sigma = \nabla p + \sigma_0 B_0^2(\boldsymbol{v}^s + \boldsymbol{v}^f). \tag{4.23}$$

Simplifying, yield

$$\nabla p = \nabla \cdot \sigma. \tag{4.24}$$

In order to derive the governing equation along with appropriate boundary conditions, it is convenient to assume that deformations are small enough. This can be justify, because we are using infinitesimal theory in modeling the governing dynamics. In the case of cylindrical geometry, only the radial components of the displacement and velocity are non zero. In this configuration; stress components can be written as

$$\sigma_{rr} = (\lambda + 2\mu)\frac{\partial u}{\partial r} + \beta\lambda\frac{u}{r}, \tag{4.25}$$

and

$$\sigma_{\theta\theta} = (\lambda + 2\mu)\frac{u}{r} + \lambda\frac{\partial u}{\partial r} + (\beta - 1)\frac{u\lambda}{r}, \tag{4.26}$$

where λ and μ are **Lame** constants, and $\beta = 0, 1, 2$ correspond to the cartesian (x, y, z), cylindrical (r, θ, z), and spherical (r, θ, ϕ) geometries, respectively. For the case of planar geometry, σ_{rr} is simply σ, at $r = x$, and $\sigma_{\theta\theta} = 0$. For the spherical geometry, $\sigma_{\theta\theta} = \sigma_{\phi\phi}$ due to the symmetric configuration. Remaining components of the stress are considered to be zero for the case of simplicity due to their negligible contribution. Therefore, divergence of the stress, in the radial

direction can be written as [50]

$$(\nabla \cdot \boldsymbol{\sigma})_r = \frac{\partial \sigma_{rr}}{\partial r} + \beta \left(\frac{\sigma_{rr} - \sigma_{\theta\theta}}{r} \right). \qquad (4.27)$$

From equations (4.25)-(4.27), we get

$$(\nabla \cdot \boldsymbol{\sigma})_r = H_a \frac{\partial \phi}{\partial t}, \qquad (4.28)$$

where

$$\phi = \frac{1}{r^\beta} \frac{\partial}{\partial r} (r^\beta u), \qquad (4.29)$$

where $H_a = \lambda + 2\mu$ is the aggregate modulus. Form of equation (4.3), we have

$$\frac{\partial v}{\partial r} = 0. \qquad (4.30)$$

The velocity in the radial direction can be found by integrating equation (4.30) as follows

$$v_r = \frac{v(t)}{r^\beta}, \qquad (4.31)$$

where $v(t)$ is the constant of integration. From equations (4.22), (4.24), (4.28) and (4.29), we get

$$\frac{\partial p}{\partial r} = H_a \frac{\partial}{\partial r} \left(\frac{1}{r^\beta} \frac{\partial}{\partial r} (r^\beta u) \right) = \frac{1}{k(\phi)} [1 + M] \frac{\partial u}{\partial t} - \frac{1}{k(\phi)} \frac{v(t)}{r^\beta}. \qquad (4.32)$$

After some algebraic simplification, we get

$$H_a k(\phi) \frac{\partial \phi}{\partial r} = [1 + M] \frac{\partial u}{\partial t} - \frac{v(t)}{r^\beta}. \qquad (4.33)$$

It is convenient to change the equation (4.33) into a single unknown function. This modification makes the governing partial differential equation more feasible for solution point of view. In order to transfer the governing equation (4.33) into a single unknown function, we have define the following transformation

$$L(\omega) = \frac{1}{r^\beta} \frac{\partial}{\partial r} (r^\beta \omega). \qquad (4.34)$$

From equations (4.33) and (4.34), we get

$$H_a \frac{1}{r^\beta} \frac{\partial}{\partial r} \left(k(\phi) r^\beta \frac{\partial \phi}{\partial r} \right) = (1 + M) \frac{\partial}{\partial t} \frac{1}{r^\beta} \frac{\partial}{\partial r} (r^\beta u) - \frac{1}{r^\beta} \frac{\partial}{\partial r} (r^\beta \frac{v(t)}{r^\beta}). \quad (4.35)$$

The term containing the velocity factor $v(t)$ vanished, because it is independent of r. From equations (4.29) and (4.35), we get

$$H_a \frac{1}{r^\beta} \frac{\partial}{\partial r} \left(k(\phi) r^\beta \frac{\partial \phi}{\partial r} \right) = (1 + M) \frac{\partial \phi}{\partial t}. \quad (4.36)$$

Now, equation (4.36) is converted into velocity free form. The equation for local fluid pressure can be found using the equation (4.32) as follows

$$\frac{\partial p}{\partial r} = H_a \frac{\partial}{\partial r} \left(\frac{1}{r^\beta} \frac{\partial}{\partial r} (r^\beta u) \right). \quad (4.37)$$

Integrating equation (4.37) gives

$$p(r, t) = \frac{H_a}{r^\beta} \left(\frac{\partial}{\partial r} (r^\beta u) \right) + c(t), \quad (4.38)$$

From equation (4.29), we have

$$\phi(b, t) = \frac{\partial u}{\partial r} (b, t). \quad (4.39)$$

The fluid flow is considered normal to the surface, this leads us to the following equation

$$\left[\frac{\partial u}{\partial r} + \beta \lambda_r \frac{u}{r} \right]_{r=a} = 0, \quad (4.40)$$

where $\lambda_r = \frac{\lambda}{(\lambda + 2\mu)}$. This in terms of ϕ can be written as

$$\phi(a, t) = \frac{\beta}{a} u(a, t)(1 - \lambda_r). \quad (4.41)$$

where $c(t)$ is the constant of integration. Figure 4.1 shows the fluid motion from central part of a spherical or cylindrical section of the shell. On the other hand, outer boundary is represented by the rigid mesh that offered negligible resistance

for the passage of the fluid. Inner radius of shell is a, whereas, b corresponds to the outer radii $(b > a)$.
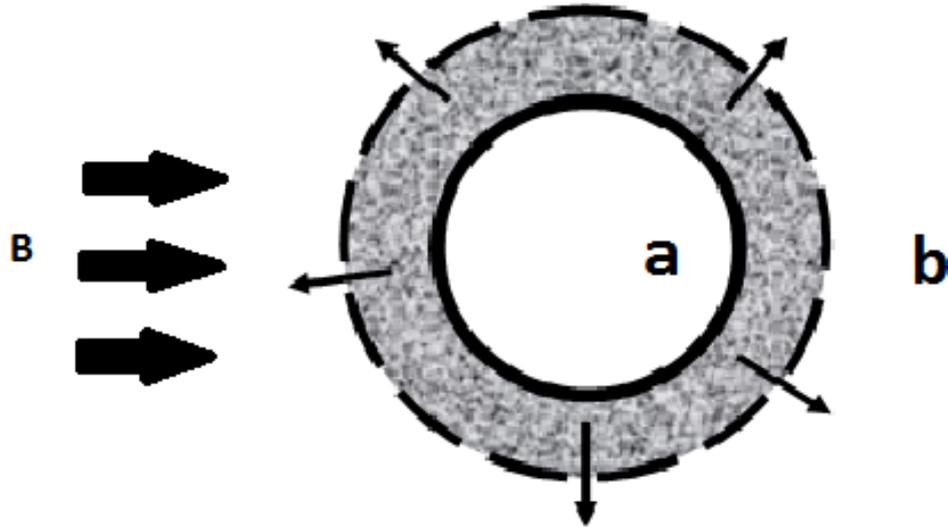

FIGURE 4.1: In this Chapter, passage of electrically conducting fluid through an elastic porous shell has been considered, in the presence of magnetic field effects. The fluid flow depends upon the loading imposed at the inner wall of shell.

Integrating equation (4.29), we get

$$u(r,t) = -\frac{1}{r^\beta} \int_r^b r^\beta \phi(r,t) dr. \tag{4.42}$$

Equation (4.42) is the required equation for the solid deformation that can only be solve when solution of the porosity $\phi(r,t)$ is known. This leads to a system of coupled partial differential equations (4.36), (4.38), and (4.42) correspond to the porosity, pressure, and solid deformation, respectively. In order to close the system, we impose displacement boundary condition $u = 0$, at $r = b$. Inserting equation (4.42) and change the limit of integration from a to b, we get

$$\phi(a,t) + \beta \frac{(1-\lambda_r)}{a^{1+\beta}} \int_a^b r^\beta \phi(r,t) dr = 0. \tag{4.43}$$

For a radial constrained boundary condition at $r = b$, we have

$$\phi(b,t) = \phi(a,t) - \frac{\nabla P}{H_a}, \tag{4.44}$$

where ∇P corresponds to the pressure. Equations (4.43) and (4.44) are the required boundary conditions for the governing partial differential equation (4.36).

Below, we introduce the dimensionless variables which we used in converting the governing system of equations in dimensionless form

$$P = H_a \phi_0 \hat{P}, \quad r = r_0 \hat{r}, \quad u = u_0 \hat{u}, \quad \phi = \phi_0 \hat{\phi}, \quad r = r_0 \hat{r},$$

$$t = \frac{r_0^2}{D} \hat{t}, \quad a = a_0 \hat{a}, \quad b = b_0 \hat{b} \quad k = k_0 \hat{k} \quad p = p_0 \hat{p}, \tag{4.45}$$

where D is the diffusion coefficient. Using these choices, equations (4.36), (4.38 and (4.42)-(4.44) can be written as

$$\frac{P}{\hat{r}^\beta} \frac{\partial}{\partial \hat{r}} \left(\hat{r}^\beta \hat{k} \frac{\partial \hat{\phi}}{\partial \hat{r}} \right) = (1+M) \frac{\partial \hat{\phi}}{\partial \hat{t}}, \tag{4.46}$$

$$\hat{p}(\hat{r}, \hat{t}) = \frac{R}{\hat{r}^\beta} \frac{\partial}{\partial \hat{r}} (\hat{r}^\beta \hat{u}) + c, \tag{4.47}$$

$$\hat{u}(\hat{r}, \hat{t}) = -\frac{S}{\hat{r}^\beta} \int_{\hat{r}}^1 \hat{r}^\beta \hat{\phi}(\hat{r}, \hat{t}) d\hat{r}. \tag{4.48}$$

Boundary conditions are

$$\hat{\phi}(\hat{a}, \hat{t}) = -\frac{\beta(1 - \lambda_r)T}{a^{1+\beta}} \int_{\hat{a}}^1 \hat{r}^\beta \hat{\phi}(\hat{r}, \hat{t}) d\hat{r}, \quad \hat{\phi}(1, \hat{t}) = \hat{\phi}(\hat{a}, \hat{t}) - \nabla \hat{P}, \tag{4.49}$$

$$\hat{p}(\pm 1, t) = 0. \tag{4.50}$$

In the following, different dimensionless variables are given which appeared while converting the governing equations into dimensionless form

$$P = \frac{H_a k_0}{D}, \quad R = \frac{H_a}{p_0}, \quad S = \frac{r_0^{\beta+1} \phi_0}{u_0 r_0^\beta}, \quad T = \frac{r_0^{\beta+1}}{a_0^{\beta+1}}. \tag{4.51}$$

Now, we have a complete system, i.e., governing equations ((4.46)-(4.48)) along with the boundary conditions ((4.49)-(4.50)).

In the following, we gave details of the solutions of governing system of equations.

4.3   Solution Methodology

In this section, we first present an exact solution of the governing system of partial differential equations for the steady state problem that is followed by numerical solution for an unsteady case. We removed hat from the equations (4.46)-(4.50) in the sections below, because the governing equations are obviously in the dimensionless forms.

4.3.1   Steady Solution

In the case of steady state problem, equation (4.46) for $k = 1$ can be written as

$$\frac{P}{r^\beta}\frac{d}{dr}\left(r^\beta\frac{d\phi}{dr}\right) = 0. \tag{4.52}$$

Integrating

$$\phi(r) = \frac{c_1}{(1-\beta)}r^{1-\beta} + c_2, \quad \text{for} \quad \beta = 0, 2 \tag{4.53}$$

where c_1 and c_2 are the constants of integration that can be found using the boundary conditions, later on.

From equations (4.53) and (4.48), we get

$$u(r) = -\frac{c_1 S}{2(1-\beta)r^\beta}(1-r^2) - \frac{c_2 S}{1+\beta}\frac{1-r^{1+\beta}}{r^\beta}, \quad \text{for} \quad \beta = 0, 2 \tag{4.54}$$

In the following, we used boundary conditions in finding the values of different constants appeared in equations (4.53) and (4.54).

For $r = a$, we have

$$\phi(a) = -(1-\lambda)\frac{\beta}{a^{1+\beta}}\int_a^1 r^\beta\phi(r,t)dr. \tag{4.55}$$

At $r = b$, we have

$$\phi(b) = -(1-\lambda)\frac{\beta}{a^{1+\beta}}\int_a^1 r^\beta\phi(r,t)dr - 1. \tag{4.56}$$

From equations (4.53), (4.55), and (4.56), we get

$$\frac{c_1}{1-\beta}a^{1-\beta} + c_2 = -(1-\lambda)\frac{\beta}{a^{1+\beta}}\int_a^1 r^\beta \phi(r,t)dr, \qquad (4.57)$$

and

$$\frac{c_1}{1-\beta}b^{1-\beta} + c_2 = -(1-\lambda)\frac{\beta}{a^{1+\beta}}\int_a^1 r^\beta \phi(r,t)dr - 1. \qquad (4.58)$$

Simplifying equations (4.57) and (4.58), we get

$$c_1 = \frac{(1-\beta)}{(a^{1-\beta} - b^{1-\beta})}, \quad c_2 = \frac{-(1+\beta)}{(1+\beta)a^{1+\beta} + \beta(1-\lambda)(1-a^{1+\beta})T}A. \qquad (4.59)$$

where $\left(\frac{2a^2 + \beta(1-\lambda)(1-a^2)T}{2(a^{1-\beta} - b^{1-\beta})}\right)$. Using values of the constants c_1 and c_2 in equations (4.53) and (4.54), for $\beta = 0, 2$ gives

$$\phi(r) = \frac{r^{1-\beta}}{a^{1-\beta} - b^{1-\beta}} - \frac{1+\beta}{(1+\beta)a^{1+\beta} + \beta(1-\lambda)(1-a^{1+\beta})T}B, \qquad (4.60)$$

where $\lambda = 0.5$, $a = 0.5$ (thick wall shell), $a = 0.8$ (thin wall shell), and $B = \left(\frac{2a^2 + \beta(1-\lambda)(1-a^2)T}{2(a^{1-\beta} - b^{1-\beta})}\right)$. Exact solution of the solid displacement can be written as

$$u(r) = -\frac{S(1-r^2)}{2(a^{1-\beta} - b^{1-\beta})r^\beta} + \frac{S(1-r^{1+\beta})}{\left((1+\beta)a^{1+\beta} + \beta(1-\lambda)(1-a^{1+\beta})T\right)r^\beta}B \quad (4.61)$$

For $\beta = 1$, general solution of the porosity and solid displacement can be written as

$$\phi(r) = c_3 log(r) + c_4, \quad u(r) = \frac{-1}{r}\left[c_3(-0.25 - 0.5r^2 log(r) + 0.25r^2) + \frac{c_4}{2}(1-r^2)\right], \qquad (4.62)$$

where c_3 and c_4 are the integration constants that were computed as follows

$$c_3 = \frac{1}{log(a) - log(1)}, \quad c_4 = \frac{-2log(a)(2a - 0.25 - 0.5a^2 log(a) + 0.25a^2)}{(log(a) - log(1))(4a + 1 - a^2)}. \qquad (4.63)$$

The complete solution for $\beta = 1$ upon inserting the integration constant can be written as

$$\phi(r) = \frac{log(r)}{log(a) - log(1)} - \frac{2log(a)}{log(a) - log(1)} \left(\frac{2a - 0.25 - 0.5a^2 log(a) + 0.25a^2}{4a + 1 - a^2} \right),$$

$$(4.64)$$

and

$$u(r) = C(-0.25 - 0.5r^2 log(r) + 0.25r^2) + D \left(\frac{(2a - 0.25 - 0.5a^2 log(a) + 0.25a^2)}{4a + 1 - a^2} \right),$$

$$(4.65)$$

where $C = \frac{-1}{r(log(a) - log(1))}$, and $D = \frac{(1 - r^2)log(a)}{r(log(a) - log(1))}$. Equations (4.60), (4.64) and (4.61), (4.65) are the required solution for the porosity and solid displacement, respectively. Below, a comparison of exact solution for ϕ and u for the fluid flow through different geometries is presented.

Figures 4.2 and 4.3 are used to described change in the porosity and solid displacement for different radial constrained geometries when thick wall elastic porous shell $(0.5 \leq r \leq 1)$ is considered. These graphical results obtained using the exact solutions for planar, cylindrical and spherical geometries. In plotting these curves, we considered a fixed value of the permeability parameter $k = 1$ by assuming slow rate of the compression.

It is interesting to see that medium remains in deformation throughout the course of compression, whereas, the cylindrical shell shows more expansion in the middle and less toward the ends. Similar dynamics is observed for the case spherical geometry. These dynamics are due to the annular stretching of the elastic medium of the shell as the radius of the inner region increases for both cylindrical and spherical geometries. The other critical observation is related to annular expansion more than indemnify for the radial contraction $\frac{du}{dr}$ in inner region.

The planar case shows clear filtration while applied pressure is kept same and filtering the smaller size particles in heavily compressed downstream regime. This particular physical phenomenon is observed in applications of filters in membrane filtration, where the goal is to separate the macro-molecules associated with the fluid flow when the flow dynamics stopped. It is to be noted that in cylindrical

geometries captures larger molecules as compared to planar case in which large size molecules are excluded from the medium.
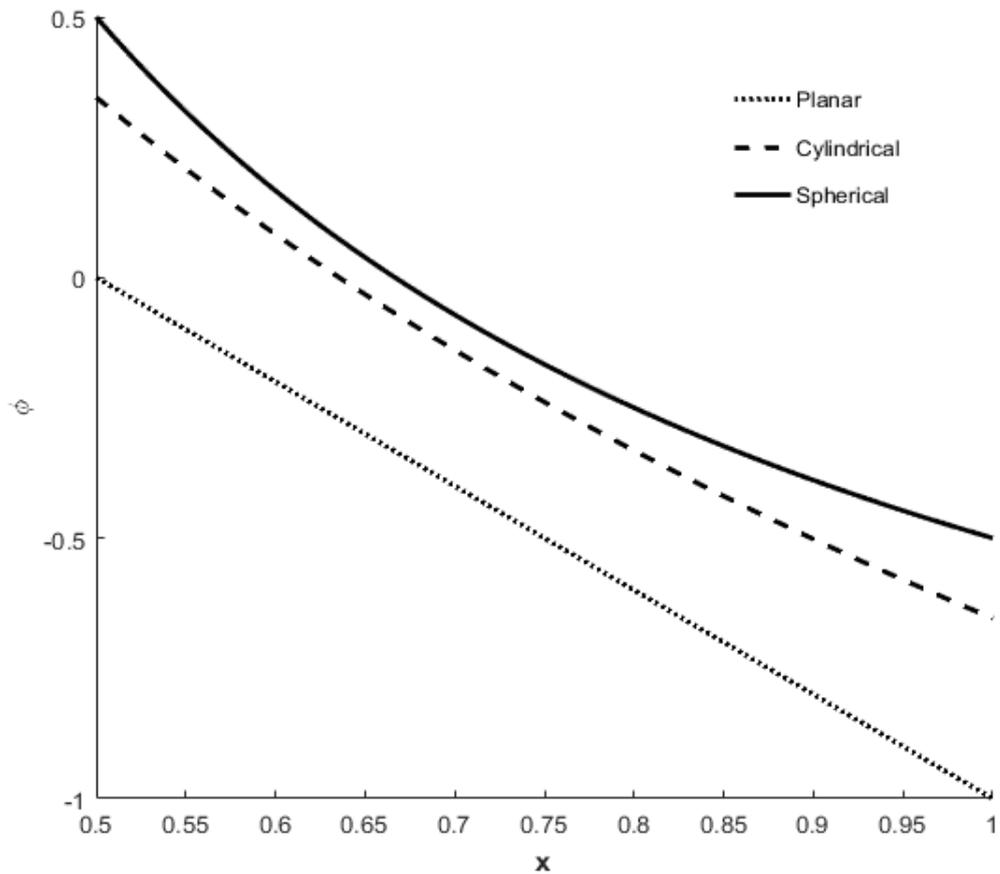

FIGURE 4.2: The changes occurred in the porosity Vs different geometries.

Interestingly, moderate size particles able to advance before being trapped which elevates the possibility for them to remain constantly trapped while the fluid flux is stopped. For the case of solid deformation, we have used equation (4.61) in finding the variation in solid displacement under loading circumstances for different geometrical constrained.

In Figure 4.3, change in the solid displacement was plotted against radius of the porous shell ($0.5 \leq r \leq 1$) for both planar and radial geometries. The maximum initial volume was reported for cylindrical geometry, however, a larger deflection can be seen for planar case. This is due to the fact that elastic solid for planar case drained maximum wage out during fluid fluxes.
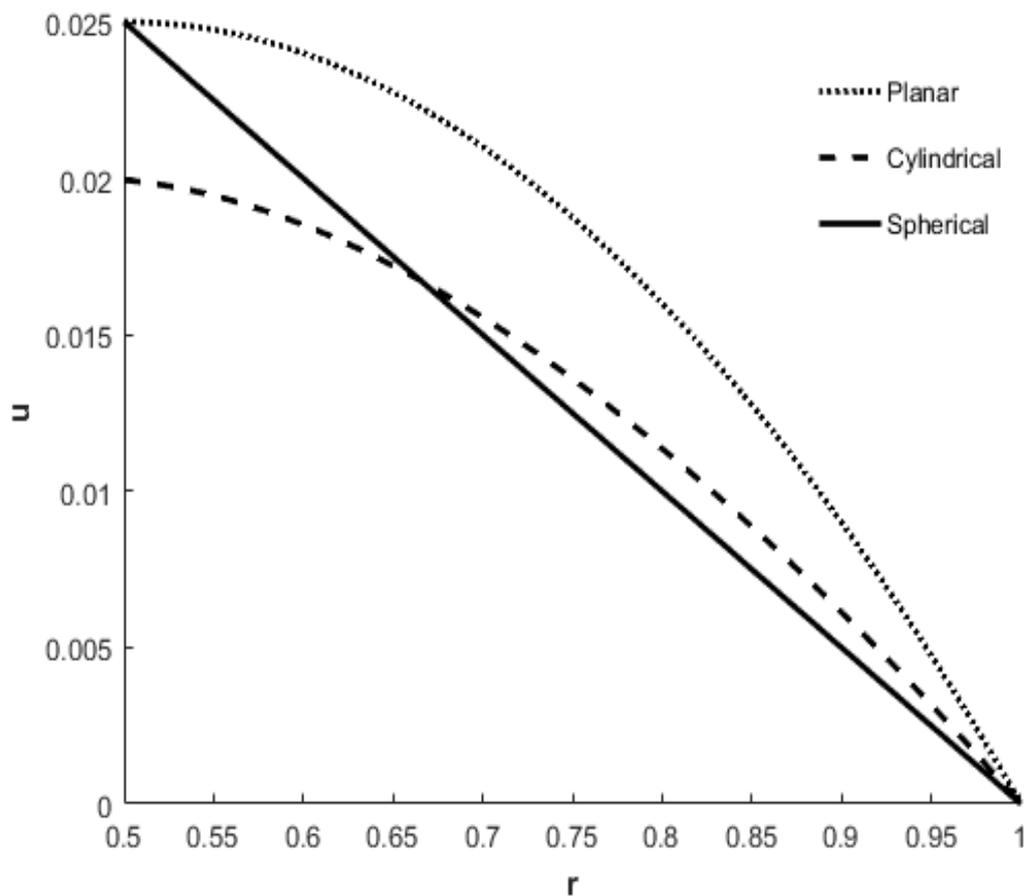
FIGURE 4.3: Solid deformation Vs different geometries.

Theses graphical results used to described the influenced of geometries on fluid flux when medium remain under loading. The planar geometry experienced more pressure effects as compared to the radial geometries. This result leads to the fact, when maximum infiltration is required the planar geometry is more suitable, however, for microorganism separation cylindrical and spherical geometries are preferable.

Graphical results in this section show the dynamics of fluid flow while keeping the permeability of shell constant more precisely linear permeability has been used. In section below, we have used strain-dependent permeability dynamics in exploring solid deformation and fluid pressure in different graphical outcomes.

4.3.2 Unsteady Solution

In present section, we gave some detail describing the numerical scheme used in solving the governing system of partial differential equations, in case of time depended problem. It is worth mentioning here that the main difficulty in solving equation containing the porosity was existence of unknown variable (ϕ) both in the governing PDE and boundary conditions. Particulary, the porosity parameter appeared in the form of an integral equation in both left and right boundary conditions. In handling this problem, we coupled the trapezoidal rule with the primary numerical scheme MOL in solving the equation (4.46) numerically.

From the modeling point of view by setting $M = 0$, we recover the system of equations described in [50]. This legitimated the rule used in deriving the governing equations, in the presence of Lorentz forces. We have solved the governing system of equations using the numerical scheme method of lines (MOL) [121, 122]. MOL required to approximate the special derivatives using finite difference, leaving the time variable continuous. The resulting system of ODEs then solved using well established MATLAB ODEs solver like ode15s, ode23 etc. The governing equation (4.46) using central difference can be written as

$$\frac{\partial \phi}{\partial t} = \frac{Le^{m\phi_j}}{r(1+M)} \left(r \left[\frac{\phi_{j+1} - 2\phi_j + \phi_{j-1}}{h^2} \right] + (\beta + mr) \left[\frac{\phi_{j+1} - \phi_{j-1}}{2h} \right] \right), \quad (4.66)$$

where $L = Pk_0$, $h = \frac{(1-a)}{n}$, and $j = a, a+h, a+2h.......a+(n-1)h, a+nh = 1$. The boundary conditions for the equation (4.66) are

$$\phi(a,t) = -\frac{\beta(1-\lambda_r)T}{a^{1+\beta}} \int_a^1 r^\beta \phi(r,t) dr, \quad (4.67)$$

and

$$\phi(1,t) = \phi(a,t) - \nabla P. \quad (4.68)$$

Using the solution of porosity in the integral equation containing solid deformation, we find the solid displacement. In the following, we present graphical results

to highlight the effects of different physical parameters on porosity and solid displacement.
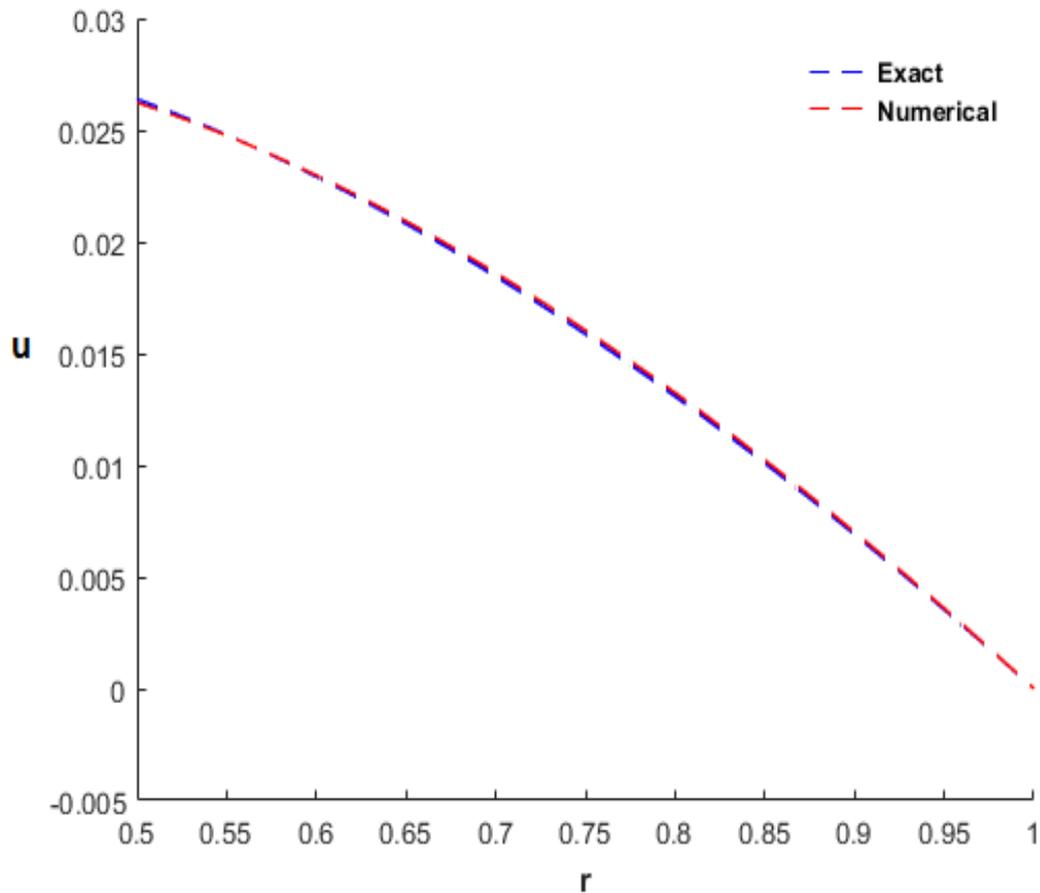

FIGURE 4.4: Comparison between the exact and numerical solutions for linear permeability of the deformable porous shell ($k = 1$).

In Figure 4.4, we compared the numerical and exact solutions for solid displacement, in the case of cylindrical geometry. The Dashed-blue curve corresponds to the exact solution for the steady-state problem, whereas, the dotted-red curve represents numerical solution, for $k = 1$. These two curves show the change in the solid displacement for a thick wall deformable porous shell. An excellent agreement can be noticed between both the solutions that validated the proposed numerical scheme used in solving the governing equations.

In Figure 4.5, solid displacement is plotted against the radial distance for four different times, i.e., $t = 0.005, 0.01, 0.015$ and 0.02. The dotted curve in this graph

shows a stage when equilibrium is achieved. This figure shows the change in the solid displacement when linear form of the permeability relation is considered as was the case in [50].
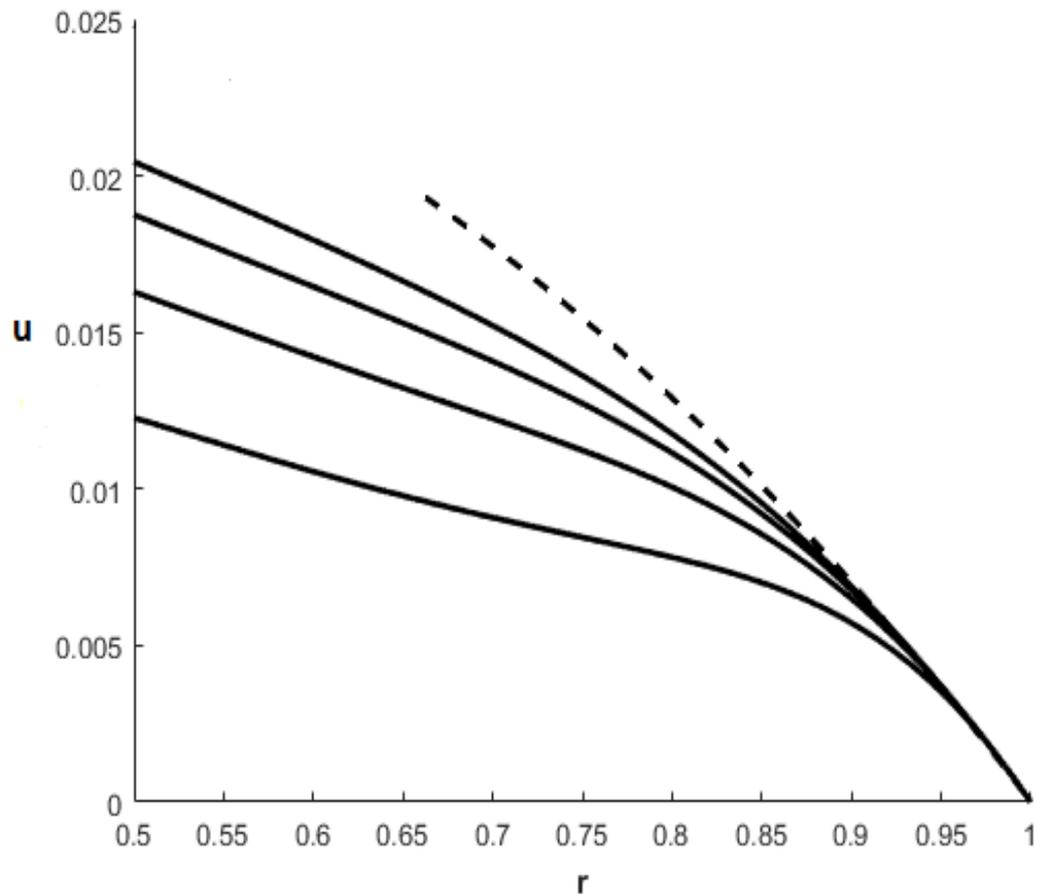

FIGURE 4.5: Solid displacement Vs various values of the normalized time t. This plot shows the similar dynamics as was in [50] when $M = 0$.

A similar dynamics is also reported by Barry and coauthor for the change in solid displacement before attaining equilibrium, in their publish article [50].

Figure 4.6 shows the change in porosity for cylindrical geometry for four different values of the magnetic parameter ($M = 0, 2, 4, 6$). In plotting theses curves, we used a constant permeability that was independent of the nonlinear effects. Four different curves show the effects of the applied magnetic field on the porosity of the deformable porous shell. When the value of the magnetic parameter increased,

it offer more resistance for the passage of fluid. In this particular situation, equilibrium reached much faster. Initially, shell behaves like an elastic medium for M=0 and reported maximum deflection at the middle part of every curve. These dynamics become linear, when process moves toward the end. This is due to the annular expansion in the elastic medium of the shell due to applied pressure while draining fluid.
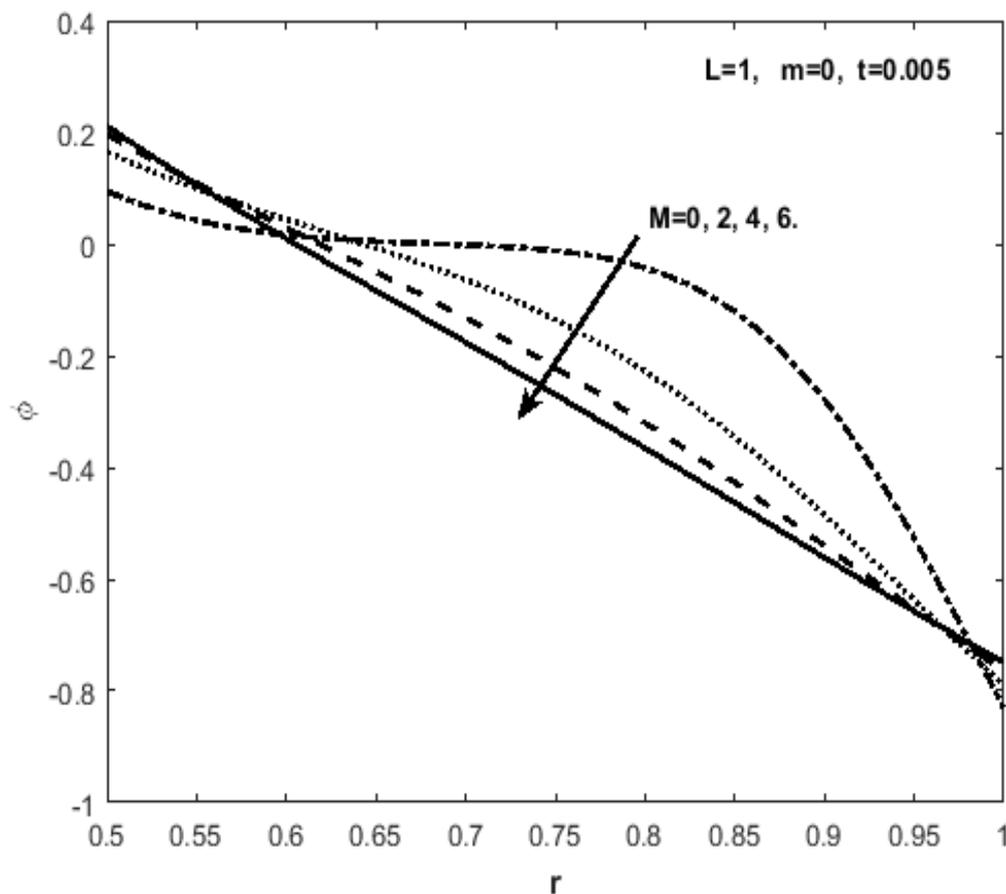
FIGURE 4.6: The porosity Vs different values of the magnetic parameter M. In plotting these curves four different values of magnetic parameter M have been taken ,i.e., $M = 0, 2, 4, 6$.

In this process an increase in the local porosity of the shell occurred that produced changes in the permeability of the solid matrix. When magnitude of the magnetic parameter is increased, it clearly results linear behavior in the solid deformation. The solid line in this graph corresponds to $M = 6$ for which medium remains in loading throughout the course of compression.

In Figure 4.7, porosity is plotted against the radius of deformable porous shell for different values of strain-dependent permeability. This graphical result is used to study the consequences of strain-dependent permeability on the fluid flow dynamics. A maximum initial value of the porosity ϕ is reached to 0.1, at $m = 0$. which gradually decreased by increasing magnitude of m or k (k is function m). An opposite behavior is noticed at the right boundary of the shell. This result shows that the permeability parameter can be used in controlling the growth rate of porosity by increasing non-linear effects in the fluid flow dynamics.
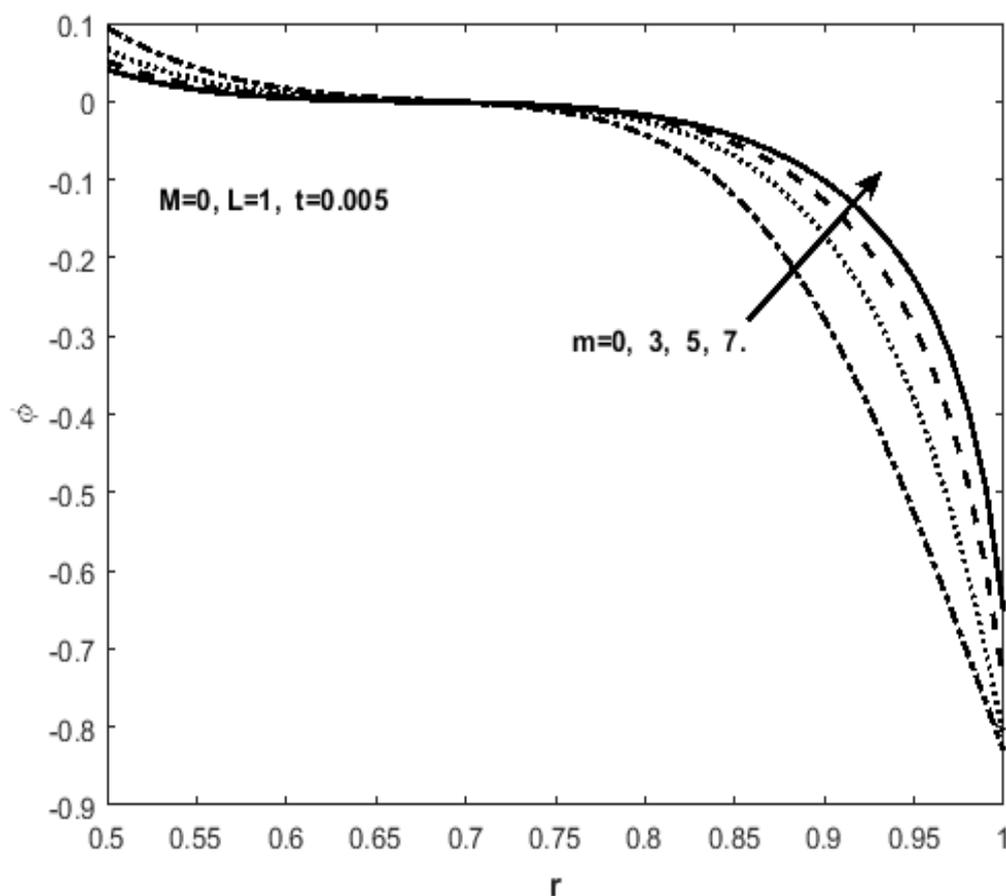
FIGURE 4.7: Change in the porosity Vs various values of nonlinear permeability k.

On the other hand, equilibrium attain by the elastic porous medium of the shell become much slower, when value of m goes on increasing. This is due to the enhancement of resistance forces during fluid-solid interaction while passaging of fluid through the deformable porous shell. This fact can be seen in the solid curve

for $m = 7$ that reported maximum deflection for the same applied pressure taken in plotting other curves in this graph.

In Figure 4.8, solid displacement is plotted against the radial distance r of the shell for various values of the magnetic parameter (M). In this plot, we considered constant permeability effects for the cylindrical geometry. It can be noticed that the solid deformation increased in accordance with the strength of the magnetic parameter (M) taken in each case.
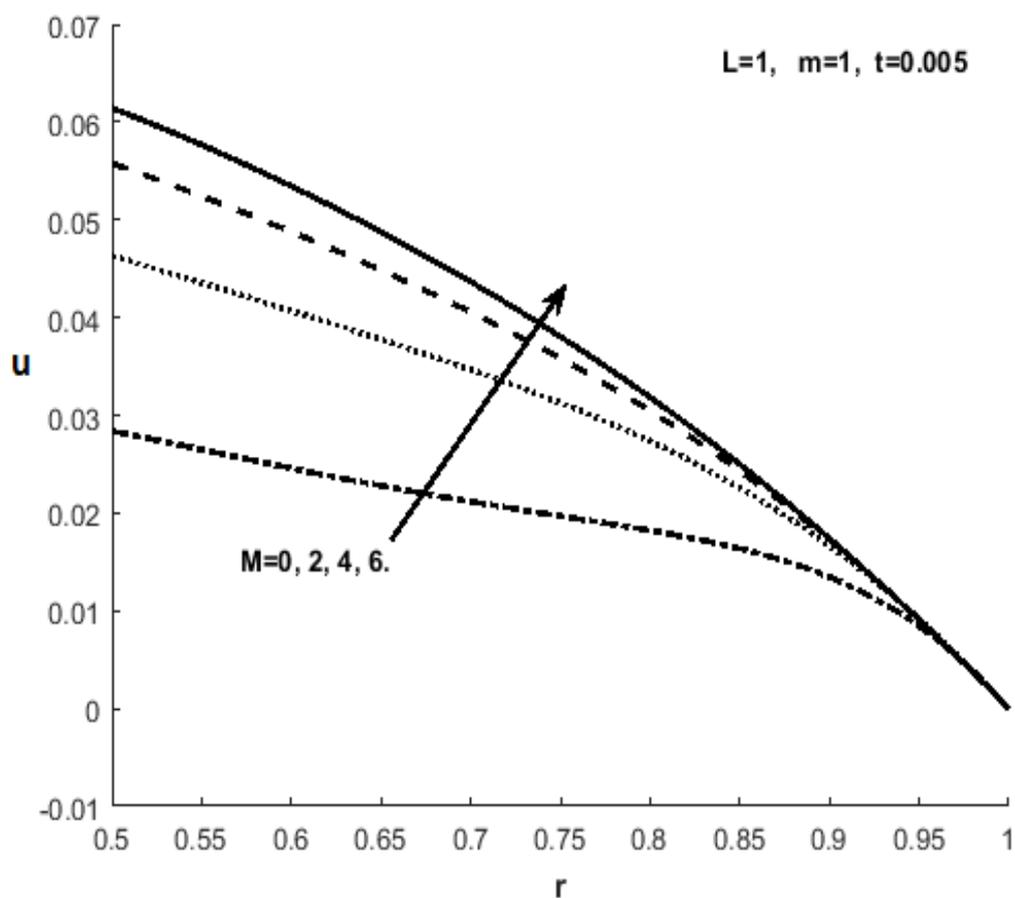
FIGURE 4.8: Solid deformation Vs different values of the magnetic parameter M. These curves show the fluid flow behavior during passage of fluids through cylindrical geometry.

At $r = 1$, maximum solid displacement is reported that corresponds to the limit of consolidation for applied pressure acting on the elastic solid matrix. The influence of strain-dependent permeability on the porosity is presented in Figure 4.9 while

keeping other parameters constant. This figure shows that the porosity of the solid decreases when nonlinear effects in the permeability parameter m increases. This result also depicts that a highly compressed region is formed at the radially constrained porous edge due to the increase of non-linearity in the system during fluid flow in compression.

The porosity ϕ and displacement u for a constrained cylindrical shell are graphed for various values of normalized times, in Figures 4.10 and 4.11, respectively.
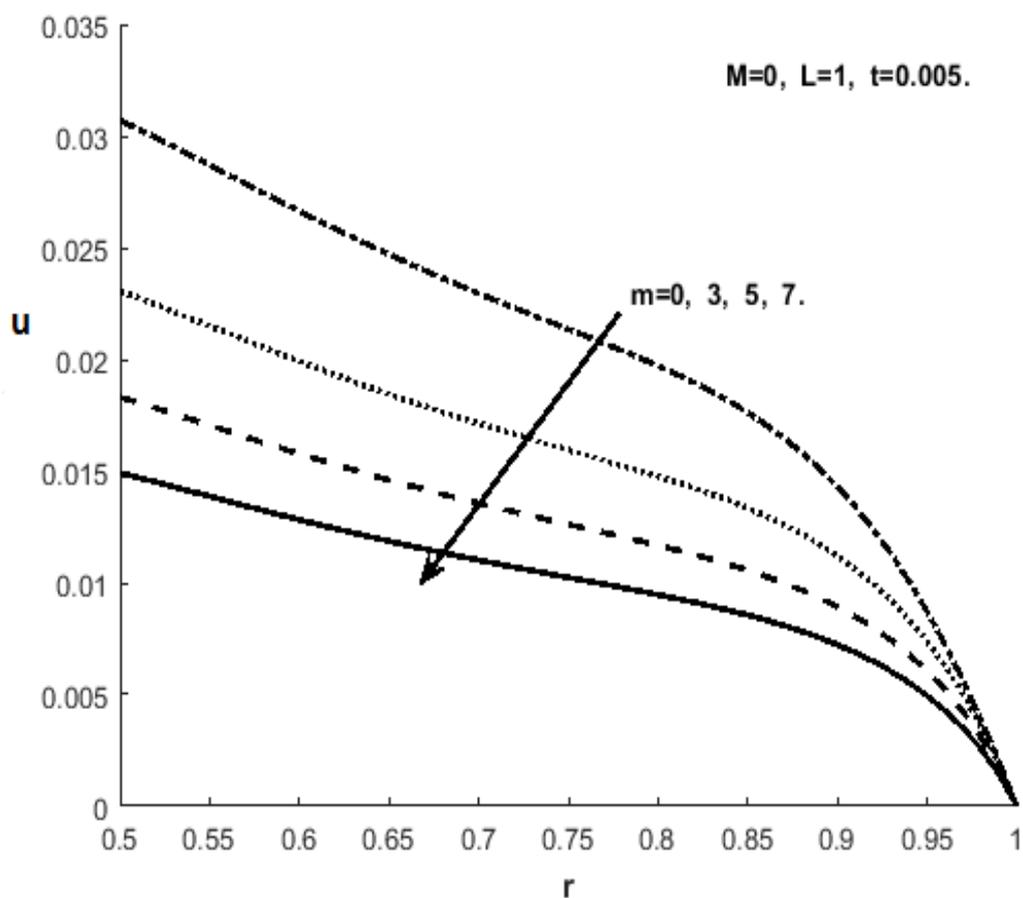

FIGURE 4.9: Changes in the porosity Vs different values of strain-dependent permeability k.

The full time dependent behavior of the radial flow is obtained using the numerical scheme, which may not be possible by solving the governing equations analytically, even, in case of small time.

Figure 4.10 shows the change in porosity at four different values of time after the application of unit step change in pressure function. The applied pressure contribution comes through the right boundary condition while solving the governing equations numerically. The expansion in the inner region of the elastic porous boundary grows with time. This fact leads to the conclusion that a compressed region is formed at the constrained boundary that is separated inwards when time varies from 0.005 to 0.02.
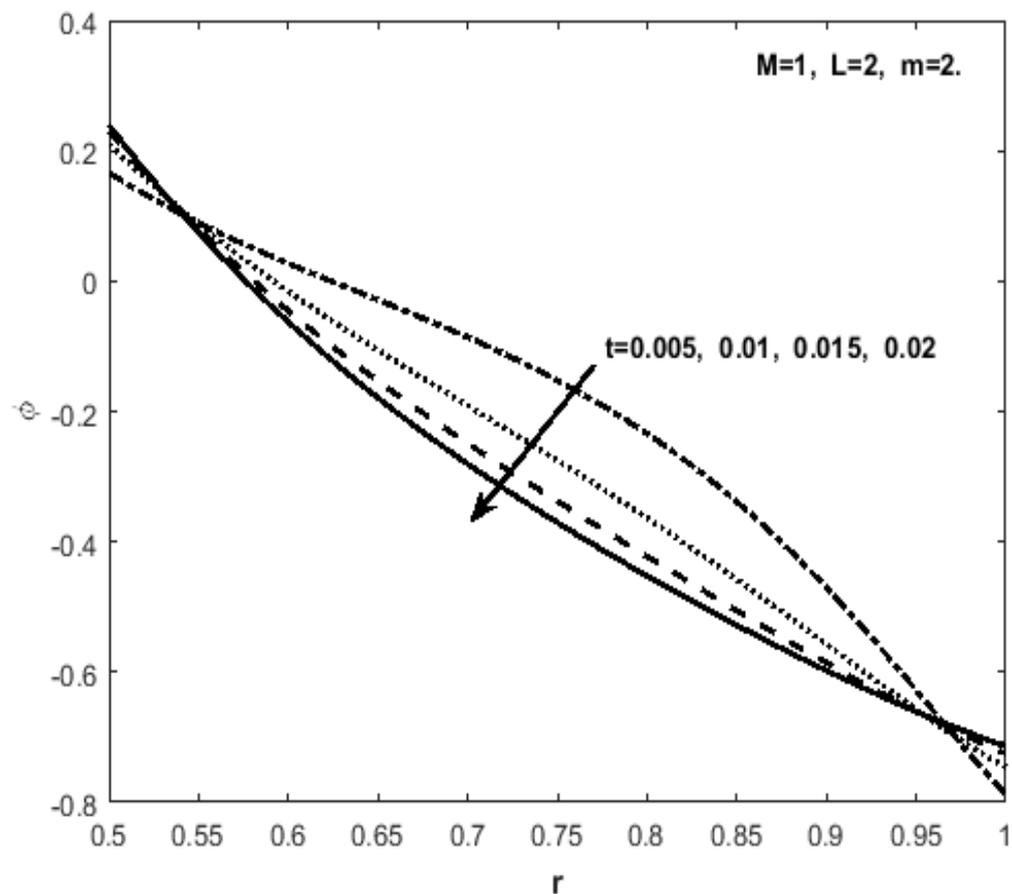
FIGURE 4.10: Change in the porosity Vs various values of the normalized time t. In plotting these curves, values of time have been changed from 0.005 to 0.02 with a regular step.

This finding shows a sensation of growth rate of medium's porosity with time.

Figure 4.11 presents solid deformation as a function of radius of porous shell for various times. It can be observed that a consolidation region is formed which grows with time. A change in solid displacement is reached to a value 0.071, at $t = 0.02$,

which corresponds to a maximum solid deformation achieved by the deformable shell in this plot.
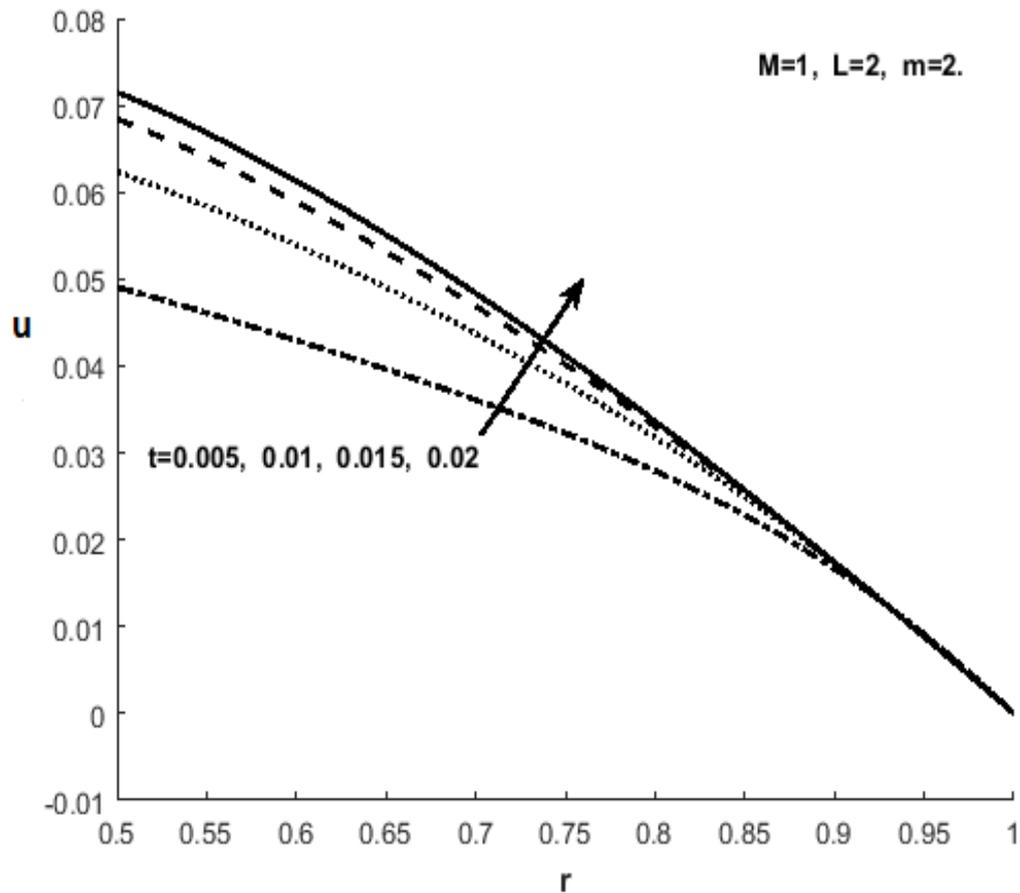
FIGURE 4.11: Solid deformation Vs various values of normalized time t.

In Figures 4.12 and 4.13 porosity and solid deformation are plotted against the radius of a thin wall (i.e. $0.8 \leq r \leq 1$) deformable porous shell, respectively. We considered four different values of the magnetic parameter M in plotting different curves in this graph.

The equilibrium state is achieved in a thin wall shell much faster as compared to the thick wall shell. This was the main reason due to which maximum value of the time taken in this graph is 0.00125, because for greater values of the time shell moves toward equilibrium much faster. Almost, a uniform behavior can be seen in both the cases when the magnetic parameter M exceeds from 1. This particular

behavior was due to the wall thickness, because the shell is essentially thin enough to react as a uniform elastic medium through out the course of compression.
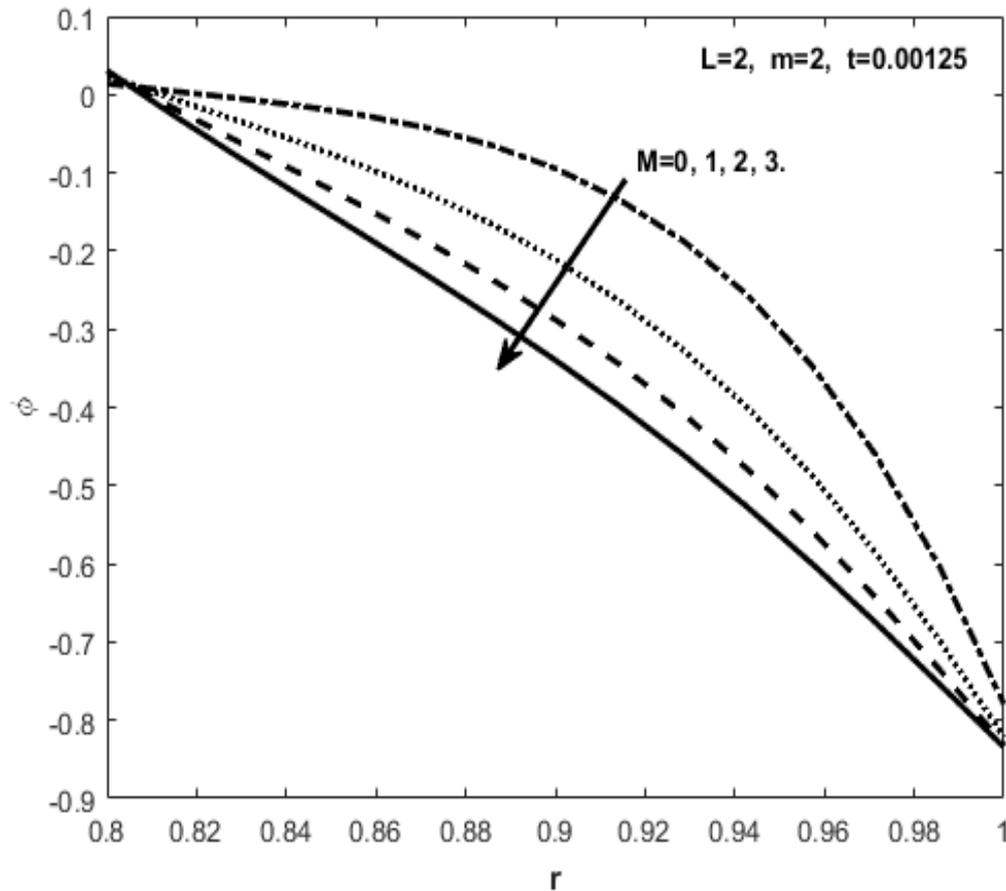
FIGURE 4.12: Variation in the porosity Vs various values of the magnetic parameter M.

This fact shows the a small value of the magnetic parameter is sufficient for establishing high resistance for a thin wall deformable porous shell. From the analysis of boundary thickness of the elastic porous media, it is clear that equilibrium controlled by the boundaries of elastic shell through which fluid flow occurred. Particularly, when loading imposed on the wall, thin shell react more faster as compared to the thick wall shell. This fact is due to the filtration of micromolecules associated with the flow dynamics that have been draped within the porous medium of shell when wall thickness was taken large enough to manage the applied compression.
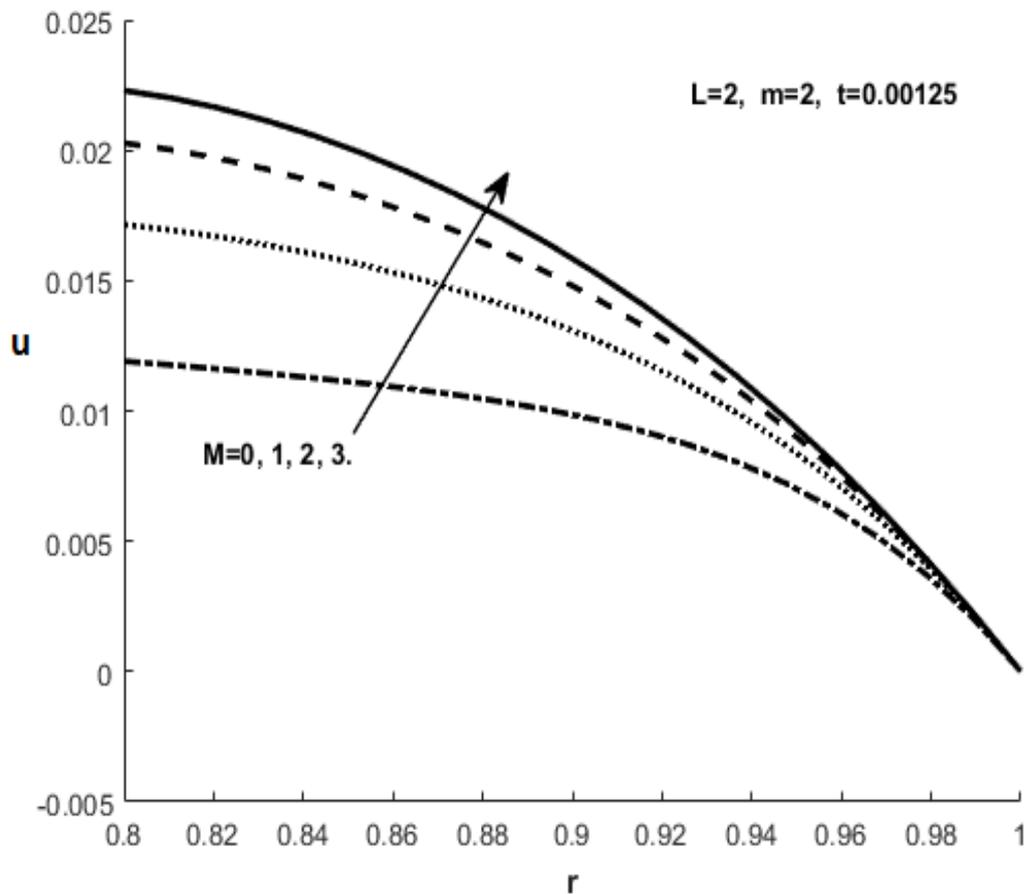
FIGURE 4.13: Solid deformation Vs different values of magnetic parameter M.

In the following, concluding remarks of the present study are given.

4.4 Conclusion

Results have already summarized in different sections, here we only point out some main features of the present study. It has been noticed that the applied pressure has sufficient effects on the fluid flow dynamics as compared to the inertial forces. A system of coupled non-linear partial differential equations is obtained which prescribed the physics of the geometry. Generally, the system was derived for planar, cylindrical, and spherical geometries. By changing the value of a single parameter $(\beta = 0, 1, 2)$, switched the governing system from planar to radial geometry. In the case of a steady-state problem, an exact solution is given. The graphical results

are used to explore the effects of magnetic parameter and normalized time range both on the porosity and solid deformation.

The magnetic parameter not only controlled the growth rate of the porosity and solid deformation also affects the equilibrium in loading circumstances. By increasing the magnitude of the magnetic parameter reported the opposite effects that were reported for the normalized time on the solid deformation. In the case of thin wall elastic porous shell more profound effects of the time and magnetic field have been noticed on flow dynamics due to attaining the equilibrium much faster. A comparison between fluid flows through different geometries legitimated the fact that planar geometry experienced more loading effects as compared to the cylindrical and spherical geometries.

The theoretical framework based upon which we derived the governing dynamics in the present study having sufficient background both in the biological and non-biological settings. The binary mixture theory approach reported by many researched in describing the fluid flow dynamics through soft tissues as well as fluid flux through deformable porous materials. This theory successfully address flow behavior for constant and strain dependent permeability through many types of elastic porous solids. The present study will helps in understanding the magnetic effects on the flow of charged fluid through planar, cylindrical, and spherical geometries. The theoretical results of the present study are further improve by incorporating different physical parameters like gravity, inertial forces, etc. In this study, these effects have been ignored due to their small contribution and can be included in the modeling where the interactions of such effects play critical role in future work for industrial applications.

Chapter 5

Radial Flow of non-Newtonian Fluid through Deformable Porous Shells and its Impact on Porosity and Solid Deformation

5.1   Introduction

In this Chapter, we have incorporated power-law model in the governing equations of continuum mixture theory for a radial fluid flow through an elastic porous shell. The main motivation in this study was in modeling the influence of different grades fluids on the solid deformation produced in an elastic shell. A parabolic type partial differential equation is derived for the porosity along with an integral equation containing the solid deformation. The numerical solution is computed for the transient case, whereas, an exact solution is provided for the steady state problem. Graphical outcomes highlights the influence of power-law fluids, normalized time, and wall thickness on the equilibrium achieved by the elastic porous shell during loading circumstances. Furthermore, changes occurred in the porosity and solid displacement are reported for planar, cylindrical, and spherical geometries.

In fact, majority of the fluids like air, water and oils, have been treated as Newtonian in engineering and scientific research. However, in many cases, assumption of Newtonian behavior not remain valid and reported more complex non-Newtonian response while driving the governing behavior [123]. Particularly, these types of situations arise in the chemical engineering process involved in preparation of different products and plastics processing industry. Moreover, non-Newtonian behavior is also encountered in the mining industry, where slurries and mud are often handled, and in applications of fluids lubrication through soft biological tissues where a variety of non-Newtonian fluids exist. The simulation of non-Newtonian fluid flow phenomena is therefore of importance to industry as well as biomedical science. Furthermore, surfactant used in controlling heating and cooling systems in advanced technology having great importance for energy savings [124]. In incorporating the non-Newtonian behavior into a dye-streak, an effective flow tracer has been molded. These types of tracers having great importance because they allow both turbulent and separated flows. These non-Newtonian tracers have been developed based upon the idea of drag-reduction technology. The basic concept is to incorporate the shear induced state. These tracer fluids can be ejected into the turbulent flow as a dye-streak that resists dispersion as well as breakup in the flow path. In the case of Newtonian fluids, the multiphasic deformation has been derived in understanding the dynamics of inkjet printing [125], Earth sciences [126], and fluid flow through the soft biological tissues [93, 127], etc. Barry and Aldis [50] have been formulated the problem of radially directed fluid flow through an elastic porous shell. This study used the Newtonian flow behavior while driving the governing dynamics. They derived nonlinear diffusion equations applicable to spherical, cylindrical and planar geometries. For the case steady flow, they calculated an exact integral along with the perturbation solutions for some special cases. In case of unsteady flow, perturbation methods have been used in finding small time solutions with a solution valid for slow rate of compression. These solutions have been used while investigating the deformation of the porous material along with the comparisons of fluid flows through the planar and radial geometries. In this Chapter, we extended Barry and Aldis [50] work by incorporating

non-Newtonian flow dynamics using power-law model.

We have formulated the non-Newtonian fluid flow through an elastic porous shell using mixture theory approach. The main focus in this study was in exploring the fluid flow behavior through planar and radial geometries, particularly, for the non-Newtonian fluids cases. The continuum mixture theory approach has been used in modeling the Newtonian [74, 100, 128] as well as non-Newtonian [129, 130] flows dynamics through the deformable porous materials. In the present Chapter, we incorporated power-law index in the basic constitutive equations of binary mixture and developed a mathematical model describing the passage of non-Newtonian fluids through a deformable porous shell. In the following, a summery of work presented in the present Chapter is given.

Section 5.2 contains the mathematical formulation of governing dynamics. In section 5.3.1, the steady state solution of governing system of equation is computed, whereas, section 5.3.2 devoted for the numerical solutions of time dependent problem. At the end, section 5.4 contains the concluding remarks.

5.2 Theory and Model

The mathematical model is developed on the basis of continuum mixture theory. In this type of modeling, fluid is considered to be incompressible and occupies each material point within the mixture. The components of the mixture are assumed elastic, homogeneous, anisotropic, and individually incompressible. The historical development of our modeling is based on the mixture theory given by Bowen [11]. A more elaborated version of this theory was discussed by Atkin and Crain [10]. However, most recent developments in the governing equations can be found in the book written by Rajagopal and Tao [12] as well.

Recently, this modeling approach is employed by Barry and Aldis [100] and Mow *et al* [54, 56], in deriving the dynamics of fluid flow through biological tissues. The necessary and relevant details of the modeling technique that we used in

formulating the solid deformation in the present article is based on the study of Barry and Aldis [50] for Newtonian fluids, and Siddique and Anderson [130] for the power-law fluids. The details of constitutive equations of the mixture theory are given in the Chapter 1. The classical laws of mass conservation for each phase given in equation (2.20) can be added to give the following equation

$$\nabla \cdot \mathbf{v} = 0, \tag{5.1}$$

where $\boldsymbol{v} = \phi^s \boldsymbol{v}^s + \phi^f \boldsymbol{v}^f$ is known as composite velocity or macroscopic velocity, s and f correspond to solid and fluid phases, respectively. Form equation (2.21), momentum balance after ignoring the inertial forces for small velocity and infinitesimal solid deformation along with negligible body force can be written as

$$\nabla \cdot \boldsymbol{T}^\alpha = -\boldsymbol{\pi}^\alpha, \tag{5.2}$$

where $\boldsymbol{T}^\alpha$ is the stress tensor $(\alpha = s, f)$. However, in the rest of the derivation, we considered that $\sigma^f = 0$ and $\sigma^s = \sigma$, for detail see [50, 66, 131]. Using this assumption, equations (2.22) and (2.23) can be written as

$$\boldsymbol{T}^s = -\phi^s p \boldsymbol{I} + \boldsymbol{\sigma}, \qquad \boldsymbol{T}^f = -\phi^f p \boldsymbol{I}, \tag{5.3}$$

and

$$-\boldsymbol{\pi}^s = K(v^s - v^f)^n - p\nabla\phi^s, \qquad \boldsymbol{\pi}^f = K(v^s - v^f)^n - p\nabla\phi^s. \tag{5.4}$$

Inserting equations (5.3) and (5.4) into (5.2), we get

$$-\nabla \cdot (\phi^s p \boldsymbol{I}) + \nabla \cdot \boldsymbol{\sigma} = K(\boldsymbol{v}^s - \boldsymbol{v}^f)^n - p\nabla\phi^s, \tag{5.5}$$

and

$$-\nabla \cdot (\phi^f p \boldsymbol{I}) = -K(\mathbf{v}^s - \mathbf{v}^f)^n + p\nabla\phi^s, \tag{5.6}$$

where n corresponds to the power-law index, K is the drag coefficient, p is the fluid pressure, $\boldsymbol{\sigma}$ is the solid stress, and $\mathbf{I}$ is identity tensor. Equation (5.5) and (5.6)

can be rewritten as

$$-\nabla(\phi^s p) + \nabla \cdot \boldsymbol{\sigma} = K(\boldsymbol{v}^s - \boldsymbol{v}^f)^n - p\nabla\phi^s, \tag{5.7}$$

and

$$-\nabla(\phi^f p) = -K(\boldsymbol{v}^s - \boldsymbol{v}^f)^n + p\nabla\phi^s. \tag{5.8}$$

After some algebraic simplifying, yields

$$\nabla \cdot \boldsymbol{\sigma} = K(\boldsymbol{v}^s - \boldsymbol{v}^f)^n + \phi^s \nabla p, \tag{5.9}$$

and

$$\mathbf{0} = -K(\boldsymbol{v}^s - \boldsymbol{v}^f)^n + \phi^f \nabla p. \tag{5.10}$$

Eliminating the fluid pressure p from equations (5.9) and (5.10), we get

$$\nabla \cdot \boldsymbol{\sigma} = \frac{K}{\phi^f}(\mathbf{v^s} - \mathbf{v^f})^{\mathbf{n}}. \tag{5.11}$$

From the expression of macroscopic velocity relation $(\boldsymbol{v} = \phi^s\boldsymbol{v}^s + \phi^f\boldsymbol{v}^f)$, we have

$$\mathbf{v}^f = \frac{\boldsymbol{v} - \phi^s\boldsymbol{v}^s}{\phi^f}. \tag{5.12}$$

From equation (5.12) and (5.11), we get

$$\nabla \cdot \boldsymbol{\sigma} = \frac{1}{k}(\frac{\partial \boldsymbol{u}}{\partial t} - \boldsymbol{v})^n, \tag{5.13}$$

where $k = \frac{(\phi^f)^{n+1}}{K}$ (k is the permeability), and $\boldsymbol{v}^s = \frac{\partial u}{\partial t}$ (u is the solid displacement). In the following, the relation between the fluid pressure (p) and stress can be found using equations (5.9) and (5.10)

$$\nabla p = \nabla \cdot \sigma \tag{5.14}$$

Equation (5.13) is well explained in physical terms by considering the Darcy's law and expressing it relative to the movement of solid, whereas, the equilibrium equation of elasticity ($\nabla p = \nabla \cdot \sigma$) is governed by stress in the solid matrix. From

equations (5.13) and (5.14), we get

$$\nabla p = \nabla \cdot \sigma = \frac{1}{k}\left(\frac{\partial \mathbf{u}}{\partial t} - \mathbf{v}\right)^n. \tag{5.15}$$

In the case of cylindrical geometry, the only radial components of displacement and velocity are considered non-zero, whereas, the permeability parameter (k) depends upon the change in the porosity (ϕ) of the shell. The permeability parameter that justifies material properties of the present problem [50] is of the following form

$$k = k_0 \cdot e^{m \cdot \phi}, \tag{5.16}$$

where k_0 and m are material constants. The constitutive relation for the divergence of stress in the radial direction can be written as

$$(\nabla \cdot \boldsymbol{\sigma})_r = \frac{\partial \sigma_{rr}}{\partial r} + \beta \left(\frac{\sigma_{rr} - \sigma_{\theta\theta}}{r}\right). \tag{5.17}$$

It is important to mention here that the parameter β is used to specify different geometries, i.e., $\beta = 0$ (planar), $\beta = 1$ (cylindrical), and $\beta = 2$ (spherical). So, by changing the value of β, we switch from one geometry to the other in a single governing partial differential equation. Inserting equations (2.24) and (2.25) into (5.17), we get

$$(\nabla \cdot \sigma) = H_a \left[\frac{\partial^2 u}{\partial r^2} - \beta \left(\frac{r\frac{\partial u}{\partial r} - u}{r^2}\right)\right], \tag{5.18}$$

where $H_a = \lambda + 2\mu$ is the aggregate modulus. From equation (5.18), we have

$$(\nabla \cdot \boldsymbol{\sigma})_r = H_a \frac{\partial}{\partial r}\left[\frac{1}{r^\beta}\frac{\partial}{\partial r}(r^\beta u)\right] = H_a \frac{\partial \phi}{\partial r}, \tag{5.19}$$

and

$$\phi = \frac{1}{r^\beta}\frac{\partial}{\partial r}(r^\beta u). \tag{5.20}$$

We considered that the fluid flow depends upon the loading imposed on the inner radius of the shell. So, fluid flow and solid deformation are large enough in the direction of applied pressure only. This restriction leads the problem into a unidirectional framework. Now, what follows is to convert the vector forms of the

equations into uni-directional form. In this setting, equation (5.1) can be written as follows

$$\frac{\partial v}{\partial r} = 0. \tag{5.21}$$

Integrating equation (5.21), yields

$$v_r = \frac{v(t)}{r^\beta}, \tag{5.22}$$

where $v(t)$ is a constant of integration. Using the value of v_r from equation (5.22) into equation (5.15), we get

$$\frac{\partial p}{\partial r} = (\nabla \cdot \boldsymbol{\sigma})_r = \frac{1}{k}\left(\frac{\partial u}{\partial t} - \frac{v(t)}{r^\beta}\right)^n. \tag{5.23}$$

From equations (5.19), (5.20) and (5.23), we get

$$\frac{\partial p}{\partial r} = H_a\frac{\partial}{\partial r}\left(\frac{1}{r^\beta}\frac{\partial}{\partial r}(r^\beta u)\right) = \frac{1}{k}\left(\frac{\partial u}{\partial t} - \frac{v(t)}{r^\beta}\right)^n. \tag{5.24}$$

In equation (5.24), $v(t)$ is a constant. It seems quite easy for the solution point of view to model the problem in pressure govern dynamics as compared to the velocity, because it is easy to find the driving pressure. This requires to eliminate unknown constant $v(t)$ from equation (5.24). For this, we defined following transformation

$$L(\omega) = \frac{1}{r^\beta}\frac{\partial}{\partial r}(r^\beta\omega). \tag{5.25}$$

Using transformation (5.25) on the equation (5.24), we get

$$\frac{1}{r^\beta}\frac{\partial}{\partial r}\left[r^\beta\left(H_ak(\phi)\frac{\partial}{\partial r}\left(\frac{1}{r^\beta}\frac{\partial}{\partial r}(r^\beta u)\right)\right)^{-\frac{1}{n}}\right] = \frac{\partial}{\partial t}\frac{1}{r^\beta}\frac{\partial}{\partial r}(r^\beta u) - \frac{1}{r^\beta}\frac{\partial}{\partial r}\left(r^\beta(\frac{v(t)}{r^\beta})\right). \tag{5.26}$$

Now, equation (5.26) become velocity free, because it is independent of r. From equations (5.20) and (5.26), we get

$$\frac{\partial \phi}{\partial t} = \frac{1}{r^\beta}\frac{\partial}{\partial r}r^\beta\left(H_ak(\phi)\frac{\partial \phi}{\partial r}\right)^{-\frac{1}{n}}. \tag{5.27}$$

The partial differential equation (5.27) is the required governing equation for the

porosity ϕ. Now, what follow is to outline the boundary conditions required for completing the governing equation (5.27) both for planar and radial geometries.
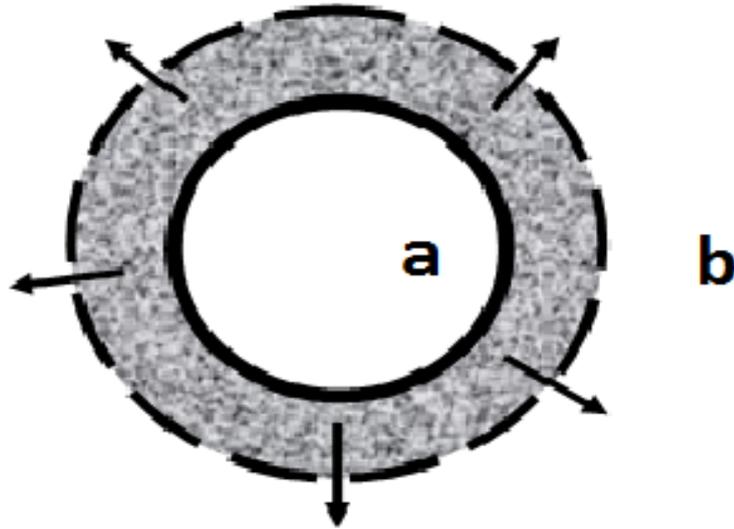
FIGURE 5.1: The non-Newtonian fluids flow through an elastic porous shell was consider in this Chapter. The outer boundary of the shell is considered rigid mesh that offers negligible resistance during passage of the fluid.

Figure 5.1 shows the fluid flow outwardly through the central part of spherical or cylindrical an elastic porous shell. We assumed that inner radius of the shell is a, whereas, b is used to represent outer radius $(b > a)$. The displacement boundary condition at the porous mesh is $u = 0$, at $r = b$. The boundary condition for ϕ can be derived using the equation (5.20) as follows

$$\phi(b,t) = \frac{\partial u}{\partial r}(b,t). \tag{5.28}$$

The inner boundary at $r = a$ can be written as [50]

$$\sigma_{rr}(a,t) = 0. \tag{5.29}$$

Simplifying equation (5.29), we get

$$\left[\frac{\partial u}{\partial r} + \beta \lambda_r \frac{u}{r} \right]_{r=a} = 0, \tag{5.30}$$

where $\lambda_r = \frac{\lambda}{(\lambda+2\mu)}$. In term of ϕ, we have following equation

$$\phi(a,t) = \frac{\beta}{a}u(a,t)(1-\lambda_r).\tag{5.31}$$

Integrating equation (5.20), we get

$$u(r,t) = -\frac{1}{r^\beta}\int_r^b r^\beta\phi(r,t)dr.\tag{5.32}$$

Equation (5.32) is the required governing equation for the solid displacement (u). Substituting the value of u from equation (5.32) into (5.31) and changing the limit of integration, we get

$$\phi(a,t) + \beta\frac{(1-\lambda_r)}{a^{1+\beta}}\int_a^b r^\beta\phi(r,t)dr = 0.\tag{5.33}$$

The boundary condition at the outer boundary $(r = b)$ can be written as

$$\phi(b,t) = \phi(a,t) - \frac{\Delta P(t)}{H_a},\tag{5.34}$$

where $P(t)$ is used for the pressure function. Equations (5.33) and (5.34) are boundary conditions for partial differential equation (5.27). We follow [131], to find the potentially important position of the inner boundary (a) that is usually of the following form

$$a = a^0 + u(a^0,t),\tag{5.35}$$

where a_0 is the initial boundary position, and a is the new position that is found once displacement u is known which we computed numerically, later on. In solving the governing equation, many researchers applied the boundary condition at the original position (initial position) instead of the new position by considering the moving domain. On the other hand, the initial deformation is not large enough to change the permeability parameter, so, it is seems physical to take $k = 1$ for this particular situation. This justification allows us to take the boundary condition $r = a$ instead of $r = a(t)$, because we are using infinitesimal theory to model the problem of fluid-solid interaction. We assumed that medium not deformed enough

away from the initial position. So, the non-linear moving boundary is not subject of the present study and left for the future work. On the other hand, our main focus in this study was in exploring the affects of power-law index on the porosity and solid displacement during passage of fluid flow through deformable porous shell. However, there is the possibility of error associated with the numerical approximation due to the moving non-linear boundary. These problems are well fixed by experimental study, which we are unable to perform due to the lack of resources. From the modeling and solution point of view, we justify the present work by comparing the results with Barry and Aldis [50], in solution section. We have reproduced their graphical results for both porosity and solid deformation.

Below, we introduced the dimensionless variables that were used in converting the governing system of equations into dimensionless form

$$P = H_a \phi_0 \hat{P}, \quad r = b\hat{r}, \quad k = k_0 \hat{k}, \quad u = u_0 \hat{u}, \quad a = b\hat{a}, \quad \phi = \phi_0 \hat{\phi}, \quad t = t_0 \hat{t}, \tag{5.36}$$

where p_m is the typical pressure. Using these choices in the governing system of equations, we get

$$\frac{\partial \hat{\phi}}{\partial \hat{t}} = \frac{t_0}{\hat{r}^\beta} \frac{\partial}{\partial \hat{r}} \hat{r} \left[\hat{k} \frac{\partial \hat{\phi}}{\partial \hat{r}} \right]^{-\frac{1}{n}}, \tag{5.37}$$

$$\hat{u}(\hat{r}, \hat{t}) = -\frac{Q}{\hat{r}^\beta} \int_{\hat{r}}^1 \hat{r}^\beta \hat{\phi}(\hat{r}, \hat{t}) d\hat{r}, \tag{5.38}$$

$$\hat{\phi}(\hat{r}, \hat{t}) = \frac{1}{Q\hat{r}^\beta} \frac{\partial}{\partial \hat{r}} (\hat{r}^\beta \hat{u}(\hat{r}, \hat{t})), \tag{5.39}$$

$$\hat{\phi}(\hat{a}, \hat{t}) = -R\beta \frac{(1 - \lambda_r)}{\hat{a}^{1+\beta}} \int_{\hat{a}}^1 r^\beta \hat{\phi}(r, \hat{t}) d\hat{r}, \tag{5.40}$$

$$\hat{\phi}(\hat{b}, \hat{t}) = \hat{\phi}(\hat{a}, \hat{t}) - \Delta \hat{P}, \quad \hat{b} = 1. \tag{5.41}$$

In the following, we gave the dimensionless parameters that appeared during non-dimensionalizing the governing equations.

$$t_0 = \frac{b^{n + \frac{1}{n}}}{H_a^{-\frac{1}{n}} k_0^{-\frac{1}{n}} (\phi_0)^{\frac{1-n}{n}}}, \quad Q = \frac{r^{\beta+1} \phi_0}{u_0 r^\beta}, \quad R = \frac{r^{\beta+1}}{b^{\beta+1}}. \tag{5.42}$$

Now, we have a system of equations ((5.37)-(5.39)) along with boundary conditions ((5.40)-(5.41)). In the following section, details of the solutions are given.

5.3   Solution Methodology

For the solution point of view, we have considered two different values of the inner radii of the shell, i.e., $a = 0.5$ (thick wall shell) and $a = 0.8$ (thin wall shell). The motivation of behind this consideration was to study the effects of wall thickness on both the porosity and solid deformation.

In the next sections, we first discuss the steady state solution of the governing system of partial differential equations that is followed by the numerical solution of the unsteady problem.

5.3.1   Steady Solution

For the steady-state case, equation (5.37) can be written as

$$\frac{1}{r^\beta}\frac{d}{dr}r^\beta\left(k\frac{d\phi}{dr}\right)^{-\frac{1}{n}} = 0. \tag{5.43}$$

If $k = 1$, the general solution of differential equation (5.43) can be written as

$$\phi(r) = \frac{c_1}{1-n\beta}r^{1-n\beta} + c_2. \tag{5.44}$$

From equations (5.39) and (5.44), we get

$$u(r) = \frac{c_1 r^{2-n\beta}}{(1-n\beta)(2+\beta(1-n))} + \frac{c_2}{1+\beta}r + \frac{c_3}{r^\beta}, \tag{5.45}$$

where c_1, c_2 and c_3 are constants of integration which we find using the following boundary conditions

$$\phi(a) = -\beta\frac{(1-\lambda_r)}{a^{1+\beta}}\int_a^1 r^\beta\phi(r)d\hat{r}, \tag{5.46}$$

and

$$\phi(1) = \phi(a) - \Delta P, \quad u(1) = 0, \tag{5.47}$$

where $\lambda_r = 0.5$, and $\Delta P = 1$. Using boundary conditions (5.46) and (5.47) for $\beta = 0$ (planar geometry) into equation (5.44), we get

$$c_1 a + c_2 = 0, \quad c_1(b=1) + c_2 = -1. \tag{5.48}$$

After some algebraic simplification, we get

$$c_1 = \frac{1}{a-1}, \quad c_2 = \frac{a}{1-a}. \tag{5.49}$$

Using the rigid boundary condition for solid displacement $(u(1) = 0)$, yields

$$c_3 = \frac{2a-1}{2(a-1)}. \tag{5.50}$$

For cylindrical geometry $\beta = 1$, we have

$$\frac{c_1}{1-n}a^{1-n} + c_2 = -\frac{1}{2a^2}\int_a^1 r\phi(r)dr, \quad \frac{c_1}{1-n}b^{1-n} + c_2 = -\frac{1}{2a^2}\int_a^1 r\phi(r)dr - 1. \tag{5.51}$$

After some mathematical manipulation, we get

$$c_1 = \frac{1-n}{a^{1-n}-1}, \quad c_2 = \frac{-2(1+(5-2n)a^{3-n})}{(3-n)(a^{1-n}-1)(3a^2+1)} \tag{5.52}$$

From equations (5.45) and (5.52) at $u(1) = 0$, gives

$$c_3 = \frac{(1+(5-2n)a^{3-n}) - (3a^2-1)}{(3-n)(3a^2+1)(a^{1-n}-1)}. \tag{5.53}$$

Similarly, we can find values of constants, c_1, c_2 and c_3 for spherical geometry($\beta = 2$) as follows

$$c_1 = \frac{1-2n}{a^{1-2n}-1}, c_2 = \frac{-3(1+(3-2n)a^{4-2n})}{(4-2n)(a^{1-2n}-1)(2a^3+1)}, c_3 = \frac{(1+(3-2n)a^{4-2n}) - (2a^3-1)}{(4-2n)(2a^3+1)(a^{1-2n}-1)}. \tag{5.54}$$

Exact solution of the porosity can be written as

$$\phi(r) = \frac{r}{a-1} + \frac{a}{1-a}, \qquad\qquad\qquad \beta = 0, \qquad (5.55)$$

$$\phi(r) = \frac{r^{1-n}}{(a^{1-n}-1)} - \frac{2(1+(5-2n)a^{3-n})}{(3-n)(a^{1-n}-1)(3a^2+1)}, \qquad \beta = 1, \qquad (5.56)$$

$$\phi(r) = \frac{r^{1-2n}}{(a^{1-2n}-1)} - \frac{3(1+(3-2n)a^{4-2n})}{(4-2n)(a^{1-2n}-1)(2a^3+1)}, \qquad \beta = 2. \qquad (5.57)$$

The exact solution of solid deformation can be written as

$$u(r) = \frac{1}{2(a-1)}r^2 + \frac{a}{1-a}r + \frac{2a-1}{2(a-1)}, \qquad\qquad \beta = 0, \qquad (5.58)$$

$$u(r) = \frac{r^{2-n}}{(3-n)(a^{1-n}-1)} - x_1 r + x_2\frac{1}{r}, \qquad\qquad \beta = 1, \qquad (5.59)$$

$$u(r) = \frac{r^{2-2n}}{(4-2n)(a^{1-2n}-1)} - x_3 r + x_4\frac{1}{r^2}, \qquad\qquad \beta = 2. \qquad (5.60)$$

where

$$x_1 = \frac{(1+(5-2n)a^{3-n})}{(3-n)(a^{1-n}-1)(3a^2+1)}, \quad x_2 = \frac{(1+(5-2n)a^{3-n} - (3a^2-1))}{(3-n)(a^{1-n}-1)(3a^2+1)},$$
$$(5.61)$$
$$x_3 = \frac{(1+(3-2n)a^{4-2n})}{(4-2n)(a^{1-2n}-1)(2a^3+1)}, \quad x_4 = \frac{(1+(3-2n)a^{4-2n} - (2a^3-1))}{(4-2n)(a^{1-2n}-1)(2a^3+1)}.$$
$$(5.62)$$

In the following, we have presented the solutions of equations (5.55)-(5.57) and (5.58)-(5.60) graphically.

Figures 5.2 and 5.3 show change in the porosity and solid displacement, respectively. In plotting these curves, we have considered different numerical values of the power law index.

It has been noticed that the changes in porosity and displacement occurred in accordance with the value of n. The porosity decreased, whereas, solid deformation increased while increasing the value of the power-law index. In fact, pores ratio of the deformable porous shell and solid deformation show an inverse behavior for a same value of n. This particular result leads to the fact that more resistance is

experienced by elastic porous shell when viscosity of the fluid passing through it increased.

The application of expansion from the inner section of the medium for small period of time linked to the dynamics of solid and non-Newtonian fluid interaction. One has to be careful while choosing the permeability relation that provides the meaningful values for expanded medium, and an unclear situation whether permeability should be function of porosity ϕ or radial strain $\frac{du}{dr}$. If the medium is random than it is appropriate to consider permeability as a function of porosity.
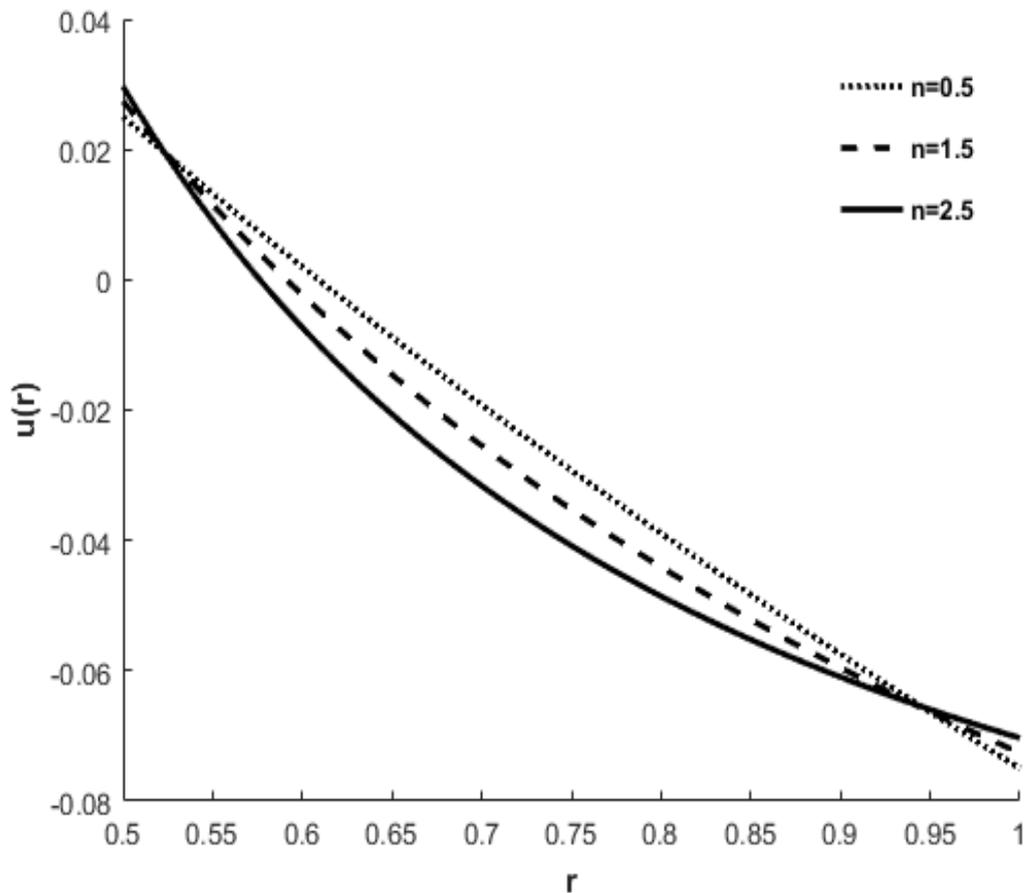

FIGURE 5.2: Change in the porosity Vs various values of power-law index n

The graphical results in this section show the variation in porosity and solid displacement for $k = 1$, however, nonlinearity during passage of fluids through the elastic porous shell is reported due to non-Newtonian nature of the fluids.
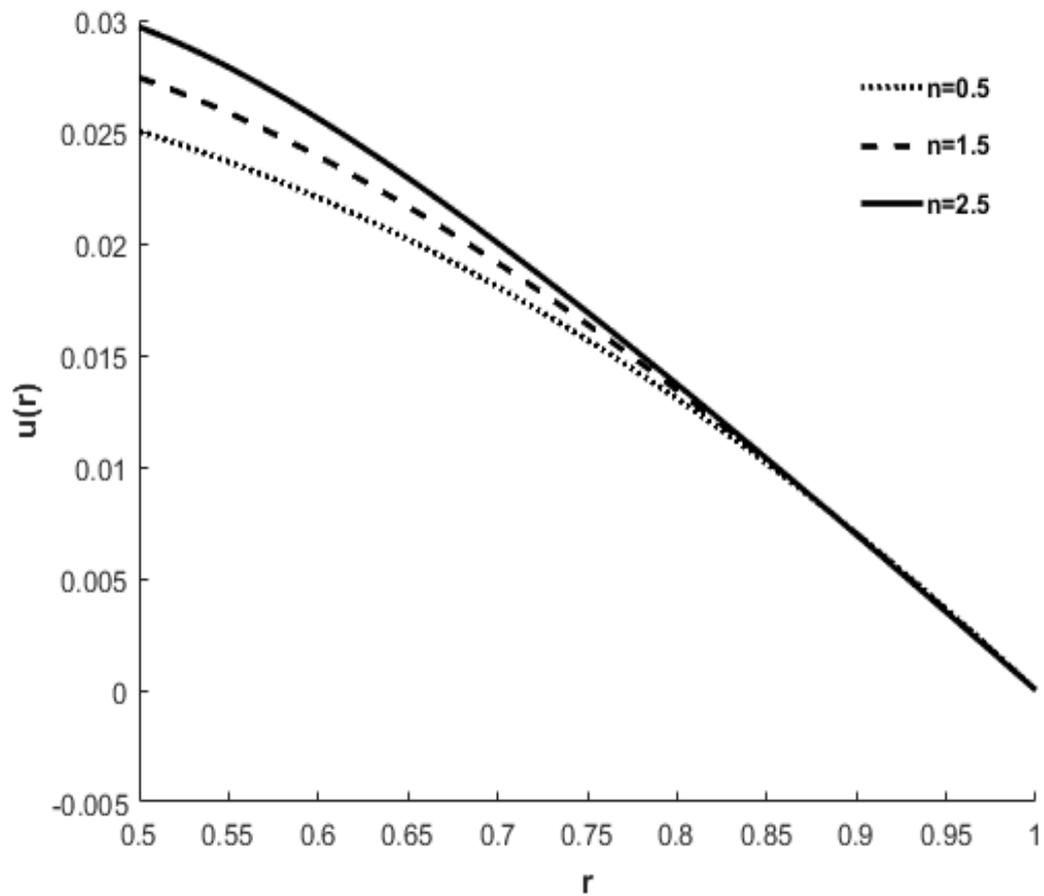
FIGURE 5.3: Variation in the solid displacement of cylindrical shell Vs various values of power-law index n.

These results described the fluid flow through different geometrical constraint that help in understanding flow behavior through planar and radial geometries. In the following section, time dependent solution of the governing system of equations is given.

5.3.2 Unsteady Solution

In this section, we presented the numerical solution of the governing partial differential equation for a unsteady problem. We have solved the equation (5.37) using numerical scheme method of lines. MOL is convergent semi-analytic numerical technique that requires to approximate the spatial derivatives using the finite

difference; however, the time variable remains continuous. The resulting system of ordinary differential equations (ODEs) that are approximated from the given PDE is solved using MATLAB ODE solver. It has been already discussed with detail the convergence of MOL on the parabolic types PDEs in Chapter 2. Now, partial differential equation (5.37) can be written as

$$\frac{\partial \hat{\phi}}{\partial \hat{t}} = \frac{1}{\hat{r}^{\beta}} \frac{\partial}{\partial \hat{r}} \hat{r}^{\beta} \left[\frac{\partial \hat{\phi}}{\partial \hat{r}} \right]^{-\frac{1}{n}}. \tag{5.63}$$

Simplifying and dropping over hat, yields

$$\frac{\partial \phi}{\partial t} = \left(\frac{\partial \phi}{\partial r} \right)^{\frac{1-n}{n}} \left[n \cdot \left(\frac{\partial^2 \phi}{\partial r^2} \right) + \frac{\beta}{r} \left(\frac{\partial \phi}{\partial r} \right) \right]. \tag{5.64}$$

The set of boundary and initial conditions are as follows

$$\phi(a, t) = -(1 - \lambda) \frac{\beta}{a^{\beta+1}} \int_a^1 r^{\beta} \phi(r, t), \tag{5.65}$$

$$\phi(b, t) = \phi(a, t) - \Delta P, \tag{5.66}$$

$$\phi(r, 0) = 0.001 e^{-r}. \tag{5.67}$$

In solving above system of equations, we have considered a step change in the pressure function ($\Delta P = 1$). The contribution of initial condition is purely dependent upon the radial direction. More precisely it is exponentially decreasing with the radius (r). By setting power-law index $n = 1$, we have recovered the governing equation as was in [50], which is the validation of our modeling. We employed the following approximation in computing the spatial derivatives involved in equation (5.64).

$$\frac{\partial \phi}{\partial r} \approx \frac{u_{j+1} - u_{j-1}}{2 \cdot h}, \quad \frac{\partial^2 \phi}{\partial r^2} \approx \frac{u_{j+1} - 2 \cdot u_j + u_{j-1}}{h^2} \tag{5.68}$$

These approximation allow us to rewrite equation (5.64) as follows

$$\frac{\partial \phi}{\partial t} = \left[\frac{u_{j+1} - u_{j-1}}{2 \cdot h} \right]^{\frac{1-n}{n}} \left[n \cdot \left(\frac{u_{j+1} - 2 \cdot u_j + u_{j-1}}{(h)^2} \right) + \frac{\beta}{r} \left(\frac{u_{j+1} - u_{j-1}}{2 \cdot h} \right) \right], \tag{5.69}$$

where $h = \frac{(b-a)}{m}$ also $j = a, a + h, a + 2h, \cdots a + (m-1)h, a + mh = b$, where m

corresponds to the numbers of mesh (nodes) points. A simple trapezoidal rule is given as follows

$$f(x) = \frac{h}{2}\left(f(x_0) + 2(f(x_1) + f(x_2) \cdots f(x_{m-1}) + f(x_m))\right). \tag{5.70}$$

The boundary condition (5.65) using the rule define in (5.70) takes the following form

$$\phi(a, t) = \frac{-4a^\beta}{(1 + 4a^\beta)} x_5, \tag{5.71}$$

where

$$x_5 = [2((a+h)\phi(a+h, t) + \cdots (a + (m-1)h)\phi(a + (m-1)h, t) + b\phi(b, t))].$$

The right boundary condition (5.66) can be written as

$$\phi(b, t) = \frac{-4a^\beta}{(1 + 4a^\beta)} x_6, \tag{5.72}$$

where

$$x_6 = [2((a+h)\phi(a+h, t) + \cdots (a + (m-1)h)\phi(a + (m-1)h, t) + b\phi(b, t))] - 1.$$

The governing equation (5.69) together with the boundary conditions (5.71) and (5.72) was used in finding the porosity (ϕ), numerically. On the other hand, solid deformation can be found using following equation

$$u(r, t) = -\frac{1}{r^\beta} \int_r^1 r^\beta \phi(r, t) dr. \tag{5.73}$$

It is worth mentioning; equation (5.73) can only be solve when solution of porosity is available. In the following, we presented graphical results for porosity and solid displacement. We explore the influence of different physical parameters on the porosity and solid deformation along with the compression between the Newtonian and non-Newtonian fluid flow through an elastic porous shell.

Figure 5.4 shows the change in porosity for $n = 1$ at $K = 1$. This graphical

result shows an identical result that was presented in [50] for various values of the normalized time. It is interesting to note that expansion occurs in the medium at the inner boundary as time increases.
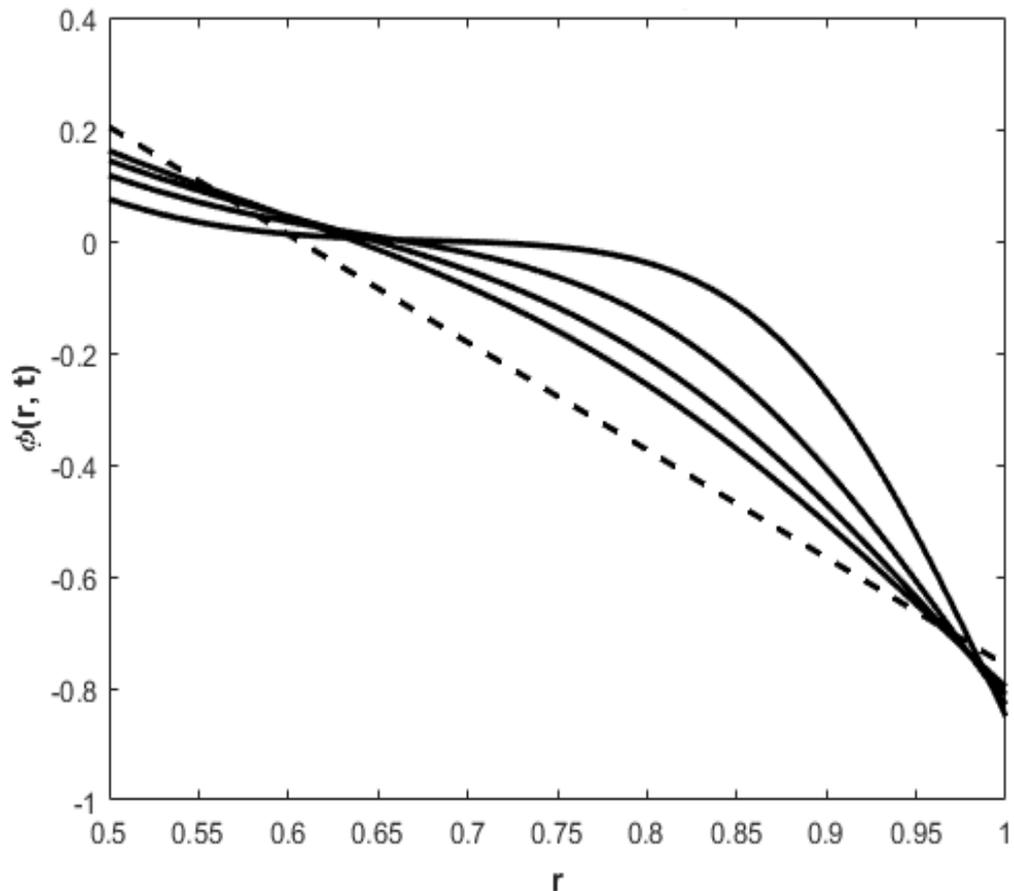

FIGURE 5.4: The changes in the porosity against the radius of deformable porous shell. In plotting these curves, Newtonian fluid flow behavior has been considered for the linear permeability of the solid matrix. This plot shows the same dynamics as was in [50] for the case of Newtonian fluid flow behavior.

The compression occurs at the constrained boundary and spreads towards the inner direction with the passage of time. The growth consolidated region in time is represented as a maximum value of displacement gradient attained for a radius equal to 1, which is the limit of consolidation. The dynamics of fluid flows are plotted for the thin wall shell due to the comparison with Barry and Aldis published article result [50]. This justification of the numerical scheme used in solving

the governing system of equations serves as a starter for non-Newtonian fluids for both the shear thinning and shear thickening fluids cases.
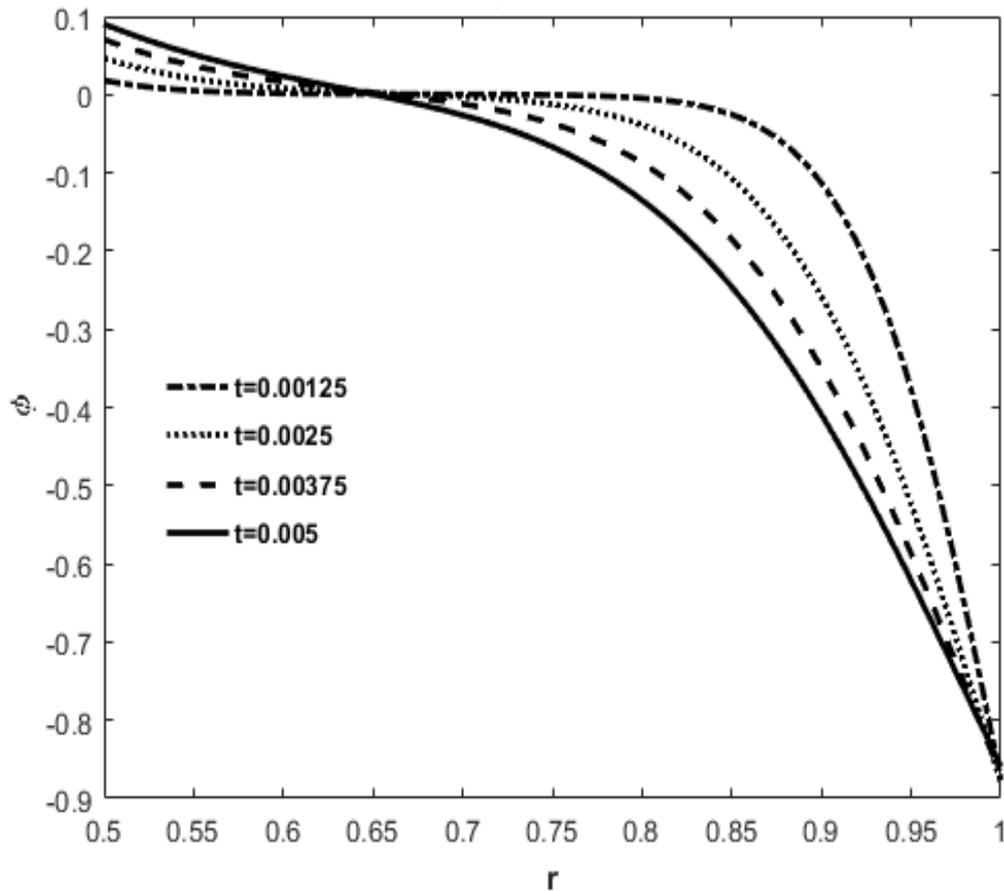
FIGURE 5.5: The changes in the porosity Vs four different values of normalized time t.

Figure 5.5 shows variability in porosity ϕ as a function of radial distance for various values of time after imposing unit step change in pressure. The change in ϕ represents the expansion of the medium at the inner boundary in accordance with the values of time taken in plotting different curves. It is interesting to note that high compressed region is formed at the constrained boundary and as time evolves it spreads in the inward direction.

In Figure 5.6, we plotted solid deformation against radial direction of the deformable porous shell. The displacement figure shows the validity of these results

as the existence of a consolidated region growing with increase of times. In plotting this figure, power law index value is taken to be $n = 1.5$ (shear thickening). The consolidation process slows down for the shear thickening fluid as the seepage of fluid decreased through the porous shell.
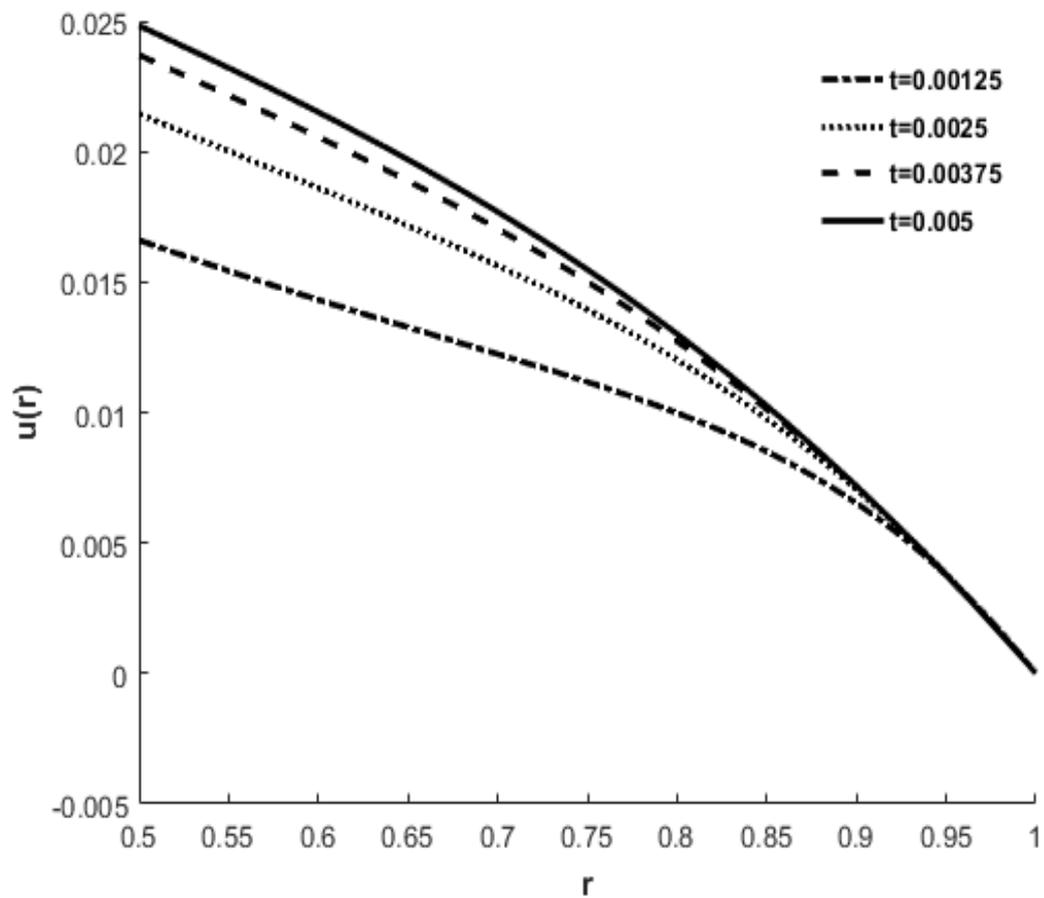
FIGURE 5.6: Solid deformation Vs various values of the normalized time t.

On the other hand, for the case of shear thinning fluid, large consolidation of the solid matrix is reported due to more fluid flow out from the porous shell which in turn causes more deformation.

Like previous figures, Figures 5.7 and 5.8 show change in porosity (ϕ) and solid deformation (u) as a function of radial distance during passage of both shears thinning and thickening fluids. We have made a comparison between the Newtonian $n = 1$ and non-Newtonian fluids flow through the elastic porous shell.

It is important to note that radius of the shell change from 0.8 to 1 (thin shell), i.e., a thin wall elastic shell was considered in these figures. The reason behind this motivation was to study the equilibrium effected by the wall thickness of the shell. It is interesting to note that for case of thinner shell equilibrium is attained much faster in contrast to the shear thickening fluid. An opposite dynamic is observed for shear thinning fluid case.
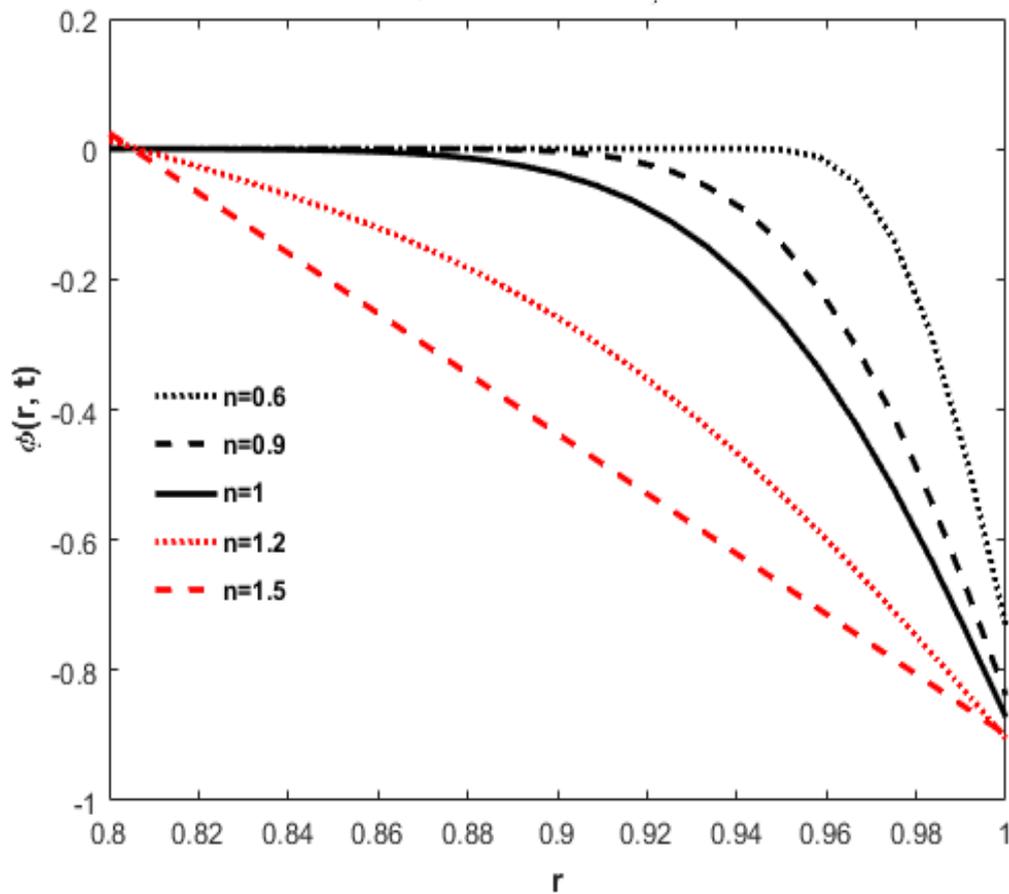
FIGURE 5.7: The changes in the porosity Vs various values of the power-law index n.

On the other hand, change in solid displacement behaves opposite to porosity dynamics for both shears thinning and shear thickening fluid as comparison to the Newtonian fluid case. It is to be noted that in cylindrical geometries captures larger molecules as compared to planar case in which large size molecules are excluded from the medium. Interestingly, moderate size particles will be able to

advance before being trapped which elevates the possibility for them to remain constantly trapped while the fluid flux is stopped.

It is important to note that this process slows down for non-Newtonian (shear thickening $n > 1$) fluids and fosters for (shear thinning $n < 1$, not shown here). The application of expansion from the inner section of the medium for small period of time linked to dynamics of solid-non-Newtonian fluid interaction.
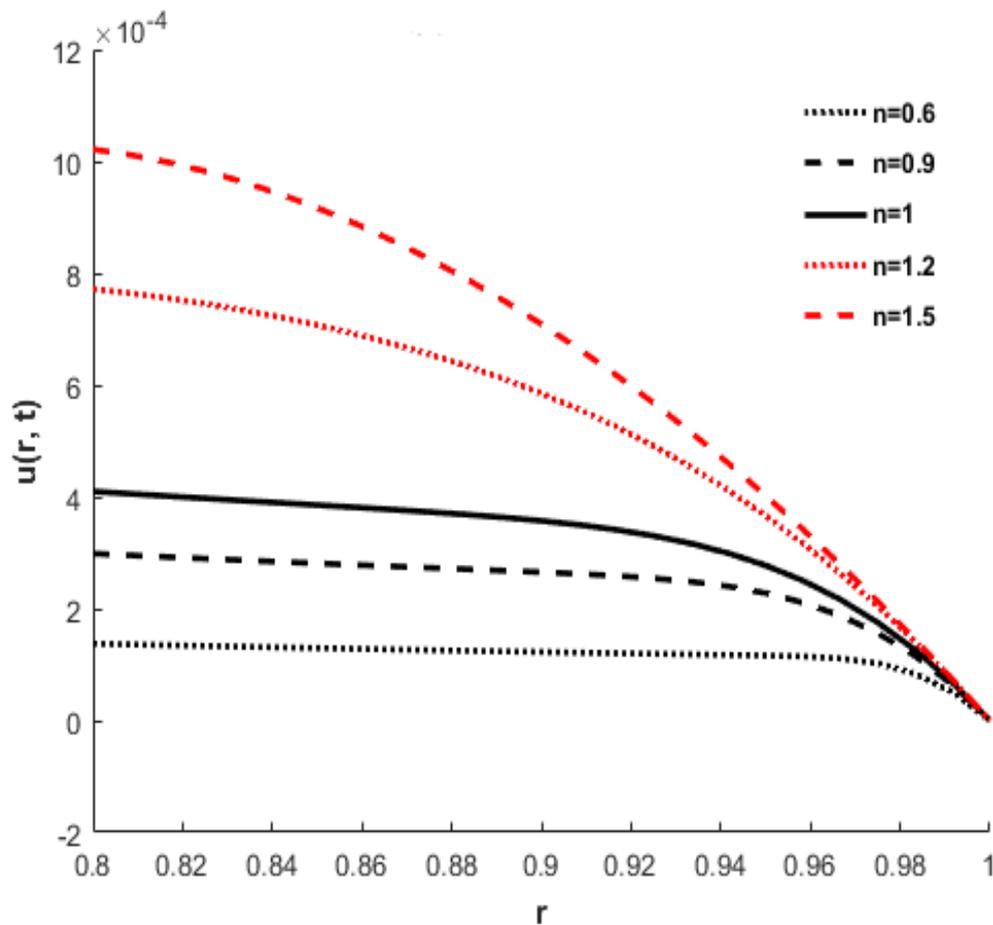
FIGURE 5.8: The change in the solid displacement Vs different values of power-law index n.

One has to be careful while choosing a permeability relation that provides the meaningful values for expanded medium, and an unclear situation whether permeability should be function of porosity ϕ or radial strain $\frac{du}{dr}$. If the medium is random than it is appropriate to consider permeability as a function of porosity.

Figure 5.9 shows the variation of porosity ϕ as a function of radial distance for a thin shell being of radius $0.8 \leq r \leq 1$ for $n = 0.7$. The region of thin wall shell attains equilibrium faster as compared to the thick wall shell due to which maximum time $t = 0.005$ is considered in plotting flow dynamics for thin wall shell. It is to be noted that there is comparatively less expansion of inner region of the shell as compared to Newtonian fluid reported in [50]. Although the results are uniform for non-Newtonian case as compared to Newtonian fluid that shows thin region act as a uniform region for most values of the time.
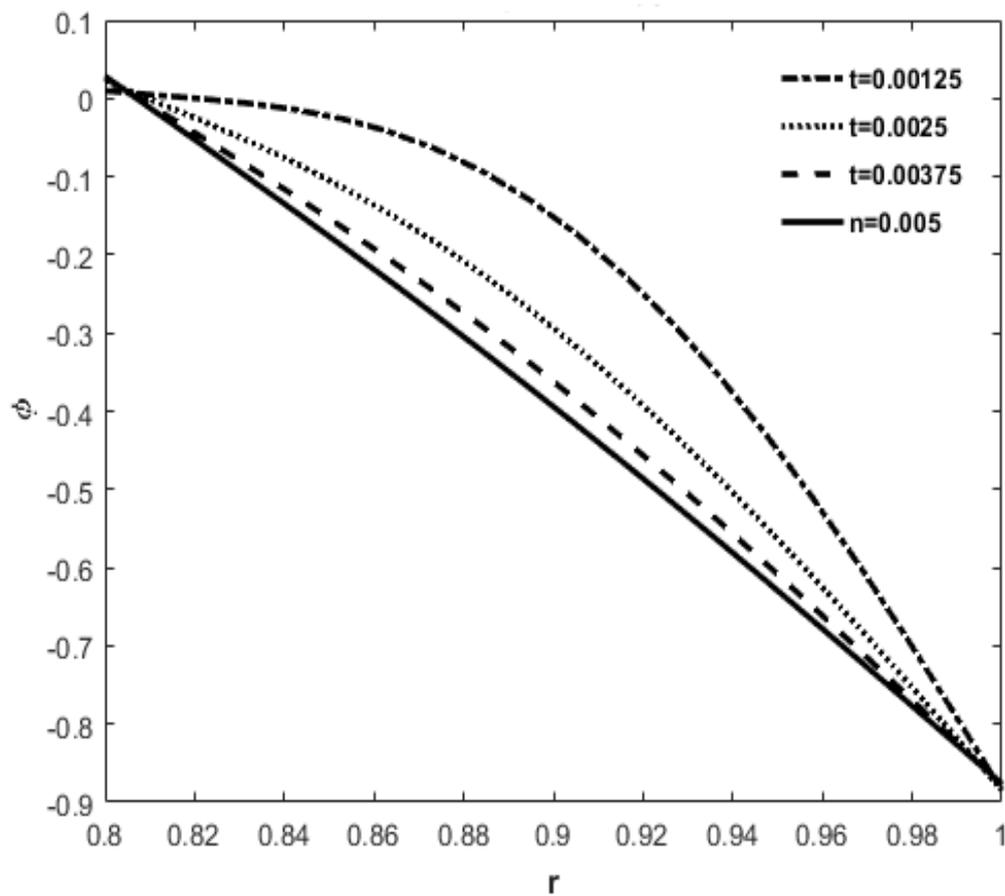
FIGURE 5.9: Variation in the porosity Vs various values of the normalized time t.

The displacement u as a function of radial distance is graphed in Figure 5.10, for various values of times $(t = 0.005, 0.0375, 0.0025, 0.00125)$ to confirm the existence of a strongly growing region in time. In plotting these curves, we have considered same grade fluid $(n = 0.7, \text{ shear thinning})$ for all cases.
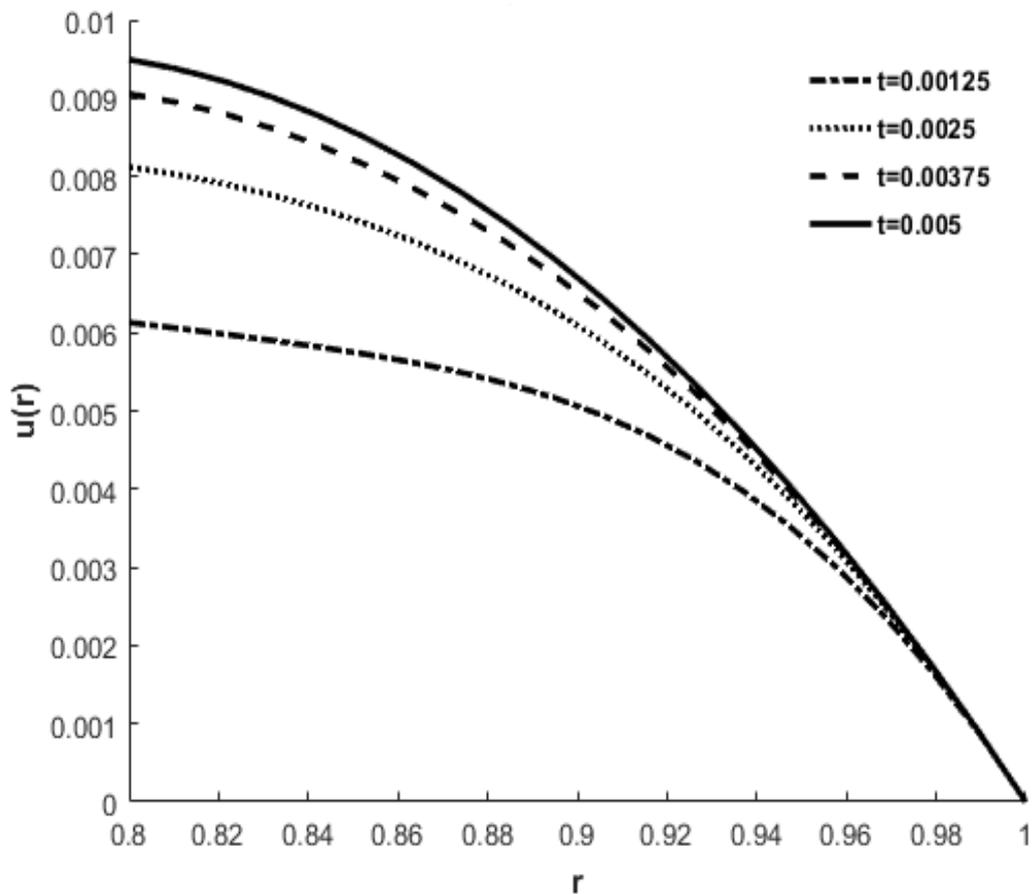
FIGURE 5.10: Solid deformation Vs four different values of the normalized time t.

It is to be noted that maximum change in displacement reaches at $r = 1$, which is our maximum limit of consolidation. It is to be noted that geometry, and type of fluid, play a very important role in dynamics of fluid flow through the elastic porous shell. Following section contain a summery of the work presented in the present Chapter.

5.4   Conclusion

The consequences of the present work were summarized already in individual sections. Here, we seek some overview of usefulness findings and present the key results of the model for radial flow and its solution. We follow the same modeling

approach as was used by Barry and Aldis [50] to develop a radially directed flow through spherical, cylindrical, and planar shells. We have computed exact solution for steady state case and numerical solution for unsteady for both planar and radial geometries. Furthermore, we considered the shell is radially constrained for two different cases, i.e., $0.5 \leq r \leq 1$ (thicker) and $0.8 \leq r \leq 1$ (thinner).

When the geometry is planar, the geometry is more compressed as compared to cylindrical shell for power fluid case due to filtration of smaller particles. This is represented by decrease of porosity in planar case. The cylindrical shell expands if the width of the cylindrical shell is wide enough. This result shows that the cylindrical filter will trap within its expanded pores when the particle size is large enough to be recovered later for non-Newtonian fluid case as compared to Newtonian case. There might be error associated with approximating the boundary condition to negate the increased accuracy when nonlinear permeability relation is incorporated in our model. The theoretical results predict that increasing the value of n (power law index) more resistance will be experienced by the fluids during the flow through porous shell. The wall thickness effects the equilibrium of the porosity and solid deformation, this effect can be controlled by the value of time as well as power-law index.

Chapter 6

Conclusion and Future Work

In this dissertation, the fluid flux through an elastic porous shell as well as fluid flow through a soft biological tissue have been reported. The theoretical framework employed in modeling the phenomenon of multiphasic deformation was based upon the well established continuum mechanics laws of mass balance and momentum balance. These laws were manipulated in developing the continuum mixture theory that was widely used in understanding the viscoelastic behavior of both soft tissues and fluid flow dynamics through deformable porous solids. The continuum mixture or more precisely binary mixture theory was the key path upon which we have derived the mathematical models in different Chapters. In the following, we have concluded the key results of present study and some possible future direction as outcomes of the present research work.

6.1   Conclusion

The fluid flow is the branch of applied mechanics that find many application in the field of engineering and biomedical sciences. Over the past few decades, numerous theoretical approaches have been used to understand the dynamics of fluid flow through different geometries under various physical conditions. Particularly, a special attention has been given in modeling the fluid-solid interaction, when

fluid flows through the deformable porous solids. These types of problems have natural intrust due to their close resemblance to the different types of biochemical processes that take place in the living organisms along with many industrial applications. In this thesis, we have formulated the solid deformation for both the soft tissue and deformable porous shell. This was based upon the mixture theory and formed an overview of the theoretical results of the field since 1967. In Chapter three, mathematical model for the coupled motion of the fluid and deformable tissues is given that is followed by Chapters four and five describing the derivation of fluid fluxes through a deformable porous shell. A system of coupled partial differential equations for the solid displacement and local fluid pressure has been derived. Furthermore, the governing systems of equations are converted into dimensionless form using appropriate dimensionless variables in different problems discussed in this thesis. At the end, both numerical and analytical solutions were found along with their graphical comparison. In some cases, we compared the graphical results of our present study with previous published articles results for the purpose of validation of both the mathematical modeling and solution methodology. In the following, we summarize the main findings of research presented in this dissertation.

1. In loading circumstances, solid volume fraction for initially saturated porous solid increases that clarify the drainage of fluid, when pressure applied to the solid matrix.

2. The magnetic parameter offers resistance for the passage of fluid through the soft tissues and these forces are enhanced in accordance with the magnitude of the applied magnetic field.

3. Increasing the value of the normalized time results in the increase of solid deformation means that solid deformation produced in the tissue is directly proportional to the time for which loading acts.

4. The permeability of the tissue affects the passage of fluid through the porous materials. In case of increasing the nonlinear effects in the permeability of the porous material result in the decrease of liquid flow through it.

5. Pressure changes produced in the deformable porous solid can also be controlled using the strain dependent permeability of the tissues.

6. In the case of elastic porous shells, permeability dependent flow controlled the growth rate of the porosity for both radial and planar geometries.

7. In case of electrically conducting fluid flow through the deformable porous shell, the magnetic parameter and time reports the opposite effects of each other on the solid deformation.

8. In case of fluid flow through deformable porous shells, width and equilibrium are correlated with each other. When the width of the shell decreases, it results in achieving equilibrium more quickly. This particular behavior shows that the solid deformation of the solid matrix depends upon the wall thickness of the shell.

9. In geometry comparison of fluid flow, planar geometry experiences more loading effects as compared to the radial geometry. Hence, when maximum fluid flow is required the planar geometry is more suited. Moreover, when micro precipitate septation is required from the solution then cylindrical or spherical geometries are better.

10. In the modeling of fluid flow through the deformable porous shell, I developed a single governing partial differential equation that prescribed both planar and radial geometries and just changing the value of one variable (parameter) switched the system from one geometry to another.

11. In case of power-law fluids, the flow or passage of the fluid offers more resistance in accordance with the value of the power-law index.

12. The expansion of the cylindrical shell effects by the permeability, power-law index, and loading imposed upon it.

13. One of the interesting findings in case of cylindrical geometry is that cylindrical filters trap within its expanded pores when large particles associated with the fluid flow.

14. In the case of numerical solution of the governing system of equation for fluid flow through deformable porous shells, the unknown variable has appeared both in the boundary conditions and governing PDE. I coupled the trapezoidal rule with the primary numerical scheme "method of lines" to handle this problem.

6.2   Future Work

From the modeling point of view, mixture theory is a well established theoretical framework used in modeling both biological and non-biological settings for constant as well as strain-dependent permeability. In this thesis, we used the biphasic mixture to derive the problems of fluid flow through deformable porous shells and soft tissue. In this thesis, a good qualitative analysis of different problems and their physical natures according to the material properties and geometry have been summarized still there is further need of improvement in models that are applicable to the real world problems. Particularly, experimental verification not only improves the quality of present work but also includes the parameters which were ignored in this dissertation due to their small contribution. Some interesting future directions in the preset work are as follows

1. Both MHD and non-Newtonian contribution in single model still need to accommodate for the fluid flow through soft tissues as well as fluid fluxes through deformable porous shell.

2. The comparison of radial and planar geometries for the fluid flow through the tissues network still needs to be performed.

3. In the derivation of governing dynamics for the fluid fluxes through the cartilage tissues, I assumed an isotropic and homogeneous nature of the tissues. For more accuracy of the theoretical results, one can take inhomogeneous and anisotropic nature of the soft biological tissues.

4. We can fixed the domain for the analysis, however, moving domain problem can be consider for future work.

5. In the present study, I model two phases, i.e, liquid and solid. The consideration of gases phase present in the pores of deformable porous shells and tissues can be studied using triphasic mixture theory approach.

6. Finally, one can compare the results of the present study by performing the experiments.

Bibliography

[1] J. Cassels, N. Hitchin, *et al.*, "Nonlinear elasticity: theory and applications," 2001.

[2] M. E. Gurtin, *Topics in finite elasticity*. SIAM, 1981.

[3] D. J. Steigmann, "Invariants of the stretch tensors and their application to finite elasticity theory," *Mathematics and mechanics of Solids*, vol. 7, no. 4, pp. 393–404, 2002.

[4] A. C. Pipkin, *Lectures on viscoelasticity theory*, vol. 7. Springer Science & Business Media, 2012.

[5] R. Christensen, *Theory of viscoelasticity: an introduction*. Elsevier, 2012.

[6] D. Ambrosi, L. Preziosi, and G. Vitale, "The insight of mixtures theory for growth and remodeling," *Zeitschrift für angewandte Mathematik und Physik*, vol. 61, no. 1, pp. 177–191, 2010.

[7] A. Menzel and E. Kuhl, "Frontiers in growth and remodeling," *Mechanics research communications*, vol. 42, pp. 1–14, 2012.

[8] W. Darcy, "Continuum mixture theory," *Z Angew Math Mech*, vol. 1, pp. 121–151, 1851.

[9] C. Truesdell and W. Noll, "The nonlinear field theories of mechanics, in in s. flügge, editor," *Handbuch der Physik*, vol. 3, p. 3, 1965.

[10] R. Atkin and R. Craine, "Continuum theories of mixtures: basic theory and historical development," *The Quarterly Journal of Mechanics and Applied Mathematics*, vol. 29, no. 2, pp. 209–244, 1976.

[11] R. M. Bowen, "Incompressible porous media models by use of the theory of mixtures," *International Journal of Engineering Science*, vol. 18, no. 9, pp. 1129–1148, 1980.

[12] L. Tao *et al.*, *Mechanics of mixtures*, vol. 35. World scientific, 1995.

[13] J. D. Humphrey, "Continuum biomechanics of soft biological tissues," *Proceedings of the Royal Society of London. Series A: Mathematical, Physical and Engineering Sciences*, vol. 459, no. 2029, pp. 3–46, 2003.

[14] V. C. Mow, S. Kuei, W. M. Lai, and C. G. Armstrong, "Biphasic creep and stress relaxation of articular cartilage in compression: theory and experiments," *Journal of biomechanical engineering*, vol. 102, no. 1, pp. 73–84, 1980.

[15] E. Myers, W. Lai, and V. Mow, "A continuum theory and an experiment for the ion-induced swelling behavior of articular cartilage," *Journal of biomechanical engineering*, vol. 106, no. 2, pp. 151–158, 1984.

[16] E. W. Washburn, "The dynamics of capillary flow," *Physical review*, vol. 17, no. 3, p. 273, 1921.

[17] B. Zhmud, F. Tiberg, and K. Hallstensson, "Dynamics of capillary rise," *Journal of colloid and interface science*, vol. 228, no. 2, pp. 263–269, 2000.

[18] T. Delker, D. B. Pengra, and P.-z. Wong, "Interface pinning and the dynamics of capillary rise in porous media," *Physical review letters*, vol. 76, no. 16, p. 2902, 1996.

[19] M. Lago and M. Araujo, "Capillary rise in porous media," *Journal of colloid and interface science*, vol. 234, no. 1, pp. 35–43, 2001.

[20] S. Davis and L. Hocking, "Spreading and imbibition of viscous liquid on a porous base," *Physics of fluids*, vol. 11, no. 1, pp. 48–57, 1999.

[21] S. H. Davis and L. Hocking, "Spreading and imbibition of viscous liquid on a porous base. ii," *Physics of fluids*, vol. 12, no. 7, pp. 1646–1655, 2000.

[22] J. R. Jones, P. D. Lee, and L. L. Hench, "Hierarchical porous materials for tissue engineering," *Philosophical Transactions of the Royal Society A: Mathematical, Physical and Engineering Sciences*, vol. 364, no. 1838, pp. 263–281, 2006.

[23] D. M. Robertson, L. St. Pierre, and R. Chahal, "Preliminary observations of bone ingrowth into porous materials," *Journal of biomedical materials research*, vol. 10, no. 3, pp. 335–344, 1976.

[24] K. Merritt, J. W. Shafer, and S. A. Brown, "Implant site infection rates with porous and dense materials," *Journal of biomedical materials research*, vol. 13, no. 1, pp. 101–108, 1979.

[25] K. Ishizaki, S. Komarneni, and M. Nanko, *Porous Materials: Process technology and applications*, vol. 4. Springer science & business media, 2013.

[26] S. Rashidi, J. A. Esfahani, and A. Rashidi, "A review on the applications of porous materials in solar energy systems," *Renewable and Sustainable Energy Reviews*, vol. 73, pp. 1198–1210, 2017.

[27] A. G. Slater and A. I. Cooper, "Porous materials. function-led design of new porous materials.," *Science (New York, NY)*, vol. 348, no. 6238, pp. aaa8075–aaa8075, 2015.

[28] K. Parker, R. Mehta, and C. Caro, "Steady flow in porous, elastically deformable materials," 1987.

[29] S. Barry, G. Aldis, and G. Mercer, "Injection of fluid into a layer of deformable porous medium," 1995.

[30] G. Cinelli, "An extension of the finite hankel transform and applications," *International Journal of Engineering Science*, vol. 3, no. 5, pp. 539–559, 1965.

[31] K. Terzaghi, "Erdbaumechanik auf bodenphysikalischen grundlagen, wien, deuticke,"

[32] V. Mow, M. Kwan, W. Lai, and M. Holmes, "A finite deformation theory for nonlinearly permeable soft hydrated biological tissues," in *Frontiers in Biomechanics*, pp. 153–179, Springer, 1986.

[33] M. Holmes, W. Lai, and V. Mow, "Singular perturbation analysis of the nonlinear, flow-dependent compressive stress relaxation behavior of articular cartilage," *Journal of biomechanical engineering*, vol. 107, no. 3, pp. 206–218, 1985.

[34] J. Philibert, "One and a half century of diffusion: Fick, einstein, before and beyond," *Diffusion Fundamentals*, vol. 4, no. 6, pp. 1–19, 2006.

[35] R. H. Christopher and S. Middleman, "Power-law flow through a packed tube," *Industrial & Engineering Chemistry Fundamentals*, vol. 4, no. 4, pp. 422–426, 1965.

[36] T. J. Sadowski, "Non-newtonian flow through porous media. ii. experimental," *Transactions of the Society of Rheology*, vol. 9, no. 2, pp. 251–271, 1965.

[37] R. Hayes, A. Afacan, B. Boulanger, and A. Shenoy, "Modelling the flow of power law fluids in a packed bed using a volume-averaged equation of motion," *Transport in porous media*, vol. 23, no. 2, pp. 175–196, 1996.

[38] Z. Kemblowski and M. Michniewicz, "A new look at the laminar flow of power law fluids through granular beds," *Rheologica Acta*, vol. 18, no. 6, pp. 730–739, 1979.

[39] T. Al-Fariss and K. Pinder, "Flow through porous media of a shear-thinning liquid with yield stress," *The Canadian Journal of Chemical Engineering*, vol. 65, no. 3, pp. 391–405, 1987.

[40] D. E. Kenyon, "A mathematical model of water flux through aortic tissue," *Bulletin of mathematical biology*, vol. 41, no. 1, pp. 79–90, 1979.

[41] V. C. Mow and W. Lai, "Mechanics of animal joints," *Annual review of Fluid mechanics*, vol. 11, no. 1, pp. 247–288, 1979.

[42] D. E. Kenyon, "A mathematical model of water flux through aortic tissue," *Bulletin of mathematical biology*, vol. 41, no. 1, pp. 79–90, 1979.

[43] C. Serra, M. J. Clifton, P. Moulin, J.-C. Rouch, and P. Aptel, "Dead-end ultrafiltration in hollow fiber modules: Module design and process simulation," *Journal of membrane science*, vol. 145, no. 2, pp. 159–172, 1998.

[44] R. M. Nerem and J. F. Cornhill, "The role of fluid mechanics in atherogenesis," 1980.

[45] G. Schettler, R. M. Nerem, H. Schmid-Schönbein, H. Mörl, and C. Diehm, *Fluid Dynamics as a Localizing Factor for Atherosclerosis: The Proceedings of a Symposium Held at Heidelberg, FRG, June 18–20, 1982*. Springer Science & Business Media, 2012.

[46] I. Howells, "Some mathematical aspects of hollow fibre ultrafiltration," 1986.

[47] D. Kenyon, "Transient filtration in a porous elastic cylinder," 1976.

[48] G. Jayaraman, "Water transport in the arterial wall a theoretical study," *Journal of biomechanics*, vol. 16, no. 10, pp. 833–840, 1983.

[49] M. Klanchar and J. Tarbell, "Modeling water flow through arterial tissue," *Bulletin of mathematical biology*, vol. 49, no. 6, pp. 651–669, 1987.

[50] S. Barry and G. Aldis, "Radial flow through deformable porous shells," *The ANZIAM Journal*, vol. 34, no. 3, pp. 333–354, 1993.

[51] V. C. Mow and W. M. Lai, "Selected unresolved problems in synovial joint biomechanics," in *Proceedings 1979 Biomechanics Symposium, Trans. ASME*, pp. 19–52, 1979.

[52] V. C. Mow and W. M. Lai, "Recent developments in synovial joint biomechanics," *Siam Review*, vol. 22, no. 3, pp. 275–317, 1980.

[53] W. M. Lai and V. C. Mow, "Stress and flow fields in articular cartilage," in *Engineering Mechanics*, pp. 202–204, ASCE, 1979.

[54] V. Mow, W. Lai, and M. Holmes, "Advanced theoretical and experimental techniques in cartilage research," in *Biomechanics: Principles and applications*, pp. 47–74, Springer, 1982.

[55] C. MOW, "Lubrication of diarthrodial joints," *Handbook of bioengineering*, 1987.

[56] V. C. Mow, S. Kuei, W. M. Lai, and C. G. Armstrong, "Biphasic creep and stress relaxation of articular cartilage in compression: theory and experiments," *Journal of biomechanical engineering*, vol. 102, no. 1, pp. 73–84, 1980.

[57] E. Myers, W. Lai, and V. Mow, "A continuum theory and an experiment for the ion-induced swelling behavior of articular cartilage," 1984.

[58] C. Armstrong, W. Lai, and V. Mow, "An analysis of the unconfined compression of articular cartilage," 1984.

[59] R. L. Spilker, J.-K. Suh, and V. C. Mow, "A finite element analysis of the indentation stress-relaxation response of linear biphasic articular cartilage," 1992.

[60] H. Guo, S. A. Maher, and P. A. Torzilli, "A biphasic finite element study on the role of the articular cartilage superficial zone in confined compression," *Journal of biomechanics*, vol. 48, no. 1, pp. 166–170, 2015.

[61] B. Cohen, W. Lai, and V. Mow, "A transversely isotropic biphasic model for unconfined compression of growth plate and chondroepiphysis," 1998.

[62] V. C. Mow, C. C. Wang, and C. T. Hung, "The extracellular matrix, interstitial fluid and ions as a mechanical signal transducer in articular cartilage," *Osteoarthritis and Cartilage*, vol. 7, no. 1, pp. 41–58, 1999.

[63] H. Muir, "Proteoglycans as organizers of the intercellular matrix," *Biochem Soc Trans*, vol. 11, no. 6, pp. 613–622, 1983.

[64] J. Siddique and A. Kara, "Capillary rise of magnetohydrodynamics liquid into deformable porous material.," *Journal of Applied Fluid Mechanics*, vol. 9, no. 6, 2016.

[65] A. Naseem, A. Mahmood, J. Siddique, and L. Zhao, "Infiltration of mhd liquid into a deformable porous material," *Results in physics*, vol. 8, pp. 71–75, 2018.

[66] A. Ahmed and J. I. Siddique, "The effect of magnetic field on flow induced-deformation in absorbing porous tissues," *Math Biosci Eng*, vol. 16, no. 2, pp. 603–618, 2019.

[67] I. Baran, K. Cinar, N. Ersoy, R. Akkerman, and J. H. Hattel, "A review on the mechanical modeling of composite manufacturing processes," *Archives of computational methods in engineering*, vol. 24, no. 2, pp. 365–395, 2017.

[68] A. W. Chan and S.-t. Hwang, "Modeling resin transfer molding of polyimide (pmr-15)/fiber composites," *Polymer composites*, vol. 14, no. 6, pp. 524–528, 1993.

[69] J. N. Reddy and A. Miravete, *Practical analysis of composite laminates.* CRC press, 2018.

[70] J. P. Cook, "Composite construction methods," *Journal of the Construction Division*, vol. 102, no. 1, pp. 21–27, 1976.

[71] D. A. Drew, "Mathematical modeling of two-phase flow," *Annual review of fluid mechanics*, vol. 15, no. 1, pp. 261–291, 1983.

[72] L. Preziosi, D. Joseph, and G. Beavers, "Infiltration of initially dry, deformable porous media," *International Journal of Multiphase Flow*, vol. 22, no. 6, pp. 1205–1222, 1996.

[73] D. Ambrosi and L. Preziosi, "Modeling injection molding processes with deformable porous preforms," *SIAM Journal on Applied Mathematics*, vol. 61, no. 1, pp. 22–42, 2000.

[74] A. Farina and L. Preziosi, "Deformable porous media and composites manufacturing," in *Heterogeneous media*, pp. 321–410, Springer, 2000.

[75] L. Billi and A. Farina, "Unidirectional infiltration in deformable porous media: mathematical modeling and self-similar solution," *Quarterly of applied mathematics*, vol. 58, no. 1, pp. 85–101, 2000.

[76] L. Mesin and D. Ambrosi, "Inertial effects during the infiltration of an elastic porous medium," *Journal of engineering mathematics*, vol. 50, no. 4, p. 379, 2004.

[77] U. Ali and J. I. Siddique, "Visco-elastic behavior of articular cartilage under applied magnetic field and strain-dependent permeability," *Computer Methods in Biomechanics and Biomedical Engineering*, vol. 23, pp. 524–535, 2020.

[78] J. Siddique, U. Ali, and A. Ahmed, "Effects of magnetic field on porosity and solid deformation for radial fluid flow through deformable porous shells," *Computers & Mathematics with Applications*, vol. 80, no. 5, pp. 1104–1116, 2020.

[79] H. P. G. Darcy, *Les Fontaines publiques de la ville de Dijon. Exposition et application des principes à suivre et des formules à employer dans les questions de distribution d'eau, etc.* V. Dalamont, 1856.

[80] J. Bear, *Dynamics of fluids in porous media*. Courier Corporation, 2013.

[81] N. T. Eldabe, G. Saddeek, and K. Elagamy, "Magnetohydrodynamic flowof a bi-viscosity fluid through porous medium in a layer of deformable material," *Journal of Porous Media*, vol. 14, no. 3, 2011.

[82] S. Sreenadh, M. Krishna Murthy, E. Sudhakara, G. Gopi Krishna, and D. Venkateswarlu Naidu, "Mhd free surface flow of a jeffrey fluid over a deformable porous layer," *Global Journal of Pure and Applied Mathematics*, vol. 11, no. 5, pp. 3889–3903, 2015.

[83] W. Lai, V. C. Mow, and V. Roth, "Effects of nonlinear strain-dependent permeability and rate of compression on the stress behavior of articular cartilage," *Journal of biomechanical engineering*, vol. 103, no. 2, pp. 61–66, 1981.

[84] M. A. Biot, "General theory of three-dimensional consolidation," *Journal of applied physics*, vol. 12, no. 2, pp. 155–164, 1941.

[85] M. A. Biot, "Consolidation settlement under a rectangular load distribution," *Journal of Applied Physics*, vol. 12, no. 5, pp. 426–430, 1941.

[86] M. A. Biot and F. Clingan, "Consolidation settlement of a soil with an impervious top surface," *Journal of Applied Physics*, vol. 12, no. 7, pp. 578–581, 1941.

[87] H. Alkhaldi, F. Kremer, T. Bierschenk, J. Hansen, A. Nylandsted-Larsen, J. Williams, and M. Ridgway, "Porosity as a function of stoichiometry and implantation temperature in ge/si1- xgex alloys," *Journal of Applied Physics*, vol. 119, no. 9, p. 094303, 2016.

[88] V. C. Mow and J. M. Mansour, "The nonlinear interaction between cartilage deformation and interstitial fluid flow," *Journal of biomechanics*, vol. 10, no. 1, pp. 31–39, 1977.

[89] F. Martini *et al.*, *Anatomy and Physiology'2007 Ed.* Rex Bookstore, Inc., 2006.

[90] V. J. Rossow, "On flow of electrically conducting fluids over a flat plate in the presence of a transverse magnetic field," 1957.

[91] A. Hussanan, Z. Ismail, I. Khan, A. G. Hussein, and S. Shafie, "Unsteady boundary layer mhd free convection flow in a porous medium with constant mass diffusion and newtonian heating," *The European Physical Journal Plus*, vol. 129, no. 3, pp. 1–16, 2014.

[92] S. Barry and G. Aldis, "Unsteady flow induced deformation of porous materials," *International journal of non-linear mechanics*, vol. 26, no. 5, pp. 687–699, 1991.

[93] M. Holmes, "Finite deformation of soft tissue: analysis of a mixture model in uni-axial compression," 1986.

[94] J. M. Mansour and V. C. Mow, "The permeability of articular cartilage under compressive strain and at high pressures.," *The Journal of bone and joint surgery. American volume*, vol. 58, no. 4, pp. 509–516, 1976.

[95] W. M. Lai and V. C. Mow, "Drag-induced compression of articular cartilage during a permeation experiment," *Biorheology*, vol. 17, no. 1-2, pp. 111–123, 1980.

[96] A. Friedman, *Partial differential equations of parabolic type*. Courier Dover Publications, 2008.

[97] O. A. Ladyženskaja, V. A. Solonnikov, and N. N. Ural'ceva, *Linear and quasi-linear equations of parabolic type*, vol. 23. American Mathematical Soc., 1988.

[98] M. H. Holmes, "A nonlinear diffusion equation arising in the study of soft tissue," *Quarterly of Applied Mathematics*, vol. 41, no. 2, pp. 209–220, 1983.

[99] M. H. Holmes, "Comparison theorems and similarity solution approximations for a nonlinear diffusion equation arising in the study of soft tissue," *SIAM Journal on Applied Mathematics*, vol. 44, no. 3, pp. 545–556, 1984.

[100] S. Barry and G. Aldis, "Unsteady flow induced deformation of porous materials," *International journal of non-linear mechanics*, vol. 26, no. 5, pp. 687–699, 1991.

[101] W. Lai, F. Mak, F. Armstrong, and V. Mow, "Compresive stress relaxation of articular cartilage with transversely isotropic permeability," *proceedings of the 4th international congress of biorehology*, pp. 127–138, 1981.

[102] K. An, S. Himeno, H. Tsumura, T. Kawai, and E. Chao, "Pressure distribution on articular surfaces: application to joint stability evaluation," *Journal of Biomechanics*, vol. 23, no. 10, pp. 1013–1020, 1990.

[103] D. Anderson, T. Brown, K. Yang, and E. Radin, "A dynamic finite element analysis of impulsive loading of the extension-splinted rabbit knee," 1990.

[104] D. Anderson, T. Brown, and E. Radin, "Stress wave effects in a finite element analysis of an impulsively loaded articular joint," *Proceedings of the Institution of Mechanical Engineers, Part H: Journal of Engineering in Medicine*, vol. 205, no. 1, pp. 27–34, 1991.

[105] R. Hooke, *Lectures de potentia restitutiva, or of spring explaining the power of springing bodies*. No. 6, John Martyn, 2016.

[106] E. Mariotte, *Traité du mouvement des eaux...* Estienne Michallet, 1886.

[107] D. Royer and E. Dieulesaint, *Elastic waves in solids I: Free and guided propagation*. Springer Science and Business Media, 1999.

[108] D. Royer and E. Dieulesaint, *Elastic waves in solids II: generation, acousto-optic interaction, applications*. Springer Science and Business Media, 1999.

[109] G. Eason, "Jd achenbach, wave propagation in elastic solids, north-holland publishing company, amsterdam (1973) cloth, 440 pp.; dfl 120.00, about us 42.10.," *Journal of Sound Vibration*, vol. 34, pp. 575–576, 1974.

[110] R. Masri and D. Durban, "Self similar dynamic expansion of a spherical cavity in elastoplastic media," in *21st International Congress of Theoretical and Applied Mechanics*, 2004.

[111] K. F. Graff, *Wave motion in elastic solids*. Courier Corporation, 2012.

[112] O. Coussy, L. Dormieux, and E. Detournay, "From mixture theory to biot's approach for porous media," *International Journal of Solids and Structures*, vol. 35, no. 34-35, pp. 4619–4635, 1998.

[113] A. Gajo, "A general approach to isothermal hyperelastic modelling of saturated porous media at finite strains with compressible solid constituents," *Proceedings of the Royal Society A: Mathematical, Physical and Engineering Sciences*, vol. 466, no. 2122, pp. 3061–3087, 2010.

[114] Y. Wang and K. Hutter, "A constitutive model of multiphase mixtures and its application in shearing flows of saturated solid-fluid mixtures," *Granular matter*, vol. 1, no. 4, pp. 163–181, 1999.

[115] C. W. McCutchen, "The frictional properties of animal joints," *Wear*, vol. 5, no. 1, pp. 1–17, 1962.

[116] E. A. Celaya, J. A. Aguirrezabala, and P. Chatzipantelidis, "Implementation of an adaptive bdf2 formula and comparison with the matlab ode15s," *Procedia Computer Science*, vol. 29, pp. 1014–1026, 2014.

[117] H. Lamba and A. Stuart, "Convergence results for the matlab ode23 routine," *BIT Numerical Mathematics*, vol. 38, no. 4, pp. 751–780, 1998.

[118] J. I. Siddique, A. Ahmed, A. Aziz, and C. M. Khalique, "A review of mixture theory for deformable porous media and applications," *Applied Sciences*, vol. 7, no. 9, p. 917, 2017.

[119] A. Naseem, A. Mahmood, J. Siddique, and L. Zhao, "Infiltration of mhd liquid into a deformable porous material," *Results in physics*, vol. 8, pp. 71–75, 2018.

[120] A. Bedford and D. Drumheller, "Theories of immiscible and structured mixtures, recent advances," *Int. J. Engng. Sei*, vol. 21, pp. 863–960, 1983.

[121] W. E. Schiesser, *The numerical method of lines: integration of partial differential equations.* Elsevier, 2012.

[122] B. P. Boudreau, "A method-of-lines code for carbon and nutrient diagenesis in aquatic sediments," *Computers & Geosciences*, vol. 22, no. 5, pp. 479–496, 1996.

[123] M. Bush, "Applications in non-newtonian fluid mechanics," in *Viscous Flow Applications*, pp. 134–160, Springer, 1989.

[124] J. Hoyt, "Some applications of non-newtonian fluid flow," in *Rheology Series*, vol. 8, pp. 797–826, Elsevier, 1999.

[125] R. K. Holman, M. J. Cima, S. A. Uhland, and E. Sachs, "Spreading and infiltration of inkjet-printed polymer solution droplets on a porous substrate," *Journal of colloid and interface science*, vol. 249, no. 2, pp. 432–440, 2002.

[126] M. Spiegelman, "Flow in deformable porous media. part 1 simple analysis," *Journal of Fluid Mechanics*, vol. 247, pp. 17–38, 1993.

[127] M. H. Holmes, "A theoretical analysis for determining the nonlinear hydraulic permeability of a soft tissue from a permeation experiment," *Bulletin of mathematical biology*, vol. 47, no. 5, pp. 669–683, 1985.

[128] V. C. Mow, M. H. Holmes, and W. M. Lai, "Fluid transport and mechanical properties of articular cartilage: a review," *Journal of biomechanics*, vol. 17, no. 5, pp. 377–394, 1984.

[129] A. Ahmed, J. Siddique, and A. Mahmood, "Non-newtonian flow-induced deformation from pressurized cavities in absorbing porous tissues," *Computer methods in biomechanics and biomedical engineering*, vol. 20, no. 13, pp. 1464–1473, 2017.

[130] J. Siddique and D. Anderson, "Capillary rise of a non-newtonian liquid into a deformable porous material," *Journal of Porous Media*, vol. 14, no. 12, 2011.

[131] S. Barry and G. Aldis, "Flow-induced deformation from pressurized cavities in absorbing porous tissues," *Bulletin of mathematical biology*, vol. 54, no. 6, pp. 977–997, 1992.

Appendix A

Exact solution

The ultimate goal in the present section is to elaborate the solution technique used in finding an exact solution of the governing partial different equation reported in chapter 3. The main theme was to construct the solution function $u(x,t)$ that satisfy the given initial and boundary conditions, for $k = 1$.

The solution of governing system of equations is found using the eigenfunction expansion method. The main motivation in finding this particular solution is to compared the results (predictions) with numerically calculated solution, in case of constant permeability. It is important to mention here that the boundary conditions for the solid displacement are non-homogeneous. It is well established fact that eigenfunction method only work when boundary condition are in homogenous form. In handling this problem, we have defined following special transformation

$$w(x,t) = \Psi_0(t) + \frac{x}{L}(\Psi_1(t) - \Psi_0(t)), \tag{A.1}$$

where Ψ_0, $\Psi_1(t)$ are the contribution of boundary conditions and $L = 1$. Using boundary conditions (3.31) and (3.32) into equation (A.1), we get

$$w(x,t) = t(1-x). \tag{A.2}$$

Now, solution of the equation (3.29) can be written as

$$u(x,t) = w(x,t) + v(x,t) \tag{A.3}$$

where $w(x,t)$ and $v(x,t)$ are new solutions for the given partial differential equation containing solid displacement. In finding v, we have following equation

$$v_t = \varrho^2 v_{xx} - (1 - x), \quad 0 \le x \le 1, \tag{A.4}$$

with following boundary conditions

$$v(0,t) = v(1,t) = 0, \quad v(x,0) = 0, \tag{A.5}$$

where $\varrho = \sqrt{\frac{R}{1+M}}$. Now, equation (A.4) for the unknown function v have homogenous boundary conditions defined in (A.5). The expression $s(x,t) = -(1-x)$ can be approximated as follows

$$s(x,t) = -(1 - x) = \sum_{n=1}^{\infty} \bar{s}_n(t) \sin(n\pi x) \tag{A.6}$$

where $\bar{s}_n(t)$ is the constant that can be found as follows

$$s(x,t) = 2 \int_0^1 (x - 1) \sin(n\pi x) dx = \frac{-2}{n\pi}. \tag{A.7}$$

Now, consider solution of $v(x,t)$ satisfy the following infinite series

$$v(x,t) = \sum_{n=1}^{\infty} \bar{v}_n(t) \sin(n\pi x) \tag{A.8}$$

Equation (A.8) allow us to rewrite v_t and v_{xx} as follows

$$v_t = \sum_{n=1}^{\infty} \frac{\partial \bar{v}_n}{\partial t} \sin(n\pi x), \tag{A.9}$$

$$v_{xx} = -\sum_{n=1}^{\infty} \bar{v}_n(t)(n\pi)^2 \sin(n\pi x). \tag{A.10}$$

Inserting equations (A.6), (A.9), and (A.10) into (A.4), we get

$$\sum_{n=1}^{\infty} \left(\frac{\partial \bar{v}_n}{\partial t} + \varrho^2 (n\pi)^2 + \frac{2}{n\pi} \right) \sin(n\pi x) = 0. \tag{A.11}$$

Simplifying

$$\bar{v}_n(t) = \frac{-2}{(n\pi)^3 \varrho^2} + B_n \cdot (e^{-\varrho^2 (n\pi)^2 t} - 1), \tag{A.12}$$

where B_n is constant that can be found to be $\frac{2}{\varrho^2 (n\pi)^3}$ using initial condition. Using equations (A.2), and (A.12) into (A.3), closed form of the solutions for the solid deformation can be written as

$$u(x,t) = t(1-x) + \frac{2}{\pi^3 \varrho^2} \sum_{n=1}^{\infty} \left(\frac{e^{-\varrho^2 (n\pi)^2 t} - 1}{n^3} \right) \sin(n\pi x). \tag{A.13}$$

From equation (A.13) and (3.30), we get exact solution for the pressure as follows

$$p(x,t) = \frac{2}{(1+\xi)\varrho^2 \pi^2} \left[1 - \frac{(1-\xi)M}{(1+\xi^2)(1+M)} \right] \sum_{n=1}^{\infty} \left(\frac{e^{-\varrho^2 (n\pi)^2 t} - 1}{n^2} \right) (\cos(n\pi x) - \cos(n\pi)) \tag{A.14}$$

This complete the solution of given system of partial differential equations.

Appendix B

MOL Algorithms

B.1   MOL Code for Chapter 3

clc;   clear all;

$N = 500;$ $K = 200;$

$a = 0;$ $b = 1;$

$dx = (b - a)/N;$

$x = linspace(a, b, N);$

$uinit = 0. * (x);$

$tinit = 0;$ $tfinal = 0.2;$

$tspan = linspace(tinit, tfinal, K);$

$RelTolVal = 10^{-6};$

$AbsTolVal = 10^{-6};$

options = odeset ('RelTol',RelTolVal,'AbsTol',AbsTolVal);

$[t, u] = ode15s(@heat - function, tspan, uin, options, N, dx);$

plot(x,u(end,:),'k-'); R=2;   M=1;   m=0;

for   j = 1 : N

$U(j) = R * (exp(m * (u(j + 1) - u(j - 1)) * (2 * dx)^- 1))$

$*(1 + M * exp(m * (u(j + 1) - u(j - 1))*$

$((2 * dx)^- 1))^- 1 * (u(j + 1) - 2 * u(j) + u(j - 1)) * (dx)^- 2;$

```
end
RHS=[U(1:N)]';
```

B.2   MOL Code for Chapter 4

```
clc;    clear all;
N=600;    K=300;
a=0.5;    b=1;
dx =(b-a)/N;
x = linspace(a,b,N);
```

$uinit = 0 * cos(0 * x);$

```
tinit = 0;    tfinal =0.00125;
tspan = linspace(tinit,tfinal,K);
```

$RelTolVal = 10^{-6};$

$AbsTolVal = 10^{-6};$

```
options = odeset ('RelTol',RelTolVal,'AbsTol',AbsTolVal);
```

$[t, u] = ode15s(@heat_function, tspan, uin, options, N, dx);$

```
plot(x,u(end,:),'k-'); L=2;    t=2;    b=1;
for    j = 1 : N
```

$U(j) = L * exp(t * u(j)) * (0.5 + j * dx)^{-}1 * (1 + M) * ((0.5 + j * dx)*$
$(u(j + 1) - 2 * u(j) + u(j - 1)) * (dx^{-}2) + (b + t * (0.5 + j * dx))*$
$(u(j + 1) - u(j - 1)) * (2 * dx)^{-}1);$

```
end
RHS=[U(1:N)]';
```

B.3   MOL Code for Chapter 5

```
clc;    clear all;
N=600;    K=600;
a=0.5;    b=1;
```

dx =(b-a)/N;

x = linspace(a,b,N);

uinit = 0.001*exp(-x);

tinit = 0;   tfinal =0.025;

tspan = linspace(tinit,tfinal,K);

$RelTolVal = 10^{-6}$;

$AbsTolVal = 10^{-6}$;

options = odeset ('RelTol',RelTolVal,'AbsTol',AbsTolVal);

$[t, u] = ode15s(@heat_function, tspan, uin, options, N, dx)$;

plot(x,u(end,:),'k-'); $t = 2$; $n = 1$;

j = 1 : N

$U(j) = abs(((u(j+1) - u(j-1))./2 * dx)^{(}1 - n)/n)*$

$(n * ((u(j+1) - 2 * u(j) + u(j-1))./(dx)^2)+$

$b./(0.5 + j * dx) * ((u(j+1) - u(j-1))./2 * dx))$;

end

RHS=[U(1:N)]';